M9605029 4

Report DOE/PC/90545-1
(Babcock & Wilcox Report RDD:94:40090-030-036:01)

TASK REPORT

FULL-SCALE DEMONSTRATION OF LOW-NO_x CELL™ BURNER RETROFIT

Long-Term Testing

Prepared for
The U. S. Department of Energy
Under Cooperative Agreement DE-FC22-90PC90545
(B&W CRD-1250)

Submitted by
Babcock & Wilcox
Research and Development Division

March 1994

FULL-SCALE DEMONSTRATION OF LOW-NO_x CELL™ BURNER RETROFIT

Long-Term Testing

TASK REPORT

March 1994

Report DOE/PC/90545-1
(Babcock & Wilcox Report RDD:94:40090-030-036:01)

Principal Investigators

C. F. Eckhart, R. F. DeVault, and S. C. Kung

Sponsored by

The U. S. Department of Energy

Work Performed Under Cooperative Agreement DE-FC22-90PC90545
(B&W CRD-1250)

DOE Program Manager

R. Corbett

Babcock & Wilcox
Research and Development Division
Alliance Research Center
Alliance, Ohio 44601-2196

LEGAL NOTICE

This report was prepared by Babcock & Wilcox (B&W) pursuant to a cooperative agreement partially funded by the U.S. Department of Energy (DOE). Neither B&W, nor any of its subcontractors, nor DOE nor any person acting on behalf of either:

a. Makes any warranty or representation, express or implied, with respect to the accuracy, completeness, or usefulness of the information contained in this report, or that the use of any apparatus, method, or process disclosed in this report may not infringe privately owned rights; or

b. Assumes any liability with respect to the use of, or for damages resulting from the use of, any information, apparatus, method, or process disclosed in this report.

Reference herein to any specific commercial product, process. or service by trade name, trademark, manufacturer, or otherwise does not necessarily constitute or imply its endorsement, recommendation, or favoring by the DOE. The views and opinions of the authors expressed herein do not necessarily state or reflect those of the DOE.

DISCLAIMER

Portions of this document may be illegible in electronic image products. Images are produced from the best available original document.

DISCLAIMER

ACKNOWLEDGMENTS

The project organization is comprised of the following groups:

- DOE — funding co-sponsor
- Babcock & Wilcox (B&W) — prime contractor, project manager and funding co-sponsor
- Dayton Power & Light (DP&L) — host site utility, operations and construction management and funding co-sponsor
- Electric Power Research Institute (EPRI) — testing consultant and funding co-sponsor
- State of Ohio Coal Development Office (OCDO) — funding co-sponsor
- Acurex Environmental Corporation (Acurex) — testing subcontractor
- Utility funding co-sponsors:
  - Allegheny Power System
  - Centerior Energy
  - Duke Power Company
  - New England Power Company
  - Tennessee Valley Authority
  - Cincinnati Gas & Electric Company
  - Columbus and Southern Ohio Power Company

DP&L agreed to be the host utility for the full-scale demonstration of the LNCB, offering the use of J.M. Stuart Station Unit No. 4 (JMSS4) as the host site. JMSS4 is a B&W 605 MW_e Universal Pressure (UP) boiler, a once-through design, originally equipped with 24, two-nozzle cell burners arranged in an opposed wall configuration.

EXECUTIVE SUMMARY

On December 21, 1989, the U.S. Secretary of Energy announced the selection of 13 projects which would further the goals of the Clean Coal III Program Opportunity Notice (PON). In brief, the primary goal of the PON was to conduct cost-shared projects to demonstrate innovative, energy efficient technologies that could be commercialized in the 1990s. Babcock & Wilcox's project to demonstrate the Low-NO_x Cell™ Burner's applicability as a retrofit system to coal-fired power plants was among those selected. A contract award was made and the program was begun on April 1, 1990.

The host site chosen for this work was Unit #4 of the J. M. Stuart Electric Generating Station owned by the Dayton Power & Light Company (DP&L), the Cincinnati Gas & Electric Company, and the Columbus Southern Power Company. The station is operated by DP&L and is located on the Ohio River near Aberdeen, Ohio, which is approximately 60 miles east of Cincinnati, Ohio. The host site consists of four Babcock & Wilcox (B&W) once-through universal pressure boilers, each with a generating capacity of 605 MW_e. Unit #4 was retrofit with Low-NO_x Cell™ Burners (LNCBs) developed by B&W and the Electric Power Research Institute (EPRI).

The goal of the project was to perform the first commercial-scale, full burner retrofit demonstration of this particular technology for utility boilers in the United States. Specific objectives for the project were:

- Demonstrate a 50% reduction in NO_x emissions compared to baseline emission levels with standard burners
- Quantify the NO_x reduction achievable and any impact on boiler operation, performance, and reliability
- Confirm that the LNCB technology is a commercially viable approach for NO_x control on cell burner units

Part of the methodology necessary to accomplish the above objectives was the inclusion of a long-term test task. Following the successful retrofit and burner optimization/characterization tasks, the unit was monitored for an 8-month period. During this time, the unit burned coal from the common coal pile and operated under dispatch per normal system demand and priority. Two primary areas of investigation and documentation took place via the long-term testing: 1) independent monitoring of gaseous emissions at the boiler's economizer outlet section and 2) a corrosion potential evaluation based on hydrogen sulfide (H_2S) exposure of metal parts. The former activity was accomplished through a subcontract with the Acurex Environmental Corporation while the latter was conducted through B&W's Alliance Research Center (ARC).

Services of the Acurex Environmental Corporation were contracted early in the overall program and included involvement in several phases of the planning, testing, and evaluation of boiler performance. Only

those results regarding Acurex's long-term efforts are included in this publication to maintain the report's focus. They can be found in Section 3.

Gaseous emissions of nitrous oxide (N_20) were measured by B&W's ARC both before and after the retrofit to quantify potential changes in the formation of this greenhouse gas as a result of the new system. These results are included in Section 2.

Both a laboratory corrosion evaluation of several alloy types and a field test using an 80-tube wide by 12-foot high corrosion panel were conducted to assess the potential corrosion rate changes which might occur in localized areas of the boiler's waterwalls as a result of the LNCB retrofit. The results of this portion of the long-term task effort are described in Section 3 of this report.

The bulk of this task report is devoted to the results of the corrosion assessment study. As already noted, this work consisted of two major areas of investigation: 1) laboratory scale tests and evaluation and 2) field tests and measurements. In the laboratory tests, mixtures of standard gases were used to expose alloy coupons to simulated boiler gases which contained H_2S levels predicted by sub-stoichiometric combustion chemistry. Three H_2S levels were used. Additionally, in a separate series of controlled laboratory tests, simulated ash deposits were used to cover duplicate metal coupons during the exposure period (1000 hours). The weight and thickness loss rates measured in the laboratory tests were compared with loss rates of the same materials which comprised the field-installed corrosion panel. The tie elements for this comparison were H_2S exposure and metal surface (tube wall) temperature. Thus, both H_2S and temperature were important field-measured variables. It was hoped that field acquired data (for metal loss) plotted according to alloy type (chromium concentration), H_2S exposure level, and temperature would have a high correlation coefficient with the laboratory data curves. Simplified predictive equations could then be used to quantify expected worst-case corrosion rates.

Generally, this effort was successful as maximum metal wastage of the base T2 tube material from the field test panel agreed reasonably well with the corrosion loss of 15 mils calculated from the developed predictive equations. However, understanding how this information relates to the LNCB retrofit is extremely difficult. All boilers are subject to various levels of corrosion and tube degradation problems which are (many times) specific to particular locations in the boiler. These can be due to both water side and fireside operating conditions. It was not a goal of the long-term task effort to quantify the metal loss rates of the furnace walls of the DP&L boiler prior to the retrofit. Therefore, a loss rate associated specifically with the change of burners made in this program cannot be calculated. Only worst-case predictions can be made based on the laboratory and field data obtained. However, it is important to note that rather extensive ultrasonic thickness (UT) tests were performed at several elevations in the boiler both before and after the long-term testing. As well, historical UT data were obtained from DP&L and used for comparative purposes. Generally, the UT data indicated that patterns of boiler tube wastage were unchanged, i.e., there were localized areas with significant loss rates (12 mpy) while most of the tube surface experienced no measurable change (refer to Section 3.3.5 for further discussion). This implies that these localized areas were experiencing exposure to some unquantified level of corrosive combustion gases prior to the retrofit. The degree to which the LNCB installation may have affected localized tube wastage is therefore uncertain. Observations over a more extended time period are necessary (refer to Section 5 — Recommendations).

Test results from the laboratory and the field which compare the capability of various alloys to resist corrosion attack via H_2S exposure are valuable in making economic and functional assessments of these materials for future field application. Presently, a longer term exposure with continued monitoring is needed to increase confidence in the existing data. Also, expanded laboratory work to assess the effect of fluctuations or cycling of both temperature and gas composition is the next step to improving predictive capabilities for boiler tube wastage rates.

Though this report focuses only on the laboratory and field corrosion evaluation activities, the general conclusions provided later in this summary also include some results of the overall retrofit, i.e., actual boiler performance compared to project goals. Through the inclusion of this "extra" information, the reader is given a perspective on the applicability of the technology to the retrofit market as well as a better understanding of the general operation of the boiler during the long-term evaluation test period.

Conclusions describing the general operation of the Low-NO_x Cell™ Burner technology are as follows:

- Data collected by B&W indicated a 55.5% reduction in NO_x emissions compared to baseline test results. These results were measured with the unit at full load with all mills in-service. Measurements of the same operating condition by the independent testing company (Acurex Environmental Corporation) indicated a 53.0% NO_x reduction.
- Furnace exit gas temperatures averaged about 10°F lower than baseline values (standard cell burners) and more importantly, are more even in distribution than baseline operation. As a result, problems with gas-pass pluggage due to bridging of ash deposits at the furnace exit have been reduced or eliminated.
- A small increase in carbon loss representing about a 0.37% average overall loss of efficiency was measured. Half of this loss was regained through a 0.16% increase in average efficiencies caused by lower economizer gas outlet temperatures.
- No change in ash composition was noted in comparing upper furnace ash samples before and after the retrofit. The original cell burners formerly produced a buildup of agglomerated "popcorn" ash on horizontal convective pass tubes. This ash buildup and associated tube erosion has been greatly reduced since the LNCB installation. Also, required maintenance associated with the airheaters, flyash handling equipment, and bottom ash handling equipment has been reduced since the retrofit.

Conclusions made as a result of the long-term task work are as follows:

- From laboratory and field results, predictive equations were developed which appear to be useful in estimating the expected worst corrosion rate of an alloy under a given combustion environment.
- The long-term corrosion panel test in J. M. Stuart Station Unit #4 (JMSS 4) indicates that the maximum metal wastage of SA213-T2 is approximately 21 mils after the 15-month operating period. This wastage rate is equivalent to a corrosion rate of 17 mpy. Based on predictive equations developed during the long-term test task, maximum metal wastage of T2 was calculated to be 15 mpy. These equations based their predictions upon: 1) the metal temperature, 2) H_2S concentration in the flue gas, and 3) Cr concentration in the alloys under the test conditions employed.
- All of the commercial high-alloy steels investigated in this task, including a popular and economical steel — SA213-TP304, appear to possess suitable corrosion resistance to the laboratory mixed gases. Their good performance was also confirmed by the field test. Therefore, the selective use of

chromia-forming alloys in areas of the boiler where chemically reducing flue gases have wall contact should alleviate the corrosion concern of many low-NO_x technologies.

- By contrast, the corrosion performance of carbon and low-alloy steels commonly used in the lower furnace of utility boilers may suffer due to sulfidation attack under reducing combustion gases. Therefore, these materials require surface protection locally in the lower furnace where reducing gases are present. However, high tube wastage was reported prior to the retrofit in JMSS4 where reducing combustion gases were suspected.
- Results of the field test suggest that a chromia-forming coating relatively free of structural defects may be locally applied to the surfaces of waterwalls to combat the above noted sulfidation attack. However, these corrosion resistant materials can be significantly affected by their microstructure integrity. When pre-existing structural defects, such as cracks, pores, and oxide stringers are present, the corrosion attack can proceed preferentially along these sites. As a result, the metal wastage can be much greater than anticipated when the surface coatings are not applied properly.
- Regarding field measurements, an accurate on-line H_2S monitoring system for the interior of a furnace was successfully developed. Also, an on-line system for monitoring levels of H_2S at the test unit's west wall corrosion panel was developed. This system was not considered as accurate as the in-furnace probe system (since some H_2S may have been destroyed by gas-phase reactions within the probe due to a slow quench rate from 1000°F to 300°F).
- In-furnace H_2S monitoring both before and after the LNCB retrofit indicate that there was no significant increase in H_2S levels on the east and north sides of the boiler between 4 and 18 feet into the furnace interior. These measurements were made at the lower burner level in all instances.
- The temporal average H_2S levels on the corrosion panel ranged from less than 20 ppmV (lower left side) to 839 ppmV (upper right side — near the center of the furnace at the lower burner level) during the post-retrofit testing in June of 1992 (prior to burner optimization for lower H_2S performance). As a result of burner optimization work in August 1992, H_2S levels monitored on the corrosion panel were reduced to less than 20 ppmV (limit of gas chromatograph detection) for three of the four corrosion panel sample ports. H_2S levels of 95 ppmV were measured through the fourth (lower right) port.
- Based on March 1993 probing of the same four ports, the benefit of the burner adjustments was observed to be dependant upon many boiler operating factors. Airheater pluggage had occurred which biased air distribution in the boiler's windbox. This altered burner performance with the effect of increasing H_2S along the corrosion panel. Additionally, it was observed that mills out-of-service alter coal/air mixing to the remaining burners and can change H_2S levels near the furnace walls. For instance, H_2S levels in the 500 ppmV range were measured through one of the corrosion port panels (lower right) in March with the burners in their optimized settings but with airheater pluggage occurring. This compares with an H_2S level of 95 ppmV (lower right port) with no airheater pluggage as measured in August 1992. Burner air distribution is considered the primary cause of this disparity.
- Regarding long-term emission monitoring, economizer outlet emissions by Acurex Environmental Corporation show consistent operation with an average NO_x value of 350 ppmV corrected to 3% excess O_2 over the 8-month monitoring period.

In summary, the JMSS 4 retrofit was successful in fulfilling all of its original objectives and is considered an economical and effective technology for obtaining significant (>50%) NO_x emission reduction for existing cell burner equipped boilers.

Recommendations for application of the technology and for future work are listed below:

- Continue the long-term corrosion evaluation effort at the host site (JMSS 4) over the next 3 to 5 outages (~5 years). Removal of about 1 foot of the corrosion panel material across all 80 tubes should be made with corresponding comparison and analyses. Also, in-furnace sampling for H_2S should be made prior to each boiler outage to measure levels of this gas species near the wall.
- Build an improved probe for sampling through the corrosion panel ports. This would likely require a water-quench system and an internal heater for maintaining the sample above the flue gas dew point (~275°F).
- Test for H_2S using coals of different sulfur content to quantitatively characterize the relationship between coal sulfur content and H_2S levels at the furnace walls.
- For future retrofits of the LNCB technology, application of coatings having compositions similar to commercial high alloy steels is recommended for sections of the boiler's waterwalls in localized areas where high metal temperatures and reducing combustion gases are most likely to co-exist.
- Use numerical modeling techniques developed in other phases of this project to aid in locating potential reducing conditions near the boiler waterwalls.
- The techniques used to apply the coatings with minimum defects proved to be important. Therefore, further work is needed to identify not only the alternative materials, but also the coating techniques. This work should also include economic analyses to optimize the selection of the coating process.

CONTENTS

CONTENTS (Continued)

ILLUSTRATIONS

ILLUSTRATIONS (Continued)

ILLUSTRATIONS (Continued)

TABLES

Section 1
INTRODUCTION

1.1 CONTRACT BACKGROUND

The Low-NO_x Cell™ Burner (LNCB) concept was developed by Babcock & Wilcox (B&W) to effectively reduce the NO_x emissions from pulverized-coal-fired boilers equipped with cell burners. These boilers were built mostly in the mid to late 1960s. Small (6-million Btu/hr) and intermediate (100-million Btu/hr) prototype versions of the concept were developed jointly by B&W and the Electric Power Research Institute (EPRI) during the mid-to-late 1980s.[1,2] The design of B&W LNCBs allows direct replacements of the originally installed cell burners without pressure-part modifications. During this U.S. Department of Energy (DOE) Clean Coal III program, Dayton Power and Light Company (DP&L) served as the host utility using its J. M. Stuart Station Unit #4 (JMSS 4) for the first full-scale LNCB demonstration. This unit has a rated output capacity of 605 MW_e.

After the LNCB retrofit and burner optimization contract phases in late 1991, JMSS 4 underwent a long-term (nine months) test period from July 1992 to March 1993. The objective of this test was to determine the overall performance of this boiler after the LNCB retrofit. The long-term test involved determinations of the boiler emission performance and evaluations of waterwall corrosion potential, as well as a study of the overall operability of the LNCB system. Specific tasks performed during this long-term test include:

1) Laboratory corrosion study
2) Field corrosion panel study
3) In-furnace gas species probing
4) Boiler emissions performance study

This report summarizes the long-term test results.

1.2 DESCRIPTION OF LONG-TERM TEST

The long-term test included four major tasks:

1) Furnace gas probing and analysis
2) Laboratory corrosion study
3) Monitoring of boiler emissions
4) Field corrosion test in JMSS 4

A brief description of each task is provided.

1.2.1 Furnace Gas Probing and Analysis

Furnace gas was analyzed by extracting the flue gas with a 28-foot-long water-cooled probe inserted into the furnace through four observation ports located in the lower burner zone. This gas probe traveled parallel to the furnace waterwalls about 12 - 18 inches away from the wall surfaces. The furnace gas was also extracted directly from four 1/2-inch sampling ports located near the corners of a test panel (to be described in Section 1.2.4). The extracted furnace gas was pumped to gas analyzers through heated Teflon tubing. The CO and O_2 concentrations in the combustion gas were determined using CO and O_2 analyzers, respectively, and the H_2S concentration was measured using an on-line gas chromatograph.

1.2.2 Laboratory Corrosion Study

The laboratory corrosion study involved evaluating various alloys and coatings in a B&W test facility under simulated reducing combustion environments. A total of five retort tests were performed, each for 1000 hours. After the tests, the corrosion rates of these materials were carefully measured and their performance was evaluated. Results of the laboratory corrosion study were to serve as the baseline information for the corrosion evaluation and materials selection, as well as for the development of predictive equations.

1.2.3 Monitoring of the Boiler Emissions

The emission performance of JMSS 4 during the long-term test was performed by both Acurex Corporation and B&W. The measurements consisted of continuous monitoring of O_2, CO_2, NO, NO_x, CO, and total hydrocarbons (THC) at the economizer outlet location using heated and unheated grab sample and continuous sample extractive systems. Additionally, B&W performed a comparative analysis of N_2O emissions before and after the LNCB retrofit. Emissions of this gas species were measured at the unit's economizer outlet using an on-line gas chromatograph and sample conditioning system as described in Section 2.4.

1.2.4 Field Corrosion Study

The field corrosion test was performed by installing a 12-foot-long by 80-tube-wide test panel in place of a portion of the west sidewall of JMSS 4 during the 1991 outage. The panel consists of four sections of commercial coatings separated by bare T2 tubing (refer to Appendix A). The test panel, extending from the bottom of the lower cell burner elevation to the top of the lower burner elevation, essentially covered the entire lower burner zone on one-half of the west sidewall (on the half closest to the front wall). Near each corner of the test panel, a 1/2-inch through-membrane sampling port and chordal thermocouples were built in. The sampling ports and thermocouples (TCs) were respectively used to extract the gas compositions and determine the metal temperatures directly on the waterwall surfaces. After a 15-month exposure time in JMSS 4 under low-NO_x operation, the top and bottom segments of the test panel were cut off and sent to B&W for metallurgical analyses and corrosion-rate determinations.

1.3 LIMITATIONS

1.3.1 Probing Accuracy

There were primarily two types of in-furnace probing conducted during the long-term phase of operation. Gas species measured were the same for both types. Only the sample collection technique and location varied. The accuracy attributed to each type of probing changed as a result of the variation in technique, but of even more importance was the variability of the process being measured. Both techniques called for sample gases to be extracted from the combustion zone of coal flames. Thus the composition of the gases were dependent upon mixing rates and ever-changing flow patterns occurring within or very near the flame envelope. Under these conditions it is considered that a sample location change of a few inches could result in significant differences in measured results. However, since overall burner flow patterns tend to remain constant for a stable combustion condition, the goal of the probing (to map H_2S, O_2, and CO gas species along the furnace walls) remained a practical, achievable approach to defining the role of H_2S in fireside corrosion of the various waterwall tube materials.

The first technique used a specially designed, water-cooled probe which was inserted into the furnace up to 18 feet in pre-selected intervals of 2 or 4 feet. The tip of the probe was 12 to 18 inches from the sidewall so that reported levels of the measured gas species are those which existed at that location and not at the gas-tube interface. This measurement location created errors in assertaining the precise quantitiy of H_2S in contact with the tube material at any given time and therefore in the amount of H_2S actually required to cause a measured corrosion rate. Therefore, to obtain a broader perspective on the range of H_2S exposure levels experience by the tubewall materials, a second sampling technique was applied. In this procedure, combustion gases sweeping the tubewalls were drawn from the furnace through openings made between the tubes. Though the measured composition of these gases might be thought to be the most representative of those at the actual gas-tube interface, this may not be the case. If metal-H_2S reactions occur to the extent that the sample gases are affected as they enter the sidewall opening, measured values may be lower than actuals. However, by comparing the measured values from both sampling techniques, a range of H_2S exposure was established which was a valuable tool in the overall corrosion study.

1.3.2 Panel Location

The waterwall test panel was about 12 feet high and 80 tubes wide (approximately 14 feet). This panel was placed on the boiler's west sidewall at the lower burner level. The basis for this placement was from historical plant data on worst-case corrosion experience and on numerical modeling results of CO predictions near the furnace walls (the regions of highest CO were considered to be indicative of H_2S). With the LNCB installation, old furnace flow patterns near the walls could change, leaving a less than optimum panel location. During initial testing performed on both sides of the boiler, it was apparent that the west, or panel side exhibited much higher CO and H_2S values than the east side. Also, since the lower burner level was exposed to the most substoichiometric combustion conditions, the selected panel location was considered to be appropriate. However, localized combustion conditions near the boiler walls could exist which experience greater exposure to potentially corrosive conditions. Only many years of exposure will reveal the location of these areas.

1.3.3 Operating Variation

Though JMSS 4 is a base-loaded unit operating most of the time at a full-load capacity, changes in operation do occur. The extent and frequency of these changes affect the accuracy of any attempt to 1) define localized corrosion rates and then 2) use these rates to predict overall corrosion for various tube materials. Consequently, the results of this study cannot be comprehensively accurate and the reader is advised to consider trends rather than absolute rates when evaluating the report findings.

1.3.4 Corrosion Rate Predictive Equations

Predictive equations were generated based on the results of the laboratory corrosion study. The predictive equations are intended to serve as a means to estimate the metal wastage of alloys exposed to the reducing combustion gases in boilers burning sulfur-containing coals substoichiometrically.

However, it must be realized that the actual boiler environments cannot be totally simulated in laboratory studies. For example, in the present laboratory tests, the alloy and coating samples are exposed to simulated combustion gases without any thermal cycling, mechanical stress, thermal fatigue, and gas fluctuations in composition (oxidizing/reducing) that commonly exist on waterwalls. The addition of these variables often accelerates the corrosion wastage of metals. It is also difficult in the laboratory study to duplicate the actual ash chemistry and thickness condensed on the boiler tube surfaces. On the other hand, the laboratory tests involve exposure of alloy samples to the simulated furnace gases constantly without any compositional variations. In other words, the materials are attacked by the employed environments at their maximum strength during the entire test period, whereas the corrosivity of actual boiler conditions tends to fluctuate, often reduces from its maximum corrosion strength due to many factors, such as partial/full load changes.

As will be seen later, the use of the predictive equations generated from the 1000-hour laboratory data can offer reasonable wastage estimates for SA213-T2, considered here as a baseline alloy, compared to those determined from the test panel exposed in JMSS 4 for 15 months. This agreement may be attributed to the fact that the absence of thermal cycling, mechanical stress, thermal fatigue, and deposit simulation in the laboratory study resulting in reduced corrosion rates is offset by the presence of maximum corrosivity in the mixed gases leading to enhanced corrosion rates. Based on the available corrosion data, it is not clear if these equations can also be used to predict the corrosion rates of alloys after longer-term furnace exposure, i.e., >15 months. Therefore, further field studies are needed to verify the limitation of these equations.

Section 2
TECHNICAL BACKGROUND

2.1 LABORATORY CORROSION STUDY

The presence of sulfur in coal may accelerate the corrosion wastage on boiler components and therefore is one of the major concerns for application of any low-NO_x technologies. Thermodynamic calculations have demonstrated that sulfur in fuels can exist in different forms under different air/fuel stoichiometric ratios.[3] In areas where the flue gas is oxidizing, sulfur can react with oxygen to form predominately SO_2 and some SO_3. However, under reducing conditions, sulfur is primarily converted to H_2S and other condensed sulfides. The formation of H_2S and condensed sulfides is attributed to an increase of sulfur chemical potential (i.e., the partial pressure of S_2) and decrease of oxygen potential in the flue gases. Consequently, higher corrosion rates may occur due to the tendency of sulfide formation on the alloy surfaces.

Alloys for use in high-temperature corrosive environments must possess the ability to form protective corrosion products (or surface scales). A protective scale is defined as the corrosion products formed on the alloy surfaces being resistant to further rapid corrosion attack, resulting in a metal wastage rate decreasing with time, while a non-protective scale permits continuing rapid growth of the corrosion products. Depending upon boiler operation and fuel chemistry, both metal oxides and sulfides may form on boiler tubes as the predominant corrosion products. However, the growth rate of a metal sulfide is, in general, a few orders of magnitude higher than that of the corresponding metal oxide. Therefore, when metal sulfides are expected to form on boiler tubes, such as in reducing zones of boilers burning high sulfur-containing coals, the corrosion rates of the tube alloys may be accelerated.

Because corrosion rates generally increase with increasing sulfur potential (S_2), and the sulfur potential influences the partial pressure of H_2S in the flue gas, the amount of H_2S can be regarded thermodynamically as an indicator of the flue-gas corrosivity. That is, when the H_2S concentration in the combustion gas is high, the flue gas is more reducing and thus more corrosive. In addition, H_2S vapors can serve kinetically as the sulfur-carrying species contributing to the sulfidation processes. B&W's preliminary laboratory tests[4] have confirmed that the corrosion rates of alloys indeed increase with H_2S in simulated reducing combustion gases. Many field experiences have also attributed high metal wastage rates to the existence of reducing combustion gases, resulting from improper mixing of fuel and air in the combustion zone of boilers even under an overall oxygen-excess condition. Consequently, successful employment of low-NO_x technologies that may locally create reducing combustion zones in boilers is likely to require proper control of the metal wastage.

Therefore, the objectives of this long-term test program were to:

1) Gain corrosion information of alloys and coatings useful for boilers equipped with Low-NO_x Cell™ Burners
2) Establish a correlation between the corrosion rates of alloys and coatings with H_2S% and temperature in the ranges practical to LNCB-retrofitted boilers
3) Recommend candidate materials to be used in the lower furnace of LNCB boilers

To extend the corrosion information, the materials data generated from B&W's previous R&D studies pertinent to this low-NO_x program (but not funded by this program) were also incorporated in the data analysis.

2.1.1 Materials Selection

Several commercial steels and high-temperature coatings were chosen for the laboratory retort study. These alloys, readily available commercially as tubing materials, included carbon steel (SA178-A), low-alloy steels (SA213-T2, SA213-T11, SA213-T22, and SA213-T9), and stainless steels (SA213-TP304L, SA213-TP309, SA213-TP310, and SA213-TP321). In addition, Alloy 253MA, considered here as a stainless steel, was also included in the test matrix.

Test coupons of all the commercial alloys were supplied by Metal Samples Inc., Munford, AL, with a typical rectangular sample dimension of ~1 inch x 0.5 inch x 0.125 inch. The coupon surfaces were thoroughly cleaned and degreased prior to the retort tests without further surface polishing.

Two types of iron-base coating materials, designated here as FeCrAl and FeNiCrAl, were also investigated. These high-temperature coating materials are usually available in powder form for thermal sprays. However, test coupons of these materials were prepared from rolled sheets, which were produced as a special order for a previous coating study at B&W. Therefore, these coating alloys were present in the retort tests as "free-standing" materials, i.e., without the existence of an underlying substrate. After cutting, the coupon surfaces were lightly ground on sandpapers to remove cutting burrs.

In addition, three types of coating systems, produced by two coating techniques, were investigated. The coating systems are:

- Al plasma-sprayed on T2
- FeCrAl plasma-sprayed on T2
- Cr/Si co-diffusion coated on T2

Table 2-1 summarizes the chemical compositions of the materials under the laboratory investigation. The Al and FeCrAl plasma sprayed coatings on T2 substrates were produced by ASB Inc., Barberton, OH, using standard commercial coating procedures.

For the Cr/Si co-diffusion coating, the process were carried out by Ohio State University (Professor R. A. Rapp) on T2 substrates using a modified pack cementation technique. The technique involved co-diffusion of Cr and Si into the substrate surfaces simultaneously at high temperatures. The coating process locally "modifies" the chemical composition of the substrate surfaces to contain high Cr and

relatively moderate Si concentrations. Both elements are known to form protective oxide scales at high temperatures, which in turn, may significantly reduce the corrosion rates of the substrates.

Table 2-1
ACTUAL CHEMICAL COMPOSITIONS OF ALLOYS AND COATING SYSTEMS SELECTED FOR THE LOW-NO_x CORROSION TESTS
(in wt, %)

ALLOY	C	Mn	S	P	Al	Si	Cr	Ni	Mo	Cu	Fe
SA178-A[1]	.25	.75	.005	.022	.070	---	---	---	---	---	bal
SA213-T2[1]	.10	.52	.016	.01	.004	.130	.72	.06	.48	.07	bal
SA213-T11[1]	.11	.38	.013	.012	---	.72	1.01	---	.49	---	bal
SA213-T22[1]	.13	.39	.004	.008	---	.25	2.12	.13	.99	---	bal
SA213-T9[1]	.12	.48	.004	.015	.002	.64	9.15	.33	1.0	.11	bal
SA213-TP304L[1]	.01	1.82	.011	.031	---	.48	18.2	8.11	---	---	bal
SA213-TP309[1]	.029	1.80	.001	.022	---	.56	22.28	14.83	.12	.13	bal
SA213-TP310[1]	.06	1.94	.001	.024	---	.68	24.87	19.72	.16	.11	bal
SA213-TP321[1]	.044	1.61	.006	.016	---	.46	17.22	9.85	.14	.10	bal
253MA[1]	.091	.55	.001	.021	---	1.71	20.9	11.0	---	---	bal
FeCrAl[2]	---	---	---	---	---	4.8	---	16.0	---	---	bal
FeNiCrAl[2]	---	---	---	---	4.0	---	17.0	8.0	---	---	bal
Al-sprayed[3]											
T2	---	---	---	---	99 min	---	---	---	---	---	---
FeCrAl-sprayed[4]											
T2	---	---	---	---	6.0	---	27.5	---	2.0	---	bal
Cr/Si co-diffused											
T2[2]	---	---	---	---	---	2-3	30-40	---	---	---	bal

1 Composition certified by the materials supplier.
2 Composition analyzed by EDX.
3 Composition of METCO 54 powder prior to plasma spray onto T2.
4 Composition of METCO 465 powder prior to plasma spray onto T2.

2.1.2 Description of the Laboratory Test Conditions

A total of five low-NO_x conditions were simulated in the laboratory retort tests. The conditions were designed to cover the full range of reducing combustion environments most likely to occur in the lower furnace of LNCB-retrofitted utility boilers. Table 2-2 summarizes the five substoichiometric conditions employed. The major differences among these conditions are in the H_2S concentration and exposure temperature.

According to thermodynamic calculations,(3) the typical H_2S concentration anticipated in the substoichiometric combustion gas in the lower furnace burning high-sulfur Illinois #6 Peabody coal can range from 0.3% to 1.6% (3000 - 16,000 ppm), with the low concentration existing at the tube-metal temperatures and high concentration at the combustion-gas temperature. Note that high-sulfur coals are defined here as those containing a sulfur content $\geq$3 wt.%. As a result, many of the eastern coals, such as the Illinois, Ohio, and Kentucky coals fall in this category. The exact H_2S concentration in the flue gas may be greatly affected by the local air/fuel stoichiometry and mixing process. It should be pointed out that the low

concentration limit of H_2S adjacent to the waterwall surfaces is what dictates the fireside corrosion, not the high concentration away from the waterwalls.

In reality, because equilibrium may not be attained during the dynamic mixing and combustion processes, the actual H_2S concentration in the flue gas may deviate from what is predicted by thermodynamic calculations. To cover the entire range of H_2S% possibly existing in the low-NO_x combustion zone of pulverized-coal-fired boilers, mixed gases containing three levels of H_2S at 0.05, 0.25, and 0.5% (or 500, 2500, and 5000 ppm) were employed in this laboratory study. A mixed gas containing 500 ppm H_2S should simulate the substoichiometric combustion of low to medium-sulfur coals at the metal temperatures.

The test temperatures employed in this laboratory study ranged from 500° to 900°F, portraying the high and low extremes of the tube-metal temperatures commonly observed on the waterwalls of modern utility and industrial boilers. All retort tests were exposed to the conditions in Table 2-2 for a total of 1000 hours.

2.1.3 Description of the Laboratory Test Apparatus

Figure 2-1 illustrates schematically the test system used in the laboratory retort study. The system consists of three major sections in sequence:

1) The gas-supply section
2) The 309SS retort section, located in a high temperature furnace
3) The effluent disposal section

The laboratory reducing mixed gases were prepared in the gas-supply section. Pure H_2S were first blended with a pre-mixed gas containing 17.61% CO_2, 5.39% CO, 0.58% H_2, and 76.42% N_2. The desired mixed-gas compositions were carefully controlled by monitoring the flow rates using two gas flowmeters — one for the H_2S and one for the pre-mixed gas. Three levels of H_2S concentrations, i.e., at the flow rates of 0.5, 2.5, and 5 ml/min, were added to the pre-mixed gas, while the combined flow rate at this point was maintained at 1 liter/min in a gas blender.

After exiting from the gas blender, water vapor was introduced to the H_2S-containing mixed gas. The water vapor was added from a water reservoir through a heated 304SS line, and a constant feed rate of 0.036 ml/min was maintained for all five retort conditions. The addition of a small amount of water vapor only slightly changed the compositions of the H_2S-bearing mixed gas. Table 2-3 summarizes the three H_2S-containing mixed gas compositions entering the gas inlet of the test retort.

The mixed gas was delivered from the front cover of the retort to the back end via a 304SS tube (3/8-inch OD). The gas exit opening was also situated on the front wall of the retort. As a result, the flow direction of the mixed gas inside the retort was from back to front. Such a flow arrangement permitted the mixed gas to be pre-heated to the test temperatures prior to contacting with the alloy coupons.

Partial chemical equilibrium of the mixed gas may have occurred during the pre-heating process. However, the achievement of a true chemical equilibrium was not necessary, as the test system was designed to simulate the actual waterwalls in boilers where, as mentioned previously, the chemical equilibrium of flue gas may not be attained quickly in a dynamic gas flow condition.

Table 2-2
EXPOSURE CONDITIONS OF THE RETORT TESTS
(H_2S)

Test #	vol %	ppm	T(°F)	Hrs
1	0.05	500	500	1000
2	0.05	500	700	1000
3	0.05	500	900	1000
4	0.25	2500	700	1000
5	0.50	5000	700	1000

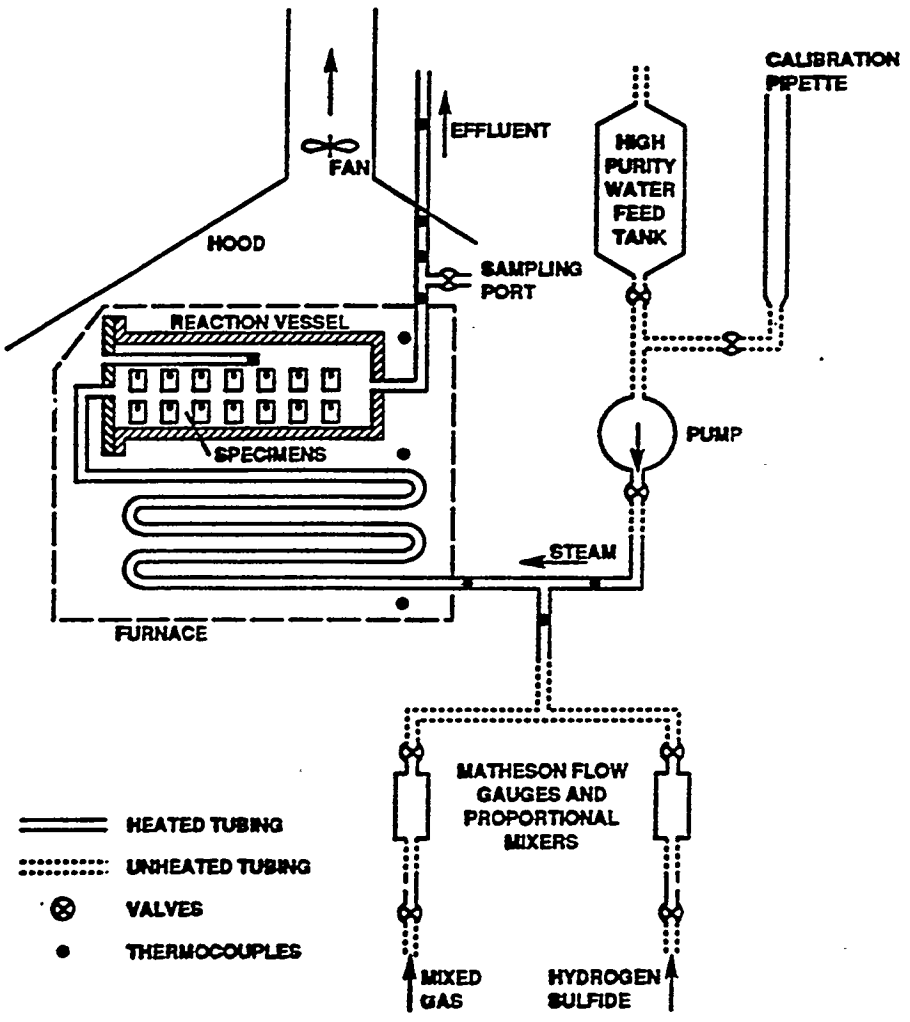

Figure 2-1 Schematic illustration of the laboratory test system employed for the retort study

Table 2-3
MIXED-GAS COMPOSITIONS AT THE RETORT GAS ENTRANCE
(vol.%)

	Initial H_2S Flow Rates (ml/min)		
	0.05	0.25	0.5
Species	Resulting Composition (%)		
CO_2	16.78	16.75	16.71
CO	5.14	5.13	5.11
H_2	0.55	0.55	0.55
N_2	72.82	72.68	72.52
H_2S	0.05	0.24	0.47
H_2O	4.66	4.65	4.64
Total	100.00	100.00	100.00

The effluent disposal section consists primarily of an H_2S scrubber. In the scrubber, a 10% NaOH solution was used to absorb the H_2S exiting from the test retort. After the absorption, the mixed gas was properly diluted with air and vented to the atmosphere.

2.1.4 Ash Deposit Simulation on the Sample Surfaces

The presence of ash deposit on boiler tubes may have profound effects on the tube-metal wastage. Many studies have shown that the presence of ash deposits can noticeably accelerate the corrosion rates of alloys compared to those without the deposits. These types of attack leading to high corrosion rates, commonly termed as "coal ash corrosion", are often found in boilers burning high-sulfur coals. For example, in the conventional utility boilers where the combustion gas is oxidizing, the formation of a sulfate-base deposit on boiler tubes, particularly alkali sulfates and iron trisulfate, is thermodynamically favored. When the sulfate deposit becomes molten at the tube metal temperatures, accelerated corrosion attack can take place by means of complex fluxing mechanisms.[5]

However, on the waterwalls of lower furnace in which the flue gas is expected to be reducing, the formation of a sulfate-base deposit may no longer be possible. Instead, a deposit consisting of other types of reducing combustion deposits, such as alkali sulfides and calcium sulfide, would form and condense on the boiler tubes. While the existence of such a deposit may still affect the corrosion rates of boiler tubes significantly, the exact impacts are not known. Therefore, the alloy performance under low-NO_x environments with the coverage of a reducing ash deposit is investigated in this study.

A simulated coal-ash deposit was synthesized from reagent-grade chemicals for the retort tests. The composition of this deposit was determined from an earlier EPRI-sponsored study[2] based on thermodynamic calculations of a combustion system burning Illinois #6 Peabody coal substoichiometrically. The study evaluated the performance of a 6-million Btu pilot-scale boiler retrofitted with LNCBs. Table 2-4 gives the chemical composition of the simulated deposit employed in this study.

Table 2-4
CHEMICAL COMPOSITION OF THE SIMULATED ASH DEPOSIT

Species	*wt.%*
SiO_2	38
Al_2O_3	16
FeS	19
CaS	18
K_2S	2
Na_2S	1
MgS	1
C	5

2.1.5 Exposure Conditions for the Laboratory Tests

Two exposure conditions were arranged for each material tested:

1) Coupons exposed to the mixed gas only, *without* the simulated deposit in Table 2-4
2) Coupons exposed to the mixed gas *with* the coverage of the simulated deposit

Two alloy coupons of each material were accommodated in an alumina crucible. The crucibles were then separated in a crucible rack positioned inside the retort. Figure 2-2 is a photograph showing an assembled sample rack prior to the retort exposure. Without the knowledge of actual deposit thickness on the waterwalls of JMSS 4, the crucibles containing the alloy samples were completely filled with the mixture. As a result, an average deposit depth of ~1 inch on the sample surfaces was employed. It will be shown that this deposit layer was too thick compared to what was found on the field-tested panel.

To minimize the possibility of any chemical contamination, the crucibles containing the ash deposit were located downstream from the gas flow direction. During the tests, all of the crucibles were covered with flat alumina disks. The flat disks served to prevent the corrosion products formed on the inner surface of the steel retort from falling into the crucibles. However, the crucibles were not tightly covered with the lids to severely hinder the diffusion of mixed gases in and out of the crucibles.

2.1.6 Determination of the Corrosion Rates of Alloys

Prior to the retort exposures, the initial weight and dimension of each of the alloy coupons were carefully measured. After the tests, at least one alloy coupon from each crucible was chemically descaled. Procedures of the chemical descaling process were as follows:

1) The exposed coupons were first immersed in an aqueous solution containing 40 g/l NaOH and 20 g/l $KMnO_4$ heated at 200°F.
2) Following Step 1, the coupon surfaces were cleaned thoroughly with distilled water.
3) Following Step 2, the coupons were immersed in a 5% HCl/inhibited solution heated on a hot plate with the solution temperature not to exceed 180°F.
4) The sample surfaces were wire brushed lightly to remove any residual scales.
5) The samples were rinsed thoroughly in distilled water and the surfaces dried.

Figure 2-2 Photograph of an assembled steel rack containing alumina crucibles prior to the retort exposure

The immersion times are not specified here because they depended vastly upon the types of alloys and corrosion products. In general, chromia-base scales required more immersion time in Steps 1 and 3 than iron oxides and sulfides. Frequent visual examinations of the sample surfaces were necessary to ascertain the optimal cleaning conditions. After the descaling process, the final weights of the exposed samples were again measured. The descaling processes and weight/dimension measurements were carried out by the same technician to minimize any human errors. Based on the weight-change data, along with the original dimension measurements, corrosion rates of the alloys investigated were derived.

2.1.7 Cross-Sectional Metallographic Examination

Cross-sectional metallography was performed on some of the exposed alloy samples. The standard metallographic procedures for the cross-sectional preparation were employed. However, for those samples covered with the simulated ash deposit during the retort tests, kerosine was used as the polishing fluid for the surface preparation so that water-soluble compounds could be preserved. The scale morphologies and their chemical compositions were determined using an SEM equipped with EDX analytical capabilities.

2.2 FIELD TEST AT JMSS 4

A test panel comprised of bare T2, aluminum-sprayed T2, Type 308 weld-overlaid T2, Type 309 weld-overlaid T2, and chromized T2 sub-panels was assembled at B&W. The test panel had an overall dimension of 12 ft long by 80 tube wide and was installed on the west sidewall of Unit #4 close to the northwest corner (i.e., close to the front wall). Several features of the test panel should be pointed out:

1) The panel was installed at the location where severe waterwall wastage had been experienced by DP&L prior to the LNCB retrofit.
2) The length of the test panel covered the lower burner zone in JMSS 4.
3) H_2S sampling ports and chordal thermocouples were built in near the four corners of the test panel.
4) The aluminum-spray coating consisted of an Al concentration ≥99 wt.%, similar to the one in Table 2-1 designed as "Al-Sprayed T2".
5) Types 308 and 309 filler wires were used for the two stainless steel weld-overlay coatings. During the depositing processes, the high Cr concentrations in the filler wires (i.e., ≥20% in the 308 filler wire and ≥24% in 309 filler wire) became slightly diluted with the substrate metal. As a result, a surface composition similar to those of SA213-TP304L and SA213-309 in Table 2-1 was produced from the Types 308 and 309 weld overlays, respectively.
6) The chromized coating was produced by B&W at the R&D center using a proprietary chromizing process. The coating consisted typically of a thick inner diffusion layer and a thin outer chromium carbide layer. The carbide layer contained a very high Cr concentration (>50 wt.% Cr). The total targeted coating thickness was 10 mils, and the coating was accomplished on both sides of the T2 panel segment. However, due to temperature and chemical variations in the coating process, the difference in coating thickness varied significantly (up to 10 mils) along the length of the waterwall tubes.

Unlike the laboratory retort tests, it was not possible to maintain a constant test condition during the panel exposure in JMSS 4. In reality, compositions of the combustion gases adjacent to the panel surfaces would have fluctuated significantly with time. The fluctuations may be attributed, for example, to coal switching and full/partial load variations. Therefore, the gas compositions, gas temperatures, and tube metal temperatures have not only altered with time, but also with the locations of the waterwalls (and thus the test panel).

The monthly average sulfur contents of coals burned during the 15-month panel exposure, as reported by DP&L, ranged from 1.10 to 1.43 wt.%. The overall average of the coal sulfur content during the entire test period was 1.3 wt.%. Using the thermodynamic calculations performed by B&W[3], an average sul-

fur content of 1.3% in coal under an air/fuel stoichiometric ratio of 0.7 would theoretically generate about 0.56% (5600 ppm) H_2S in the flue gas at 2400°F. A higher gas temperature would further increase the H_2S concentration. Again, this amount is based on the assumption of complete conversion of the sulfur to its equilibrium species. On the other hand, when the flue gas is cooled to 500° - 900°F, the H_2S concentration should be thermodynamically reduced to ~0.14% (1400 ppm). A reduction in the H_2S concentration is caused by the formation of condensed sulfides and thus, decreases the available sulfur for the H_2S formation.

In reality, when the flue gas is "quenched" from a gas temperature, e.g., $\geq$ 2400°F, to the tube metal temperature, the H_2S concentration adjacent to the waterwall surfaces would probably be higher than 0.14% due to slow chemical reactions of the flue gas at the low metal temperatures. This is assuming that the combustion gas is equilibrated rapidly at the combustion temperature but not at the metal temperature. On the other hand, if the sulfur in coal is not completely converted to its sulfur-bearing species even at the combustion temperature, the starting H_2S concentration in the flue gas would be less than 0.56% and consequently, the quenched gas adjacent to the waterwall surfaces would accordingly contain less H_2S than 0.14%. Therefore, there is some degree of uncertainty associated with these conflicting scenarios that may affect the actual H_2S concentrations present at the waterwall surfaces. In other words, when the flue gas on the furnace wall is not at equilibrium, the H_2S concentration can deviate from the theoretically predicted value.

2.3 IN-FURNACE GAS SPECIES PROBING

2.3.1 Background

The H_2S concentration in the furnace of JMSS 4 was measured in 1991, while the unit was operating with conventional cell burners.[6] The measured H_2S values were to serve as a baseline or reference against which to later compare post-retrofit values. If a significant increase in H_2S concentrations had been observed after the LNCB retrofit, an increased risk of external corrosion of waterwall tubes would then be expected.

During the baseline measurements, on-line sampling was inherently precluded by the initial design of the sampling probe, which was later modified. The ceramic filter that was fitted on the probe's tip to remove particulates from the sample stream remained effective for, at most, only five minutes. Furthermore, the sampling probe was able to provide exit gas temperatures of, at most, only 100°F to 150°F, whereas approximately 300°F was desired to prevent the loss of H_2S through condensation on the internal probe walls. Finally, the sampling probe warped during usage, thereby making it difficult to retract the probe from the furnace.

Due to the limitations of the sampling probe, an alternative method was employed to measure H_2S during the pre-retrofit tests. Gas samples were extracted from the probe's exit with a gas syringe and immediately injected into the gas chromatograph. At the majority of test points, Drager™ tube measurements were utilized to provide a check. The Drager™ tube is a device which extracts a sample gas and selectively reacts H_2S with chemicals in the tube. A color change in the chemicals is read on the calibrated tube and indicates the measured level of H_2S gas.

During the baseline tests, the highest concentrations of H_2S were found along the west sidewall of the

furnace. Levels of H_2S measured along the north and east walls were less than 20 ppmV, but values as high as 90 ppmV were recorded along the west wall. For the locations measured in the furnace, the west side of the furnace had showed greater potential for fireside corrosion. Because of operational limits related to the probe used for this testing, the actual concentrations of H_2S were determined to be as much as twice the reported values based on calculations of H_2S solubility in condensed flue gas moisture.

From the pre-retrofit measurements it was concluded that a new sampling probe design was required for the post-retrofit tests. Unless a more durable filter was obtained for the probe tip, it would not be possible to perform on-line measurements of H_2S. In addition, the probe's exit gas temperature was to be better controlled, to eliminate any possibility of condensation inside the sample tube. Finally, the probe's structure was to be strengthened, to permit easier retractability from the sampling port.

2.3.2 Post-Retrofit Work

The objective of the post-retrofit work was to measure the levels of H_2S in JMSS 4 subsequent to the change to Low-NO_x Cell™ Burners. There was a need to establish if the retrofit had increased the potential for external tube corrosion. This was to be affected by measuring the post-retrofit levels of H_2S and comparing them with the pre-retrofit values mentioned in Section 2.3.1. In addition, minimizing H_2S levels by adjusting burner settings to achieve optimum performance was considered a milestone of this work.

Among the stipulations placed on the work was that the measurements were to be made at the lower burner level of the furnace, since it would experience the most substoichiometric operation. Figure 2-3 depicts the layout of the sampling positions. The view ports probed in the pre-retrofit work were to be probed again (except for the west port on the north wall, which was inaccessible due to a lack of aspirating air). In addition, ports in a corrosion panel newly placed on the west wall of the boiler were to be probed. With the view ports, various depths in the furnace were to be probed, whereas with the corrosion panel, only the plane of the furnace wall was to be probed.

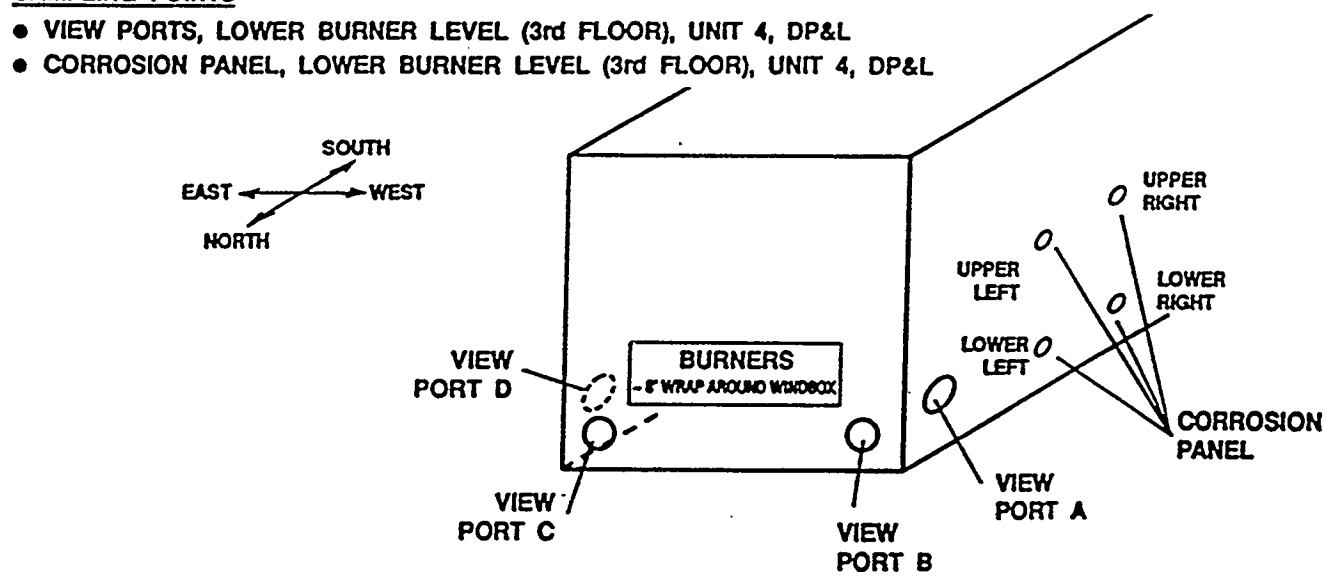

Figure 2-3 Sampling positions for on-line H_2S monitoring

Another stipulation on the post-retrofit work was that the accuracy of the measurements was to be improved, relative to the pre-retrofit efforts. In the pre-retrofit work, the measurements were merely order-of-magnitude measurements. Substantial improvement in accuracy was expected in the post-retrofit measurements.

2.3.3 Sampling System

2.3.3.1 Background. Sampling at the prescribed locations had certain ramifications on the sampling system. There was a large number of points to be probed through the view ports. Furthermore, probing the corrosion panel required the use of a severely constricted port. Following are some of the stipulations placed on the sampling system:

1) Sample extraction through a 3-inch view port as well as a 3/4-inch corrosion panel port
2) Fast turnaround of data points
3) Filtering of the sampling probe to prevent down-time induced by system pluggage

Performing the measurements accurately, imposed further stipulations on the sampling system:

4) Quenching of reactions. To avoid possible loss of H_2S by reaction with stainless steel lines, the sampling system temperature was to be maintained below 1000°F.
5) Prevention of condensation. To avoid possible losses of H_2S by its dissolving in the condensate, the sample stream was to be maintained above approximately 300°F.
6) Replication. Replicate measurements were to be made to confirm that the data were representative.
7) Redundancy. An additional test was to be utilized, to provide, at minimum, a qualitative check on the obtained H_2S data.

The resulting system was an on-line sampling train (see Figures 2-4a and 2-4b). Gas samples were extracted and maintained at approximately 300°F as they were transported to a gas chromatograph (GC), an O_2 analyzer, and two CO analyzers (low CO and high CO). For the view ports, the furnace gas was continuously extracted with a water-cooled probe which was designed to filter, quench, and maintain the gas at approximately 300°F. For the ports of the corrosion panel, the extraction was performed using a 3/8-inch stainless steel tube.

The sampled gas was transported from the respective probes to analyzers through filtered heated lines. The primary analyzer consisted of a GC which periodically provided quantitative H_2S and qualitative COS and SO_2 concentrations. Since H_2S and O_2 levels should have been inversely correlated, whereas H_2S and CO levels should have been positively correlated, simultaneous O_2 and CO readings were made with continuous analyzers as a check on the H_2S readings.

2.3.3.2 View Port Sampling Probe. The function of the view port sampling probe was to extract and quench gas samples from the interior of the furnace and provide clean, hot gas to be transported to the analyzers. The general stipulations placed on the sampling system had several implications on the sampling probe design. Following are some of the major capabilities that the sampling probe had to possess:

1) Sustained sampling. In order to minimize turnaround time between data points, the probe had to be capable of operating in the furnace for long periods of time. Consequently, the furnace could be traversed without stoppage for probe repair.
2) Durability in the 3000°F environment of the burner zone.
3) Accessing of 18 feet of the furnace's interior (after passing through the 8-foot windbox).
4) Facility of insertion and retraction through the 3-inch opening of the view port.
5) Filtering of the sample stream at the probe tip to remove particulates.
6) Quenching of the sample gas immediately (to prevent further gas phase reactions that could change the H_2S concentration), but not to temperatures below 300°F.
7) Maintenance of a wall temperature of below 1000°F for sampling tube, to prevent H_2S reactions with hot stainless steel.
8) Maintenance of the sample gas temperature at approximately 300°F through the entire length of the sample probe.
9) Safety.

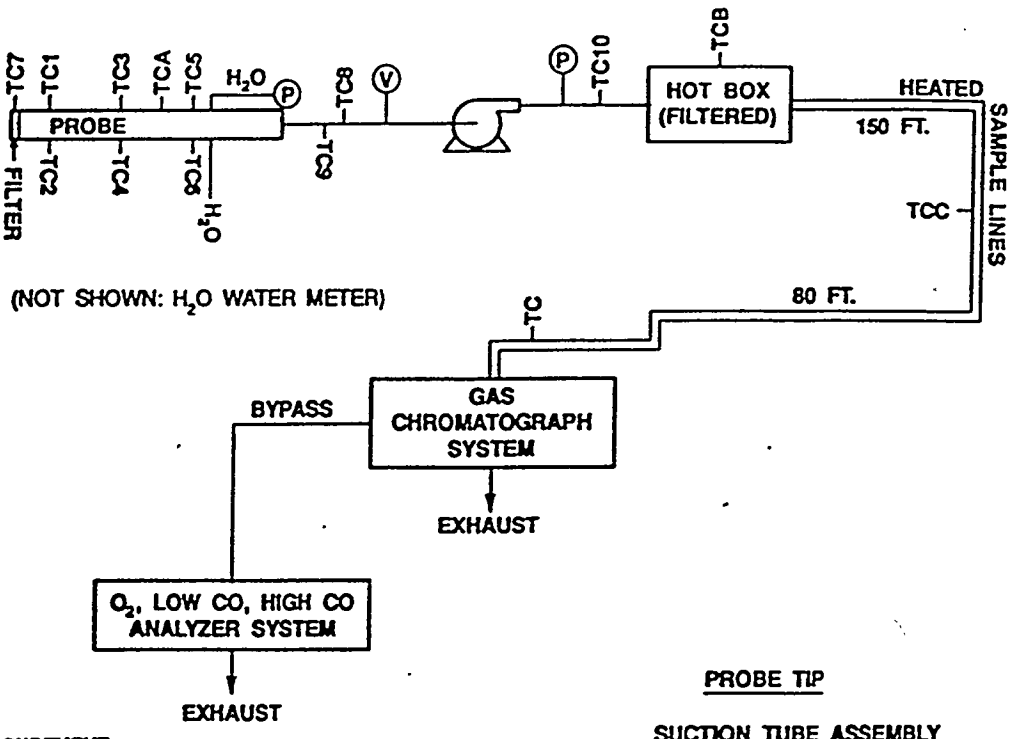

THERMOCOUPLE	MEASUREMENT
TC1	SUCTION INLET GAS
TC2	SUCTION INLET WALL
TC3	SUCTION MIDDLE GAS
TC4	SUCTION MIDDLE WALL
TC5	H_2O INLET
TC6	H_2O OUTLET
TC7	PROBE INLET WALL
TC8	PROBE-TO-PUMP HEAT TAPE
TC9	SUCTION OUTLET GAS
TC10	PUMP-TO-HOT BOX HEAT TAPE
TCA	SUCTION HEAT TAPE (ARBITRARY POSITION)
TCB	HOT BOX TUBE OUTSIDE
TCC	INTRA-SAMPLE LINES GAS
TC	GC GAS

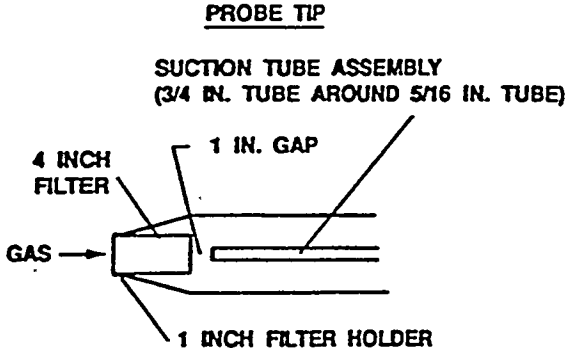

Figure 2-4a Sampling train for on-line H_2S monitoring — view ports

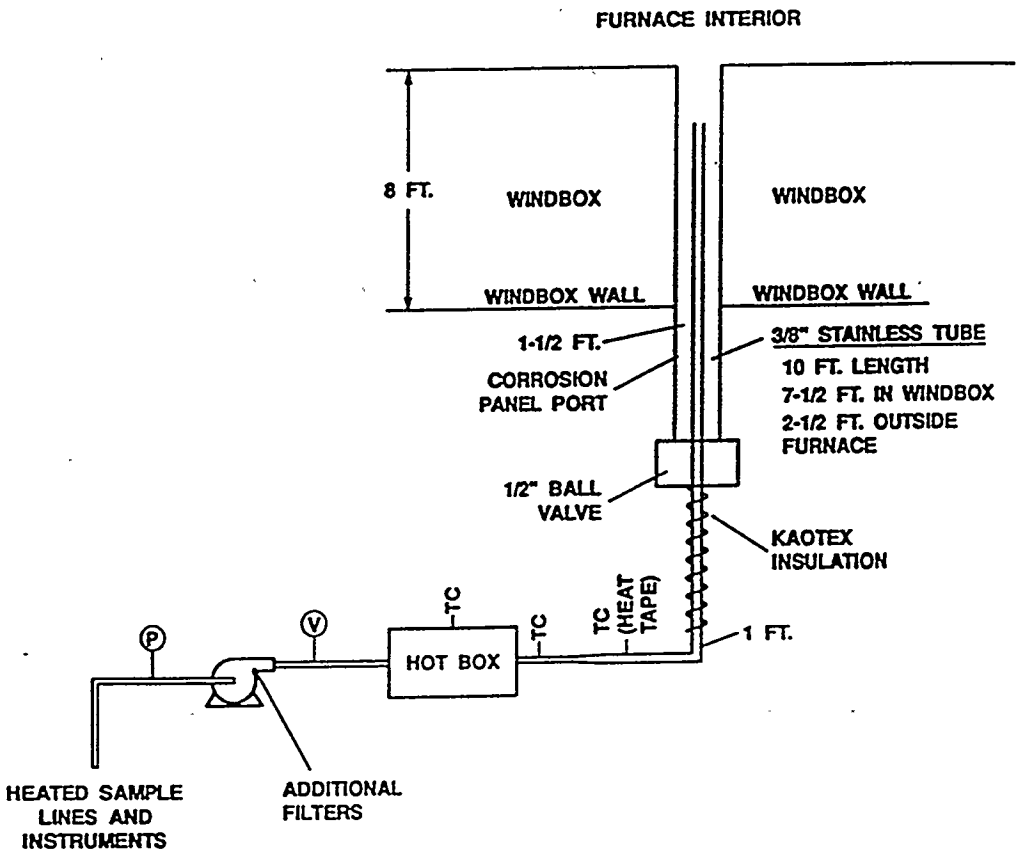

Figure 2-4b Sampling train for on-line H_2S monitoring — corrosion panel

The probe design effort consisted of three steps. The first step was the selection of a 27-foot high-velocity thermocouple (HVT) probe as a reference probe. The second step was the modification of the HVT probe to obtain a prototype H_2S sampling probe. The final step was the modification of the prototype to obtain the sustained-sampling furnace probe (SSFP).

In May 1992, the prototype H_2S probe was designed and tested under actual field conditions. The purpose of the test was to determine the changes that needed to be made to the prototype H_2S probe before its utilization for actual sample measurements in June 1992. The prototype had been designed to address three problems associated with previous probes:

1) Short useful life of the probe tip's filter (5 minutes)
2) Low sample gas temperatures at the probe's exit (maximum of approximately 100° to 150°F)
3) Probe warpage upon insertion in the furnace (irrectractable from the furnace)

Preliminary as well as in-furnace feasibility tests were performed to evaluate the prototype probe. The probe was inserted in the north port of the east sidewall, at depths of 3 feet and 16 feet into the furnace. At each sampling point, the sample stream's temperature was monitored at various positions within the probe. Due to problems with the 220V power supply, however, the sample stream's heating was achieved using an off-design 110V power source (which could thwart the attainment of high sample temperatures at low depths).

The filter at the prototype probe's tip was still quite viable even after 43 minutes of utilization in the furnace. Furthermore, the readings indicated that sample gas temperatures of approximately 300°F could be achieved, even with the lower rating of the 110V power supply. Moreover, the probe did not display any deflection when retracted from the furnace.

It was thereby concluded that the sampling probe was generally adequate for H_2S sampling. Nevertheless, it was determined that the prototype should be refined by encasing the heated suction tube in a protective steel tube. This would provide extra protection against any probe water jacket leakage and afford better seal against air leaks into the probe.

The sustained-sampling furnace probe is depicted schematically in Figure 2-5. The SSFP was a 27-foot long probe made of stainless steel with an outside diameter of 2-1/2 inches. The probe comprised an electrically heated sample jacket fitted retractably inside a water-cooled protective jacket. The SSFP was thoroughly instrumented with thermocouples to monitor the relevant temperatures. Furthermore, ground-fault interrupters were incorporated into the electric heating system as an additional safety measure.

The SSFP consisted of an assembly of five concentric tubes, fitted with a filter tip. The innermost tube was a heat-taped sampling tube. This tube was welded inside another tube to form a heated sample jacket. The heated sample jacket fitted retractably inside a double-tubed cooling water jacket. The water jacket was lined with a ribbing.

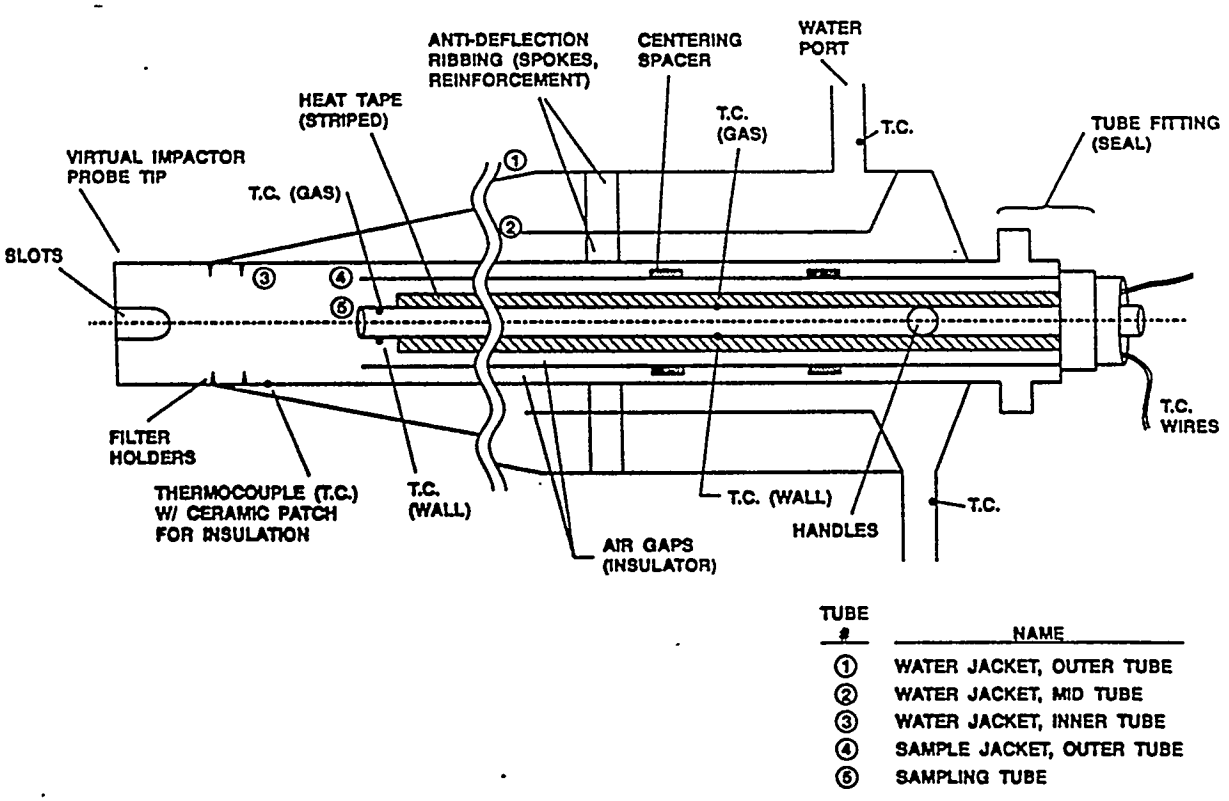

Figure 2-5 Schematic of the sustained-sampling furnace probe (SSFP)

The impactor filter tip on the SSFP, shown in Figure 2-6, possessed two significant attributes: the filter was oriented to make the probe's tip concave, and the filter rested inside the probe (protruding only about 1/8 inch). The filter acted as an impactor that successively decreased the maximum particulate size that remained in the gas stream. The larger particulates were hurled to the closed end of the filter, while the gas streamlines turned and penetrated the sides of the filter. Furthermore, the filter's concave positioning substantially increased the filter's useful surface area.

Meanwhile, the filter remained cool because it rested inside the water-cooled probe. A thermocouple mounted inside the stainless steel tube wall at the probe's tip indicated a wall temperature that ranged from 200° to 300° F. The low tip temperature increased the filter's life, as the filter was still functioning even after over 2.5 hours of continuous usage. The coolness of the probe's tip also aided sample gas quenching. The sample gas was able to quench to approximately 300°F, at a position less than 1 inch downstream of the filter.

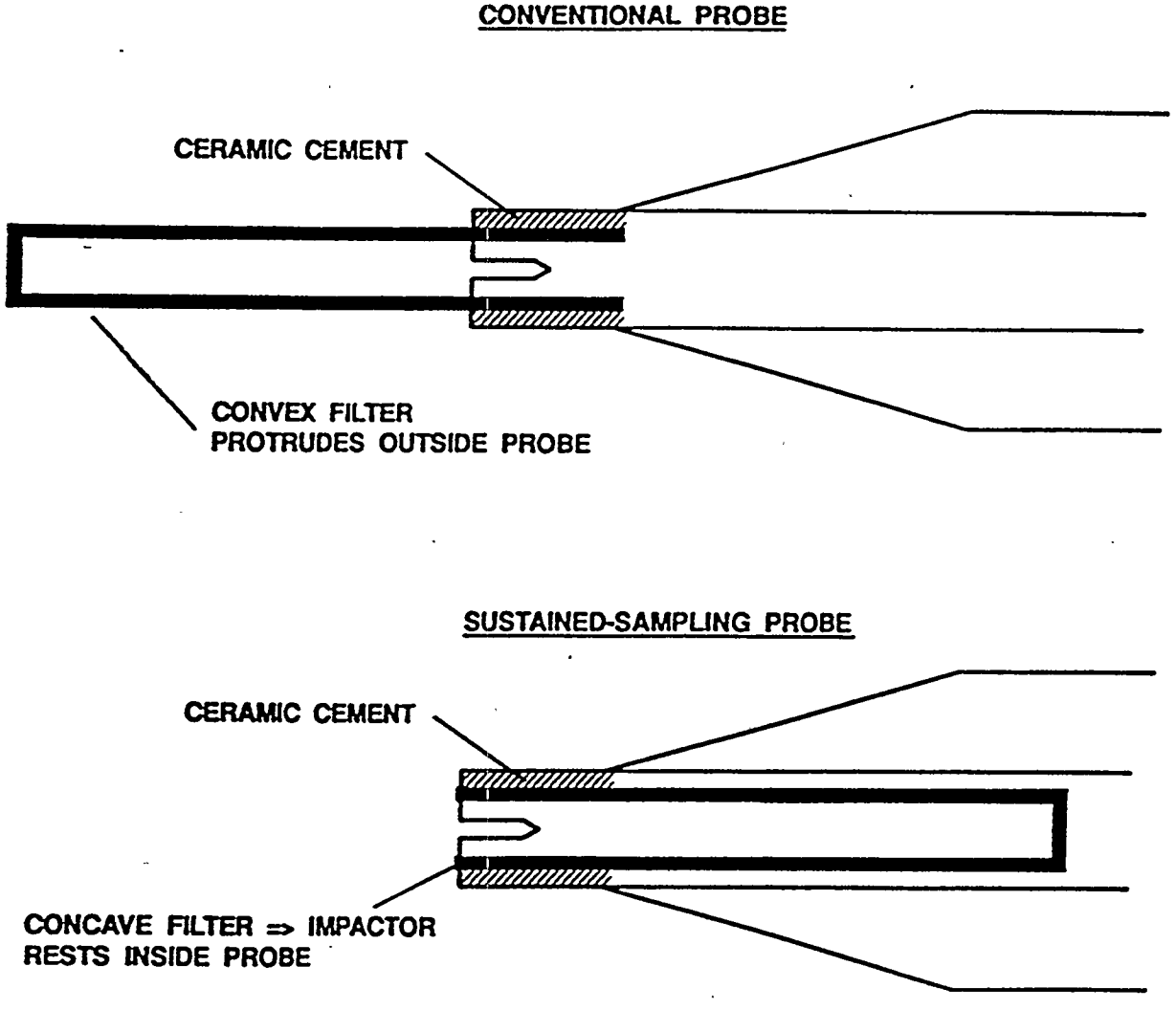

Figure 2-6 The impactor filter tip

The post-quench temperature history of the sampled gas could be controlled by the following:

1) Adjusting the distance between the end of the filter and the entrance of the heated sample jacket
2) Adjusting the power output of the sampling jacket's heat tape
3) Adjusting the water jacket's cooling water flow rate

From the probe's tip, the sample stream was drawn into the sample jacket. The sample jacket contained heat tape that compensated for sample stream heat losses induced by the surrounding water jacket. The sample jacket could attain very high temperatures due to the fact that an air gap, not a solid, was used as insulation. Thermocouples placed at the inlet, midsection, and outlet of the sample jacket indicated that tube wall and gas temperatures of approximately 300°F could be achieved by powering the heat tape with a 110V power supply (the utilization of a 220V power supply would have provided an even greater range of temperatures but was precluded by the lack of an adequate 220V ground fault breaker).

The structural integrity of the SSFP was maintained by the incorporation of the probe anti-deflection ribbing, as depicted in Figure 2-7. The ribbing was formed in the annuli of the probe's cooling water jacket and was analogous to miniature I-beams inside the annuli. The ribbing consisted of pieces of solid material that fit tightly in the annuli's radial direction. These were 1/4-inch diameter rods of weld material, as preliminary calculations suggested that the smaller the length (in the probe's axial direction) of each insert, the greater the reinforcement. The rods were built up on the inner tube of each annulus of the sampling probe and filed down in order for the outer tube to slip over them. Furthermore, each piece of solid extended only slightly in the axial and circumferential directions of the probe. At each axial position, as few as three evenly-spaced insert solids were adequate.

The probe anti-deflection ribbing reinforced the sampling probe and reduced its deflection substantially. No bending of the probe was evident even after several hours of use. In fact, the SSFP was still easily retractable from the furnace after almost 7 hours of use.

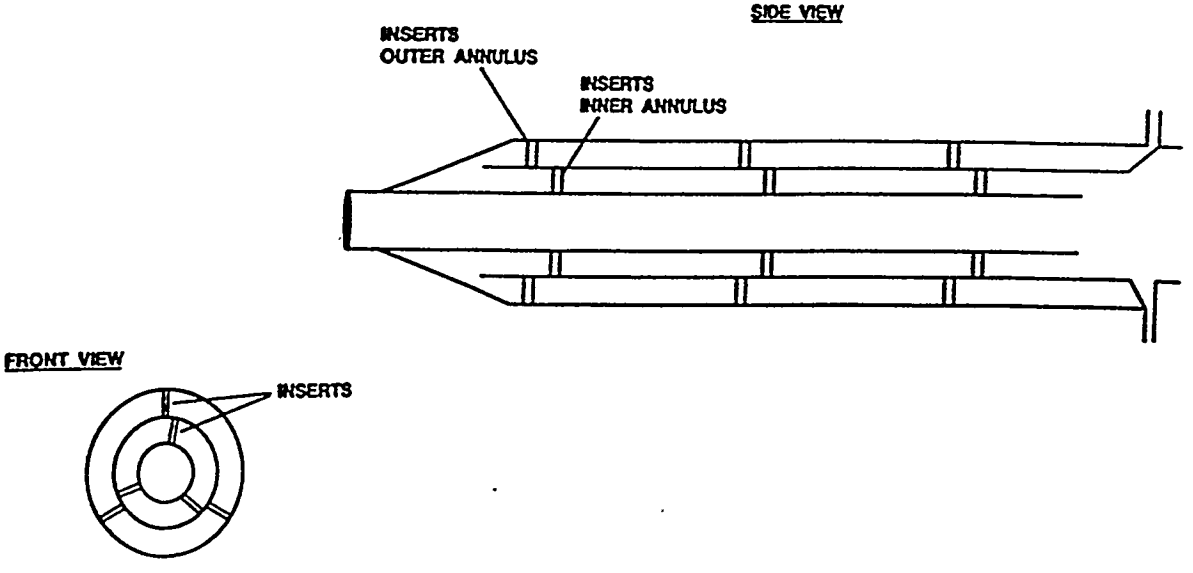

Figure 2-7 The probe anti-deflection ribbing

2.3.3.3 Corrosion Panel Sampling Probe. Ideally, the stipulations on the corrosion panel sampling probe would have been identical to those on the view port sampling probe (except for the lower ambient temperature). To achieve a determination of gas composition at the metal surface of the wall tubes, extraction of gas samples sweeping the wall were needed. Therefore, a mobile, water-cooled probe was not fabricated. Rather, a vacuum pump was used to pull gases from the furnace (see Figure 2-8). This arrangement presented some limitations compared to the probe design used for viewport sampling, but no significant compromise in data quality occurred.

The view port probe was not only used to extract gas samples from the furnace, but it was also used to filter and quench the gas samples. Quenching and filtering capabilities in the corrosion panel probe were, however, precluded by the small diameter of the corrosion panel's ports (3/4 inch). Three-quarters of an inch was just too small to fit a probe with a water jacket or a conventional filter.

Another difference between the two probes was the sampling location of their utilization. The view port probing had targeted the interior of the furnace. In contrast, the corrosion panel probing was restricted to the furnace walls.

For the above reasons, the major requirements on the corrosion panel's sampling probe were the following:

1) Able to be designed and constructed in the field within a few hours
2) Easily inserted and retracted through the 3/4-inch opening of the corrosion panel's ports
3) Maintenance of a wall temperature of below 1000°F for the sampling tube, to prevent H_2S reactions with hot stainless steel
4) Maintenance of sample gas temperatures of approximately 300°F through the entire length of the sample probe
5) Safety

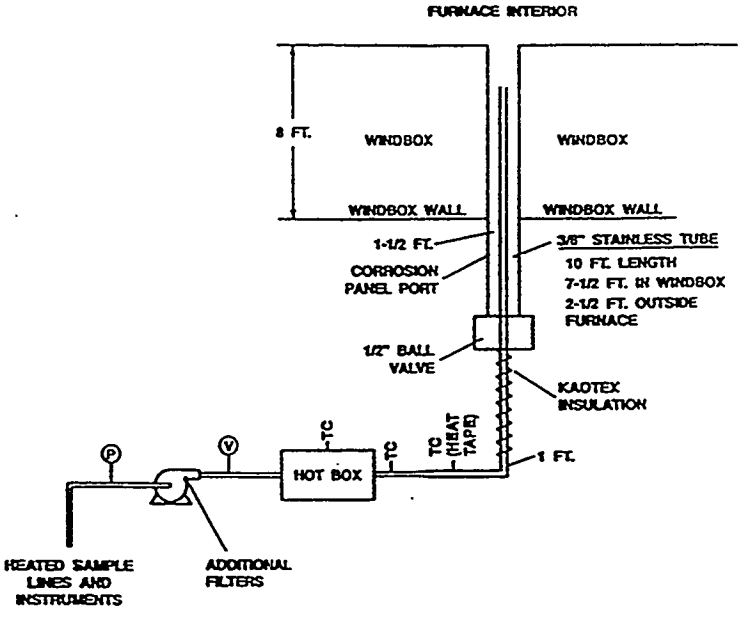

Figure 2-8 Schematic of the corrosion panel's sampling probe

The corrosion panel's probe consisted of a 10-foot length of 3/8-inch stainless steel tubing (see Figure 2-8). There was not enough space to place a filter on the probe. Consequently, the sooty material in the sample stream was filtered out downstream of the probe. Similarly, the probe could not be provided with quenching capabilities, because of spatial constraints. Moreover, the probe could not be thoroughly heat-taped. Therefore, the probe merely had its last one foot wrapped with insulation.

During sampling, the probe was inserted in the corrosion panel's port, until it was 6 inches from the furnace. The corrosion panel's port was a 3/4-inch pipe, 18 inches of which extended outside of the boiler. At the end of this pipe was a 1/2-inch ball valve. When the probe was placed inside the port, the sampled gas temperature was already below 1000°F at the probe's inlet, and it continued to decrease along the probe. Unlike the SSFP, the corrosion panel's probe was not instrumented to enable a thorough monitoring of temperature. However, the probe was thoroughly heat-taped on all surfaces outside of the port entrance. Since the port extended through the boiler's 8-foot wrap around windbox, its temperature was held steady at about 600°F. No loss of H_2S due to condensation could occur. However, reaction with the stainless steel probe surface was possible, though this was compensated for using pre- and post-test calibration data through the entire system to correct any suspected losses.

2.3.3.4 Sample Lines. The purpose of the sample lines was to transport clean, hot gas from the sampling probes to the gas chromatograph and the CO and O_2 analyzers. The gas at the exit of the probe was at 300°F, and it was the function of the sample line to maintain this temperature. The sample line was also supposed to filter the gas flow to remove any remaining particulates, to avoid damage or interference with the analyzers.

The sample lines for the view port and corrosion panel differed from one another, because of the filtering requirements. The view port sample line had little particulates loading to process, since the filter at the probe's tip had already removed the particulates. The corrosion panel's sample line, on the other hand, had a tremendous particulates loading, due to the absence of a filter from the corrosion panel's probe.

- **View Port Sample Line.** The sample line consisted of a few major pieces of equipment connected by heated or insulated tubing (see Figure 2-4a). The sampled gas was drawn from the exit of the probe through a few feet of heat-taped tubing. The sampled gas was drawn into the vacuum end of a stainless steel, dual-head pump. Subsequently, the sample stream was forced from the pressure side of the vacuum pump through another several feet of heated tubing. The sample stream entered a heat-blanketed hotbox, whose purpose was to filter the sample stream. Connected to the outlet of the hotbox was a 150-foot, 3/8-inch Teflon heated sample line. After passing through the 150-foot heated sample line, the sample gas passed into an 80-foot Teflon heated sample line. The second heated sample line transported the gas stream to the GC. At the GC, a small amount of gas was accepted, and the rest was by-passed. The by-passed sample was cooled in an ice bath to drop out water, before being passed to the gas analyzers. These gas analyzers measured the O_2 and CO content of the sample stream.

- **Corrosion Panel Sample Line.** The corrosion panel's sample line differed from the view port's in only two respects (see Figure 2-4b). First, the positions of the pump and the hot box were inverted, to protect the pump from a high exposure to the sooty material in the sample stream. Secondly, an extra filter was placed on the pump, as the filtering capabilities of the system were too low without it.

2.3.3.5 Gas Analyzers. Gas samples were transported for analysis through the Teflon heated sample lines of the sampling train to instruments housed in an air-conditioned trailer. H_2S was measured by a gas chromatograph equipped with a flame photometric detector. Concurrently, a portion of the gas stream was directed to continuous Beckman O_2 and Beckman CO analyzers for analysis.

Connected to the Teflon heated sample line of the sampling train was a 1/4 inch OD stainless steel sample line (see Figure 2-9). The stainless steel sample line was wrapped with heat tape to maintain a gas temperature of 300 ±10°F. The stainless steel sample line was also fitted with a "tee" and a valve to direct the majority of the gas sample flow through an ice bath (to remove condensates) and to the O_2 and CO analyzers.

The valve was adjusted to maintain a gas sample flow rate (as measured by the flowmeter on the vent side of the GC) of 75 ml/min through the six-port gas sample valve inside the GC. An in-line stainless steel filter was installed in the heated sample line to prevent any particulates from entering the GC. To measure the temperature of the gas sample entering the GC, a sheathed thermocouple was installed in the heated sample line. Subsequent to analysis but prior to the flowmeter, the gas stream had its moisture removed in an ice bath.

- **Gas Chromatograph (GC).** The GC used to quantify H_2S levels was a Varian Model 3400 equipped with a flame photometric detector maintained at 230°C (446°F). Nitrogen carrier gas at 30 ml/min flowed through a 30 inch x 1/8 inch OD Teflon (FEP) column packed with Porapak QS 80/100 mesh maintained at 60°C (140°F). This column provided greater sensitivity to H_2S than the column utilized during the pre-retrofit tests.

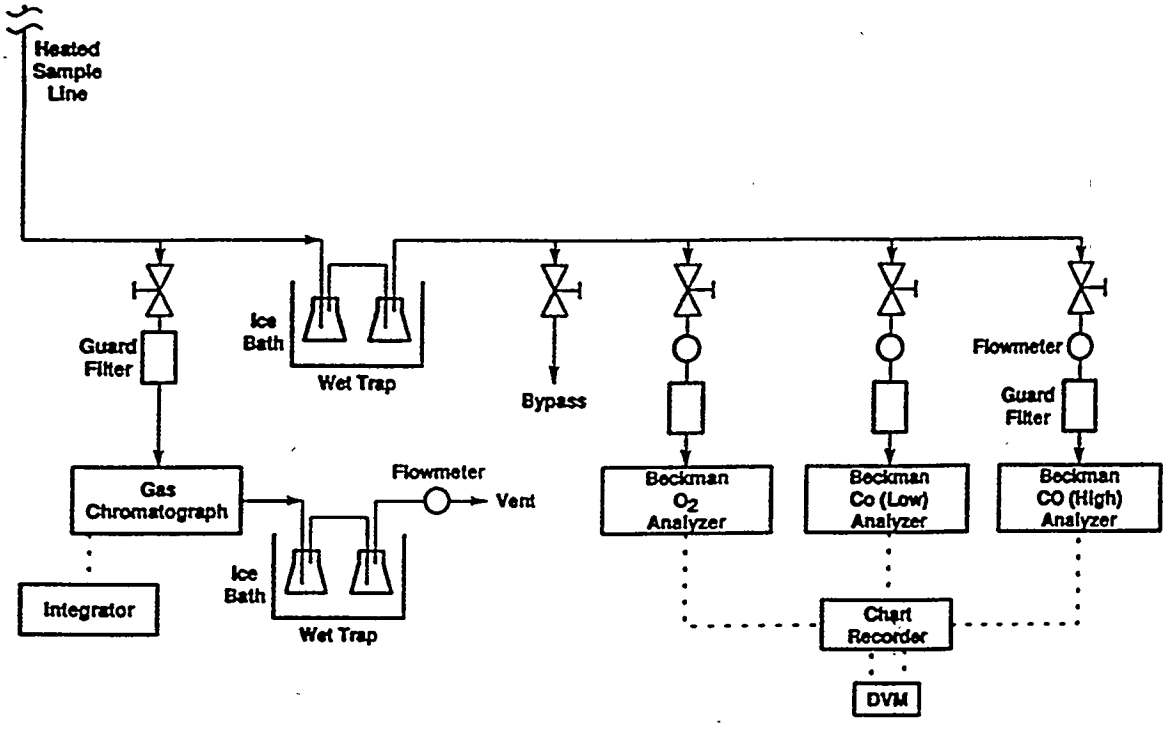

Figure 2-9 Schematic of the gas analyzer system

The GC's H_2S sampling system consisted of a four-port gas valve connected to a six-port gas valve. A selector switch handle for the four-port H_2S gas sample valve, located on top of the GC, was used to specify whether an analysis gas sample or a calibration gas standard was injected onto the column. When the selector switch handle was pointed to stream select position 1 (see Figure 2-10), the analysis gas sample flowed from the left front injection port located on top of the GC (as viewed from the front of the GC) through the constant volume (0.075 ml) sample loop and was injected onto the column. In stream select position 2, the calibration gas standard flowed from the right front injection port through the constant volume sample loop and was injected onto the column.

- **Gas Chromatograph (GC) Calibration.** The GC was calibrated for H_2S using N.I.S.T. traceable or primary bottled gas standards (Airco Specialty Gases, Riverton, NJ) in the concentration range of 10 to 500 ppmV. During calibration, the gas standards were delivered to the GC through unheated 1/4-inch OD impolene tubing at a flow rate of 75 ml/min through the gas sample loop. The calibration commenced with the highest-concentration H_2S gas standard and continued with standards of progressively lower H_2S concentration. Consequently, fewer injections of gas standard were required before the detector response equilibrated.

A typical calibration curve for hydrogen sulfide is shown in Figure 2-11. The relationship between concentration and detector response follows an exponential law, which is typical of the flame photometric detector.

- **Sample Stream Analysis.** Although H_2S was the sulfur compound of analytical interest and its retention time was only 0.9 minute, the analysis time between chromatographic runs was 5 minutes. This extra length of time was necessary in order to allow COS and SO_2, if present, to elute from the column before injecting another gas sample. Figure 2-12 shows the chromatogram obtained when H_2S, COS, and SO_2 were present.

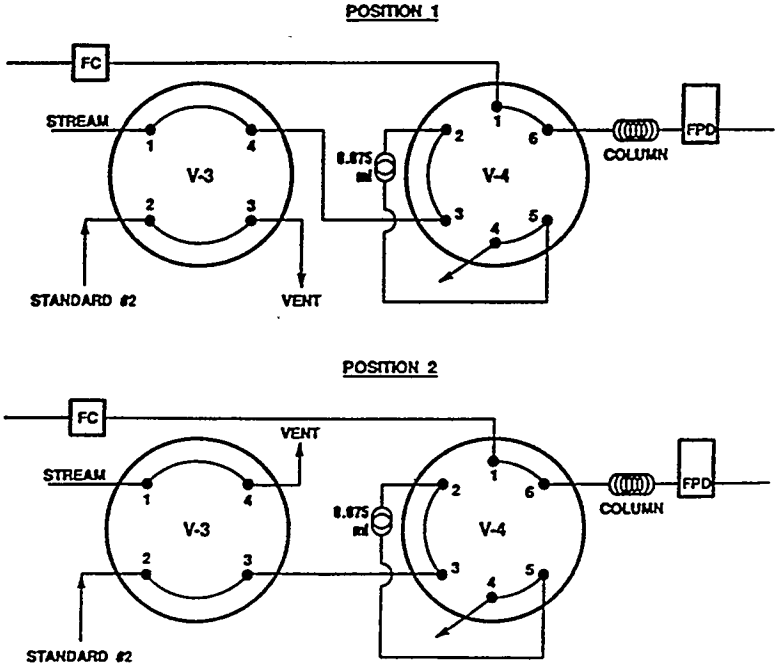

Figure 2-10 Schematic of the gas chromatograph's stream-select valves for H_2S analysis

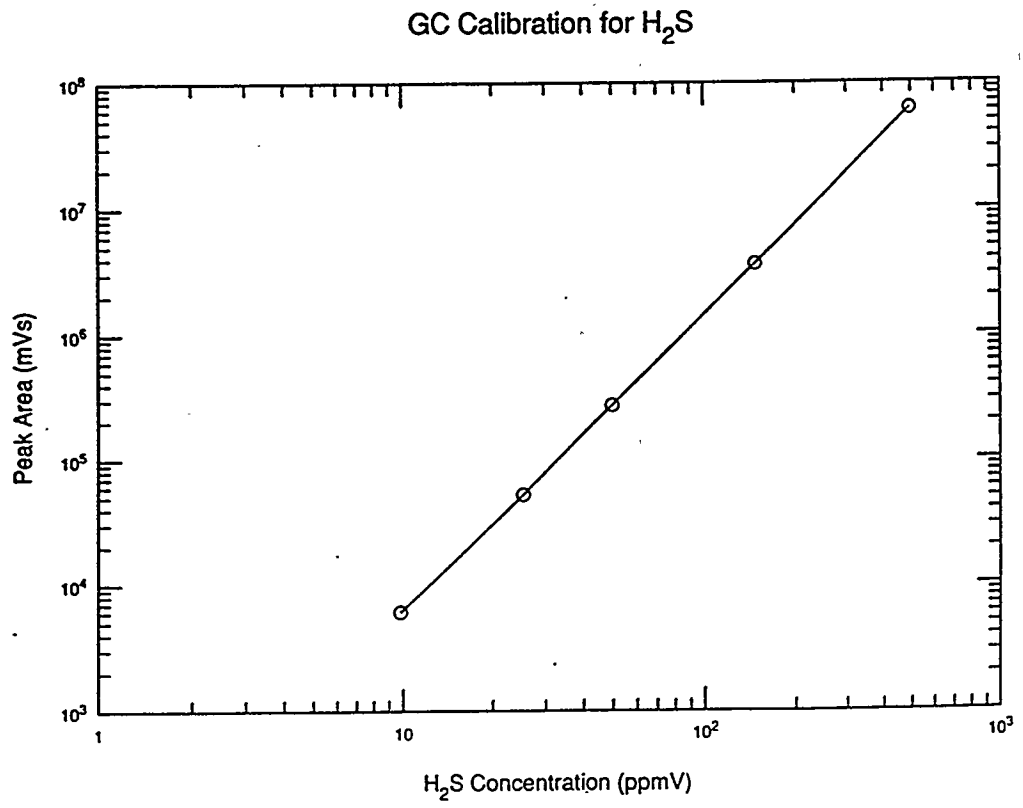

Figure 2-11 Typical gas chromatograph calibration curve for H_2S measurement

2.3.4 Sampling Procedure

Gas samples were extracted and maintained at approximately 300°F as they were transported to a GC for H_2S analysis. Simultaneous O_2 and CO readings were also made to validate the H_2S measurements. For the view ports, gas samples were extracted with the SSFP, which was designed to filter, quench, and maintain the gas at approximately 300°F. For the corrosion panel ports, the extraction was performed with a 3/8-inch stainless steel tube that laid within a 3/4-inch carbon steel support pipe which extended about 8 feet through the windbox.

The sampled gas was transported from the respective probes to analyzers through filtered heated lines. The primary analyzer consisted of a GC which provided quantitative H_2S and qualitative COS and SO_2 concentrations. Since H_2S and O_2 values should have been inversely correlated and H_2S and CO values should have been positively correlated, simultaneous O_2 and CO readings were made with continuous analyzers as a check on the H_2S readings.

Following is the list of steps of the sampling procedure for the view ports and the corrosion panel, respectively. This procedure also constituted the means of attaining quality assurance. In this procedure, emphasis was placed on the calibration of the total integrated sampling system at the same conditions as was observed during the actual sampling. Without such an integrated-system calibration, the interpretation of the signal levels generated by the GC became impossible. The GC's signal levels were sensitive to the inlet conditions of the sample supplied to the GC, i.e., temperature and pressure.

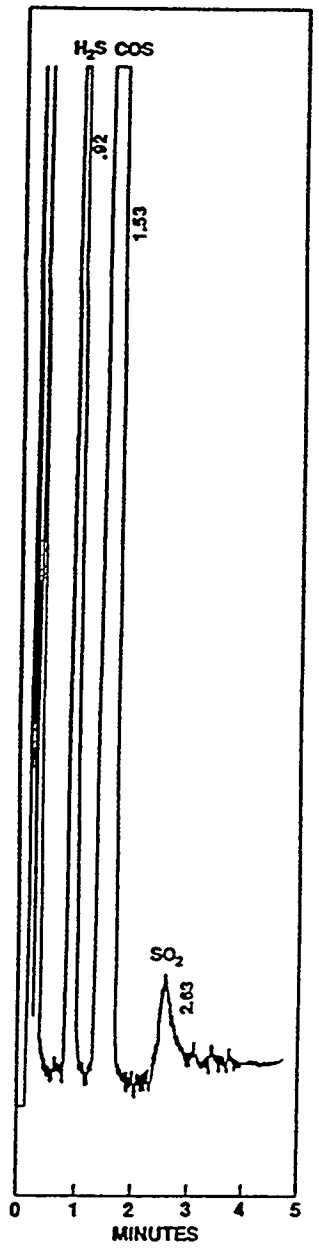

COLUMN: 30" x 1/8" TEFLON (FEP)
PACKING PORAPAK QS, 80/100
TEMPERATURE: 60°C
FLOW RATE: NITROGEN, 30 ml/min

Figure 2-12 Typical chromatogram of a furnace sample stream

2.3.4.1 View Ports.

1) Connect all appropriate lines and equipment — Ensure that probe tip's filter extends out only 1/8 inch. Also, ensure that the first 1/8 inch of the filter is coated with ceramic adhesive (cement).
2) Residence time check — After every major change of sample lines, determine length of time for sample to travel through system.
   - Purge system with H_2S - N_2 mixture until O_2 analyzer reads 0%
   - Unhook H_2S - N_2 and allow ambient air to enter through fixture at probe tip
   - Monitor O_2 level until it reaches 21%

   NOTE: System should be at ~300°F, and dual-head pump should be set at full capacity
3) Precalibration — Before probing a particular port, a precalibration should be performed (until such a point as it is established that precalibration values are reproducible; even then continued precalibration serves as a leak check).
   - As usual, maintain system at 300°F
   - Turn on pump to full capacity
   - Inject H_2S - N_2 standard through fixture at probe tip. Adjust pressure at gas tank regulator so that pressure on pump is approximately the anticipated pressure during probing.
   - Wait for required stabilization time of temperature, residence time, and O_2 readings
   - Perform two or three injections at gas chromatograph to obtain reading
4) Sampling
   - Turn on water flow to low value
   - Insert 12 feet of probe into the boiler, i.e., 4 feet in the furnace (because of 8-foot windbox)
   - Operate as with precalibration: two repetitions if readings show no H_2S; three repetitions if readings show H_2S
   - Make axial traverse — typically 4 feet, 6 feet, 10 feet, 14 feet, and 18 feet in furnace; if H_2S present, traverse in 2-foot increments
5) Post calibration — A post calibration should be performed after each port is probed (until it is established that calibration factor can be obtained reproducibly). Emphasis should be placed on maintaining:
   a) Same pump pressure as during sampling
   b) $T \approx 300°F$
   - Perform as during precalibration
6) Blow out lines with nitrogen
7) Probe accessible view ports for various operating conditions — full load, reduced load

2.3.4.2 Corrosion Panel

1) Connect appropriate lines and equipment
   - Put extra filter on pump to remove soot
   - Do not connect to the 3/8-inch, 10-foot sampling probe until ready for actual measurements
2) Assume residence time is same as for view port probing
3) Perform precalibration
   - Similar procedure as with view port probe
   - Exclude the 10-foot sampling probe from the sampling train

4) Sampling
   - Perform measurement, almost as with view port probing except:
     Only one axial position: -1/2 foot into furnace interior
     probe: 10 feet
     probe outlet to ball valve: 1 foot
     ball valve to boiler outside wall: 1 1/2 feet
     windbox: 8 feet
     NOTE: Pump should be at full capacity
5) Post calibration
   - Same procedure as with precalibration
   - Duplicate pump pressure observed during sampling
6) Purge lines (optional) — Only if significant pluggage has occurred. If line is purged, then precalibration must be performed before next corrosion panel port, otherwise continue.
7) Precalibration (optional) — Perform only if line is purged in Step 6
8) Probe next corrosion panel port

2.4 N_2O EMISSIONS PERFORMANCE

2.4.1 N_2O Measurements

It was not known whether a significant increase in N_2O would be produced in JMSS 4 after installation of the Low-NO_x Cell™ Burners. The LNCB system changed both temperature and air/fuel ratios in localized parts of the furnace when compared to an in-furnace combustion profile created by standard cell burner installations. Whether this change is conducive to increased N_2O production was not known, since the mechanisms and kinetics of the formation of this compound in substoichiometric coal combustion have not yet been established. Therefore, the objective of this portion of the post retrofit testing was to measure N_2O concentrations at the left and right economizer outlet ducts as in baseline testing and compare the results.

Through the use of a gas sampling system, flue gas samples were extracted from each of the two economizer outlet ducts at two test tap positions. The gas sampling system consisted of a sampling grid, an impinger train, a vacuum pump, and plastic tubing for conveyance of the conditioned sample. The impinger train was designed to remove sulfur dioxide (SO_2) and water (H_2O) from the continuous flue gas sample. The vacuum pump was configured to deliver a constant pressure to the system during calibrations (using bottled standard gases) and testing (flue gas sample stream). The flue gas sample was contained in plastic tubing (Impolene) prior to its analysis in a gas chromatograph.

After Phase I baseline testing, it was reported that N_2O can be adsorbed on the surface of silica gel. Therefore, a substitution was made to the contents of the impinger train so that $CaCl_2$ replaced silica gel* for H_2O removal. It should be noted, however, that no absorption of N_2O was observed during the Phase I baseline N_2O tests. Neither pre- nor post-calibration using N.I.S.T. gas standards indicated that there was any question of the validity of the baseline data.

N_2O was measured in each continuous flue gas sample stream by a GC equipped with a Ni^{63} electron capture detector (ECD). The gas chromatograph was the same instrument used for H_2S measurements.

* N_20 Mini-Workshop at METC, Morgantown, WV, June 4, 1992.

2.4.1.1 Experimental. Each continuously extracted flue gas sample was delivered to the GC for N_2O analysis via the gas sampling system shown in Figure 2-13.

The connection distance between each sampling point and the impinger train was minimized, approximately 2 feet, in order to minimize additional N_2O from forming inside the sample line before the impinger train. Impolene and surgical tubing were used to connect the sampling point to the impinger train.

The impinger train consisted of four 500 ml impingers housed in an ice bath. Each of the first two impingers had 200 ml of 3% H_2O_2 to remove SO_2. Then an empty impinger was inserted in case of carryover or bumping during sampling. Finally, the last impinger had 200 g of 4 - 8 mesh $CaCl_2$ pellets to remove H_2O.

After each sampling point, another set of impingers with fresh reagents was used.

Gas flow output from the vacuum pump was adjusted by the vent valve to deliver a constant pressure, 28 p.s.i. as measured by the gauge, to the GC.

Approximately 250 feet of 1/4-inch OD Impolene tubing was used as the sample line connecting the adjusted output of the vacuum pump to the left rear injection port of the GC (Figure 2-14).

A flow regulator valve was installed in the sample line prior to the injection port, and was adjusted to maintain a gas sample flow rate, as measured by the rotameter on the vent side of the GC, of 75 ml/min. through the six-port gas sample valve located inside the column oven of the GC.

2.4.1.2 Gas Chromatograph. The GC used to quantify N_2O was a Varian Model 3400 equipped with a Ni^{63} ECD maintained at 350°C. Nitrogen carrier gas at 30 ml/min. flowed through a 6-foot long x 1/8-inch OD SS column packed with HayeSep® D 80/100 mesh maintained at 40°C.

Similar to the gas sampling system described in Section 2.3 for H_2S, the GC had a separate gas sampling system for N_2O analyses. The differences between the gas sampling systems were:

- The N_2O gas sampling valves were located in the column oven and kept at 40°C, whereas the H_2S gas sampling valves were housed in the injection block of the GC and maintained at 140°C.
- The selector switch handle for N_2O analyses was located on the right side of the GC, instead of on top of the instrument as for H_2S.
- For N_2O analyses, a 1 ml gas sample loop was employed in the six-port gas sampling valve as compared to a 0.075 ml sample loop used for H_2S.

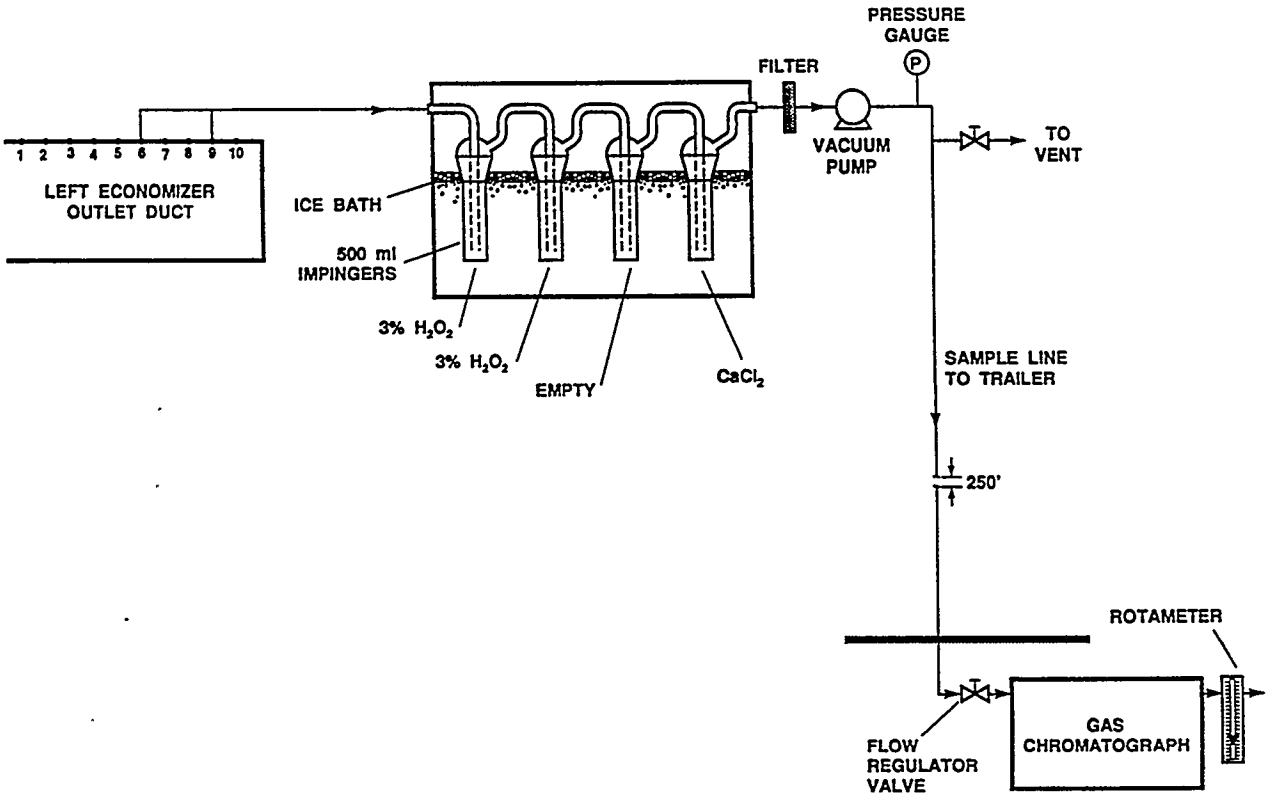

Figure 2-13 Gas sampling system for N_2O determination

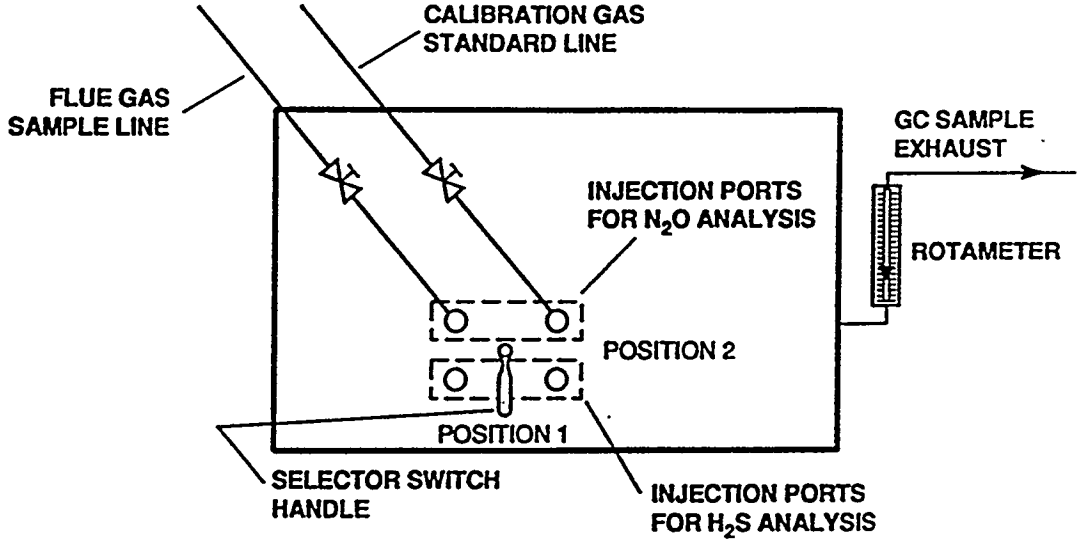

Figure 2-14 Top view of the gas chromatograph showing the location of injector ports for gas standard calibration and flue gas sampling — N_2O analyses

Section 3
RESULTS AND DISCUSSION

3.1 LABORATORY RETORT TESTS

Tables 3-1 and 3-2 summarize the corrosion rates of the alloys and coating systems obtained from the laboratory investigation. Specifically, Table 3-1 gives the corrosion rates of the materials *without* the presence of the simulated deposit, and Table 3-2 lists those *with* the deposit. All corrosion rates are expressed in mpy (mil per year), which are derived by linearly extrapolating the 1000-hour corrosion data to one year. Columns 1-5 (i.e., Tests #1-5) are data generated from this current program, and the scattered corrosion rates in the remaining columns were collected from B&W's previous studies pertaining to the current work. It is noted that in Table 3-2 no previous corrosion data involving ash deposit are available.

In general, the metal-wastage rates of the high-alloy steels in Tables 3-1 and 3-2 are significantly lower than those of carbon and low-alloy steels under the same test condition. The better performance of high-alloy steels is primarily attributed to their relatively higher Cr contents, as evidenced by the metallographic results to be discussed shortly.

Among the high-alloy steels, however, the two free-standing coating materials (FeCrAl and FeNiCrAl) appear to suffer more corrosion attack than the others, regardless of similarity in their chemical compositions compared to the other stainless steels. The high corrosion rates on these coating materials are associated with their microstructures and will be explained later.

The corrosion rates of the coating systems are somewhat erratic. A relatively low corrosion rate is observed on the CrSi/T2 samples. However, the corrosion rates calculated for the FeCrAl/T2 and Al/T2 systems are noticeably higher.

To better understand the materials performance, the alloys and coatings in Table 3-1 are divided into three groups. Group I includes the carbon and low-alloy steels, Group II contains the high-alloy steels and the two free-standing coating materials, and Group III comprises the coating-on-substrate systems. To accomplish the project objectives, the discussion followed is focused on establishing correlations between the corrosion rate and:

1) Metal temperature
2) Cr concentration in alloys
3) H_2S concentration in the mixed gas

Table 3-1
CORROSION RATES OF ALLOYS IN MIXED GAS *WITHOUT* DEPOSIT

Test#	1	2	3	4	5						
H_2S%	0.05			0.25	0.5				2.0		4.9
T(°F)	700	500	900	700	700	700	700	900	900	900	700
Time (hrs)	1000	1000	1000	1000	1000	1000	3000	1000	1000	4000	1000
178/210	5.4	1.54	14.4	5.02 6.03	11.36	8.5	4.0			41.0	19.1
T22	5.3	0.7	15.5	3.29 3.78	11.22	7.0	4.4			52.0	19.1
T11	3.9	1.5	14.3	3.81 4.36	7.61						
T9	3.2	0.5	5.2 5.82	2.57 2.79	6.69						
T2	5.3	1.16	18.3	3.24 3.40	11.69						
304	0.3	0.11	7.44 4.03	0.44	0.67	0.3	0.17	3.6	17.0	8.2 12.0	0.94
309	0.2	0.03	2.26	0.28	0.29		0.03			1.6	
310	0.2	0.06	1.77	0.30	0.20 0.34	0.08	0.05	1.6			0.14
321	N/A	N/A	0.50	1.09	2.05						
253MA	0.16	0.05	3.21	0.31	0.17 0.25						
FeCrAl	0.6	0.59	7.07 30.1	1.68	2.75						
FeCrNiAl	2.04	1.74 2.42	3.03	3.83	6.79						
CrSi/T2				0.21							
FCA/T2					2.11						
Al/T2											

Table 3-2
CORROSION RATES OF ALLOYS IN MIXED GAS *WITH* DEPOSIT

Test#	1	2	3	4	5
H_2S%	0.05			0.25	0.5
T(°F)	700	500	900	700	700
Time (hrs)	1000	1000	1000	1000	1000
178/210	4.15	1.18	8.66	6.04 6.03	11.87
T22	3.53	0.49	6.95	5.27	8.06
T11	3.00	0.84	7.12	3.77	6.29
T9	3.18	0.49	4.72	3.15 2.96	4.56
T2	3.56	0.90	10.83 11.54	5.21	8.31
304	0.68	0.15	0.99 0.81	0.80	0.67 0.73
309	0.20	0.10	0.73	0.27	0.36
310	0.40	0.07	0.87 0.83	0.43	0.45
321	N/A	N/A	2.01	3.19	1.79
253MA	0.34	0.14	3.11	0.34 0.38	0.26 0.39
FeCrAl	0.81	0.62 2.57	3.92 0.76	3.76	2.44 9.80
FeCrNiAl	1.53	3.96 1.05	13.03 13.91	2.40	5.54
CrSi/T2				0.13	0.38
FCA/T2					1.96
Al/T2					6.48

3.1.1 Variation of Corrosion Rate With Temperature

3.1.1.1 Group I — Carbon and Low-Alloy Steels. The test data generated from Tests #1, #2, and #3 are used for comparison. Variations of the corrosion rates for the Group-I alloys as a function of temperature *without* and *with* the coverage of simulated ash deposit are shown in Figures 3-1 and 3-2, respectively. Overall, the corrosion rates increase with increasing test temperature. Such a trend agrees well with the expected corrosion behavior of alloys. At the metal temperature of 500°F, the measured corrosion rates are very low — all fall below 2 mpy. However, at the highest temperature employed, i.e., 900°F, the corrosion rates become significant, with SA213-T2 exceeding 18 mpy.

In general, the low-alloy steel containing ~9% Cr, i.e., SA213-T9, suffers the least corrosion attack from the reducing mixed gas containing 0.05% H_2S at 500° - 900°F, and the corrosion resistance of all other Group-I alloys is relatively inferior than that of T9. However, the differences in their corrosion rates are not significant.

The apparent corrosion rates of the carbon steel (SA178-A) in both Figures 3-1 and 3-2 are slightly less than those of SA213-T2 at 900°F. The carbon steel has essentially zero Cr concentration, whereas T2 has ~0.7%. Such a reversed behavior between plain carbon steel and T2 may be partially attributed to the experimental errors. On the other hand, it has been reported that the presence of a small amount of Cr in alloys can in fact deteriorate the oxidation resistance of these alloys at high temperatures.[7] Such a deterioration is associated with the incorporation of Cr into the iron oxide-base scales formed, which increases the point-defect concentrations. Similarly, Cr can also increase the point-defect concentration of iron sulfide-base scales when the alloys are exposed to the laboratory mixed gases of investigation.

Literature, data, and field experience have indicated that the existence of a molten ash deposit on the surfaces of boiler tubes can expedite the corrosion attack on metals via fluxing mechanisms.[5] However, contrary to literature studies, the corrosion rates in Figure 3-2 for the alloys covered with the simulated ash deposit are somewhat less than those in Figure 3-1 without the deposit. It appears that the employed deposit has hindered the corrosion attack. The lack of negative deposit effects on the corrosion rates is quite unusual. However, it is noted that the composition of the "reducing" deposit in Table 2-4 used in this study is also quite different from those reported in the literature. The following explanations possibly leading to the apparent "beneficial" effects are suggested:

- The simulated deposit did not melt at the test temperatures. This was evidenced by the physical appearance of the deposit after the exposure from all of the retort tests. The deposit remained as loose powder after 1000 hours even at the highest temperature (900°F). Consequently, a solid deposit cannot initiate the fluxing mechanisms.
- The thick deposit layer placed on the sample surfaces (on an average of ~1 inch thick) inadvertently acted as a solid-state diffusion barrier. This barrier can impede the corrosive species in the mixed gas from arriving at the alloy surfaces. As a result, the corrosion rates are reduced. Compared to the actual deposit on the test panel, such a thick layer does not truly reflect the actual surface conditions of waterwalls in JMSS 4.
- The chemical constituents of the ash deposit listed in Table 2-4, particularly those metal sulfides, did not actively participate in the corrosion processes. It is likely that the sulfides in the mixture were already present as "inert" compounds relative to those metal constitutes in the Group-I alloys. As mentioned, the deposit chemistry was derived from thermodynamic calculations[4] based on the as-

sumption of a complete system equilibrium. Therefore, these condensed species may not be corrosive to the alloys. In other words, the metal sulfides in the simulated deposit were already at their most stable forms under the reducing environments employed.

- Again, the composition of the deposit in Table 2-4 was derived from the thermodynamic calculations in an earlier pilot-scale LNCB study.[4] If the deposit was not determined correctly, the composition may not be representive of the actual ash deposit expected to form on the lower furnace walls of JMSS 4.

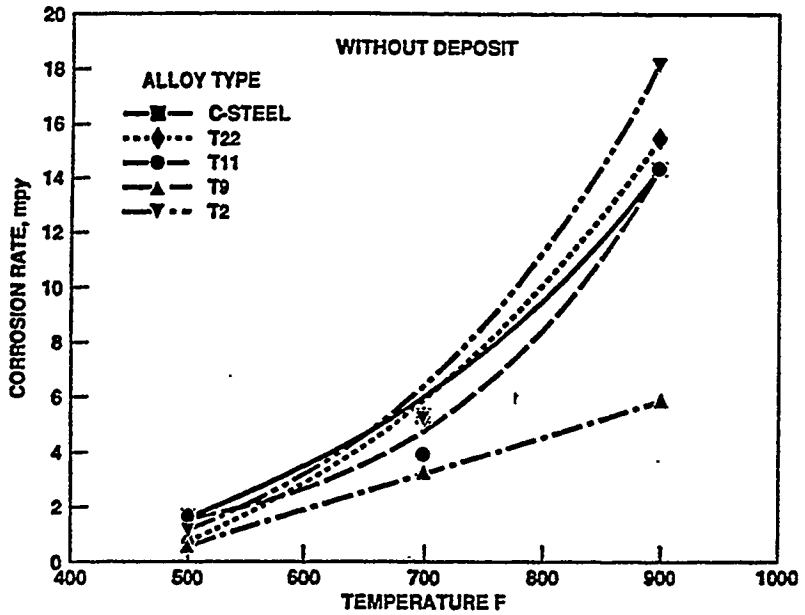

Figure 3-1 Variation of the corrosion rates with temperature for Group-I alloys without the coverage of simulated ash deposit

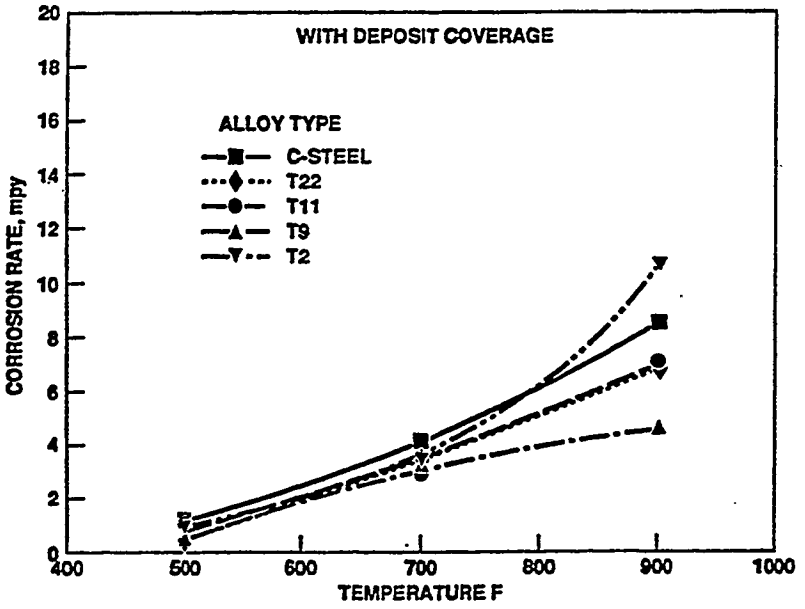

Figure 3-2 Variation of the corrosion rates with temperature for Group-I alloys with the coverage of simulated ash deposit

Cross-sectional metallographic examinations using SEM/EDX revealed that sulfidation was the predominant corrosion mode operating on the surfaces of all Group-I alloys. Figures 3-3 and 3-4 are the SEM micrographs of SA213-T11 and SA213-T9 after being exposed to the mixed gas in Test #2 (0.05% H_2S at 700°F for 1000 hours). The morphologies of these two cross sections are essentially identical in nature, i.e., both show multi-layered corrosion products formed on the alloy surfaces. The thick outermost layer is comprised of a faceted structure with a composition of nearly pure iron sulfide. Underneath the sulfide layer, a relatively porous mixed scale is present. EDX analyses suggested that the mixed scale contained some iron oxide and primarily iron sulfide (presumably Fe_3O_4 and FeS).

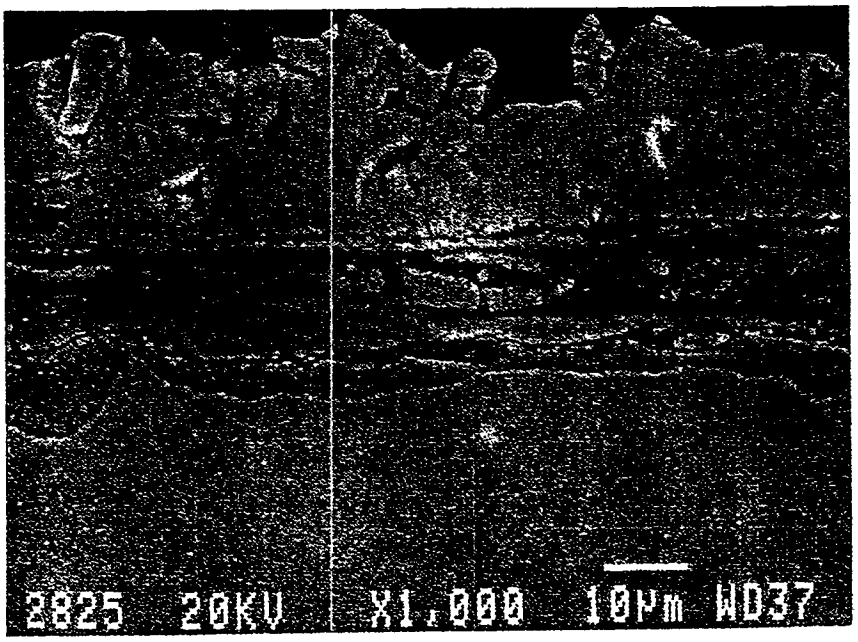

Figure 3-3 Cross-sectional SEM micrograph of SA213-T11 after exposure to the Test #2 condition

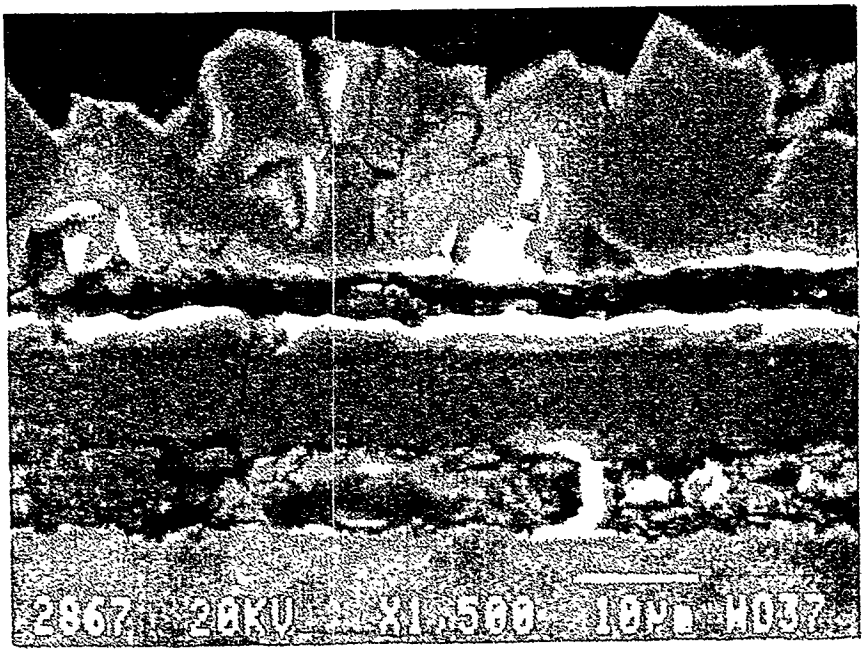

Figure 3-4 Cross-sectional SEM micrograph of SA213-T9 after exposure to the Test #2 condition

A multi-layered morphology, as those shown in Figures 3-3 and 3-4, is typical for all Group-I alloys under the Test #2 condition. Furthermore, the cross-sectional morphologies of the Group-I alloys exposed to other test conditions (i.e., different temperatures and H_2S concentrations) were also similar to those in Figures 3-3 and 3-4, although the thicknesses of the multi-layered structure vary somewhat with the test temperature and H_2S concentration.

3.1.1.2 Group II — Stainless Steels and the Two Free-Standing Coating Materials. Using the data from Tests #1, #2, and #3 in Tables 3-1 and 3-2, the corrosion rates of high-alloy steels and the two coating materials are graphically presented in Figures 3-5 and 3-6 as a function of temperature *without* and *with* the coverage of the ash deposit, respectively. In comparison, the corrosion rates of the high-Cr alloys in Group II are significantly lower than those of the Group-I alloys. Perhaps with the exception of 1) 304 and FeCrAl at 900°F in Figure 3-5 and 2) FeCrNiAl at 900°F in Figure 3-6, the corrosion rates of other Group-II alloys are all below 4 mpy. In particular, stainless steels 309 and 310 consistently exhibit very high corrosion resistance under the simulated reducing mixed gas containing 0.05% H_2S at 500° - 900°F.

Comparing Figures 3-5 and 3-6, the beneficial effects from the ash deposit covering the Group-II alloys are not as explicit as those on the carbon and low-alloy steels shown in Figures 3-1 and 3-2; however, negative effects on the corrosion rates are absent. As discussed before, the lack of negative deposit effects may be attributed to the experimental errors associated with the corrosion rate measurements, as well as those suggested above for the Group-I alloys.

Figures 3-7 and 3-8 are the cross-sectional SEM micrographs of SA213-310 and 253MA near the surfaces after being exposed to the mixed gas containing 0.05% H_2S at 700°F for 1000 hours (i.e., Test #2). Similar to the Group-I alloys, the corrosion products contain multi-layered structures, with the outer layer consisting essentially of pure iron sulfide. However, the thicknesses of the sulfide layer on the Group-II alloys are considerably less than those on the Group-I alloys. The cross-sectional morphologies are also typical for those of SA213-304L, SA213-309, and SA213-321 as well.

Unlike the Group-I alloys, however, a thin and continuous inner scale exists underneath the outer sulfide layer. EDX analysis indicated that this layer was rich in Cr and was likely to be chromia-base oxide. Chromium oxide can provide much improved corrosion resistance for alloys exposed to many corrosive environments. The satisfactory performance of these steels is therefore attributed to their high Cr concentrations.

On the other hand, the corrosion resistance of the two free-standing coating alloys (i.e., FeCrAl and FeCrNiAl) is usually achieved by their ultimate formation of an alumina scale. When exposed to high temperatures, the alloys first form a chromia scale on the surfaces, followed by slow formation of an alumina sub-scale between the chromia layer and the substrate.

However, the corrosion rates of these free-standing coating materials in Figures 3-5 and 3-6 are relatively high compared to those of the other Group-II alloys. To understand the cause of this behavior, the exposed coating materials were carefully examined under SEM/EDX. Figure 3-9 shows a cross-sectional SEM micrograph of an FeCrNiAl sample after exposure in Test #2. In general, the corrosion products on the outer surface were very thin, despite the detection of some iron sulfide by EDX. The thin corrosion products formed on the surfaces indicate that the inherent compositions of these coating materials are quite resistant to the simulated reducing combustion gases.

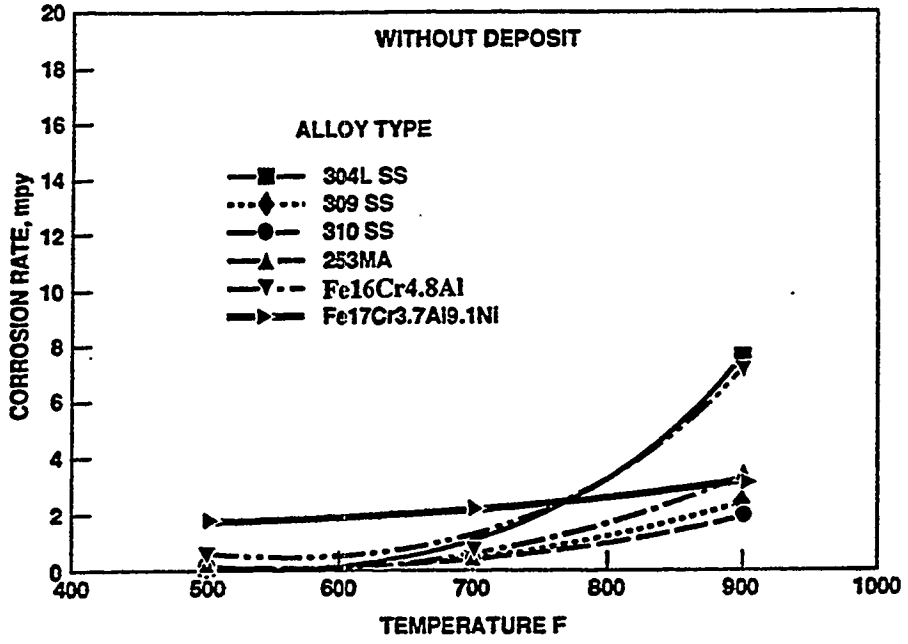

Figure 3-5 Variation of the corrosion rates with temperature for Group-II alloys without the coverage of simulated ash deposit

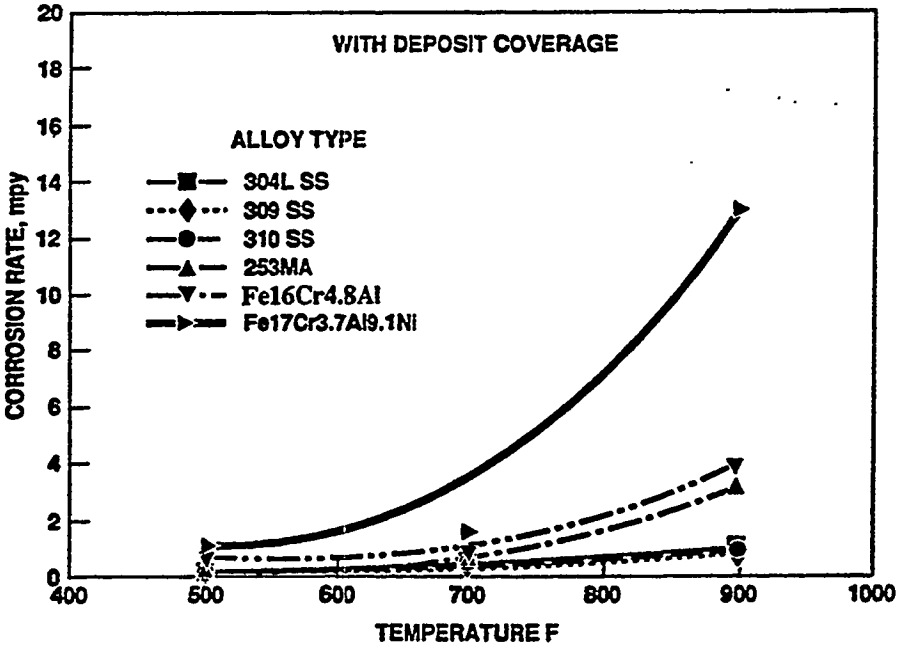

Figure 3-6 Variation of the corrosion rates with temperature for Group-II alloys with the coverage of simulated ash deposit

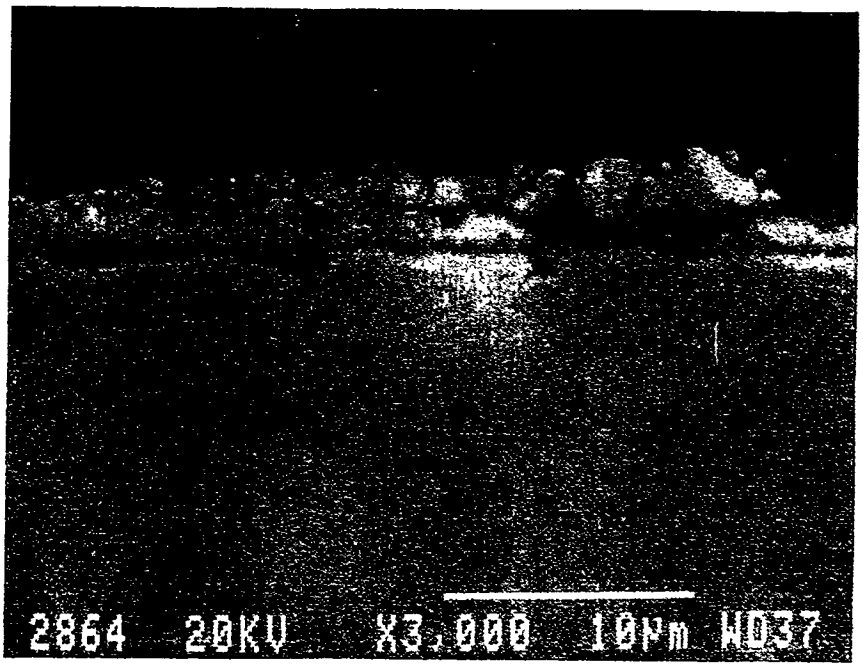

Figure 3-7 Cross-sectional SEM micrograph of SA213-310 after exposure to the Test #2 condition

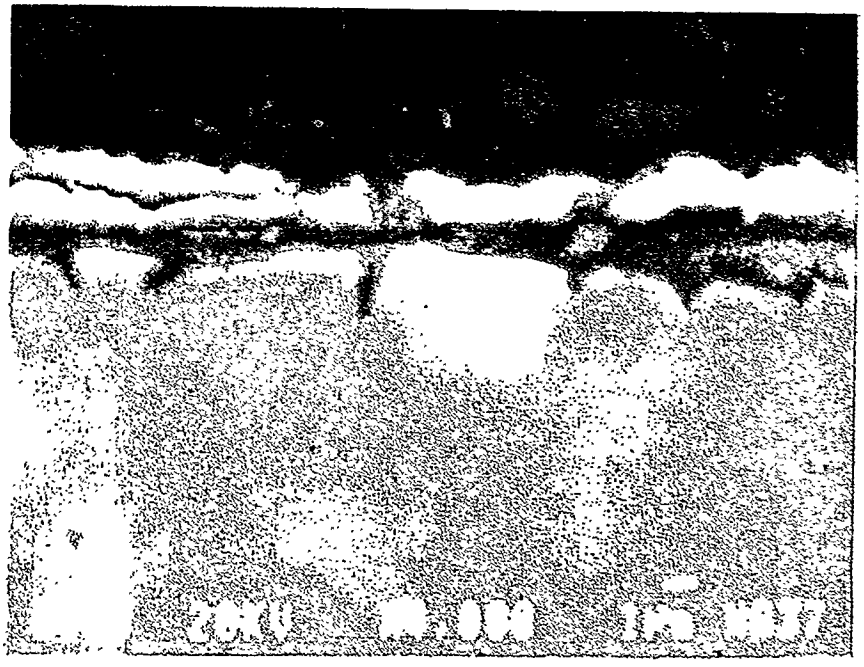

Figure 3-8 Cross-sectional SEM micrograph of Alloy 253MA after exposure to the Test #2 condition

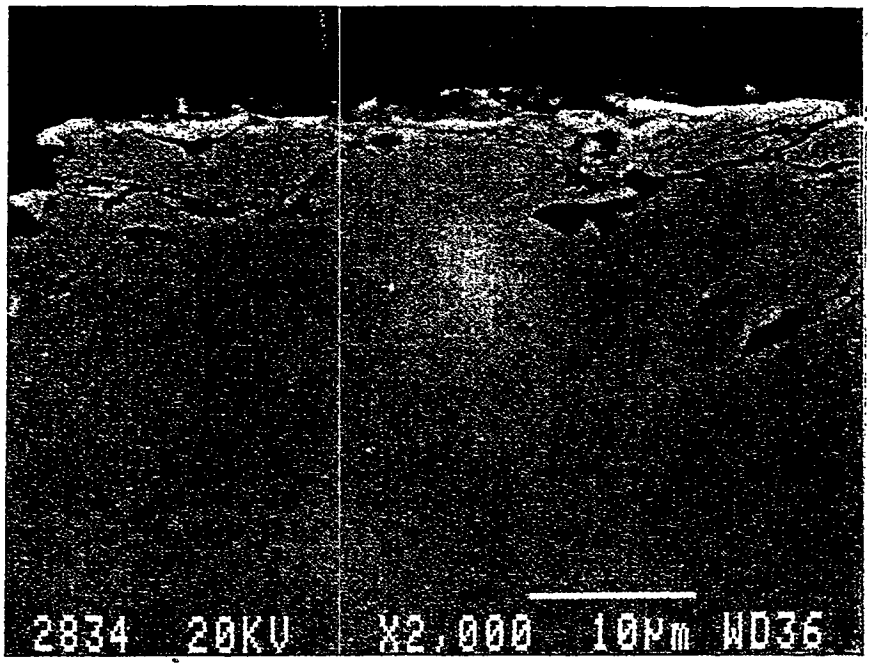

Figure 3-9 Cross-sectional SEM micrograph of an FeCrNiAl alloy after exposure to the Test #2 condition

However, localized corrosion attack occurred along the defects near the substrate surfaces. In addition to the corrosion products observed on the sample surfaces, mixed oxide and sulfide were found within the structural defects. The increased metal wastage was therefore closely associated with the presence of structural defects in the materials under the surfaces.

Both of the coating alloys are mechanically brittle due to their high Al concentrations. During the rolling operation, numerous cracks must have been created. The cracks have apparently generated additional surface areas inside the materials prior to the retort exposures. Therefore, the actual surface areas of these samples could be significantly higher than those calculated based on the apparent sample dimensions.

In addition, it is likely that, during the descaling processes, some of the material near the surfaces was separated from the alloy coupons along the structural defects where corrosion has taken place. As a result, a higher weight loss was realized. The localized corrosion attack appeared to become more severe at higher temperatures, as evidenced by a rapid increase in the "apparent" corrosion rates with temperature, shown in Figures 3-5 and 3-6.

Differences in the corrosion rates among the Group-II alloys suggest that the structural integrity of the materials is very important and cannot be overlooked. Structural defects introduced from materials processing can profoundly have a negative impact on the materials performance. As demonstrated by the two coating materials which are often thermal sprayed onto the substrate surfaces, the corrosion attack may proceed preferentially along the structural defects, such as coating porosity, while the magnitude of the corrosion attack cannot be easily detected by the appearance.

3.1.1.3 Group III — Coating Systems. The calculated metal wastage rates for 1) plasma-sprayed Al coating on SA213-T2, 2) plasma-sprayed FeCrAl coating on SA213-T2, and 3) co-diffusion Cr/Si coating on SA213-T2 are given in Tables 3-1 and 3-2 *without* and *with* the deposit coverage, respectively. Because only a few coated samples were made, these coating systems were not tested in all of the retort conditions. The lack of complete data prohibited graphic presentations of the coating performance. However, their corrosion resistance can be qualitatively evaluated by comparing their corrosion rates to those of Groups I and II alloys.

The corrosion rates of Al/T2, FeCrAl/T2, and CrSi/T2 in Table 3-2 from Test #5 (0.5% H_2S at 700°F with the deposit) are 6.48, 1.96, and 0.38, respectively. The metal-wastage rate of Al/T2 appears to be comparable to those of Group-I alloys, while the corrosion rates of FeCrAl/T2 falls between those of Group-I and Group-II alloys. It is noted that the corrosion rate of FeCrAl/T2 is almost the same as that of the free-standing FeCrAl. On the other hand, the metal-wastage rate of CrSi/T2 is relatively low, equivalent to those of stainless steels. This low corrosion rate suggests that CrSi/T2 performed in the laboratory low-NO_x environments as good as, or slightly better than, the Group-II high-Cr alloys.

The excellent performance of the CrSi/T2 system was repeatedly demonstrated by the low corrosion rate shown in Table 3-1 from Test #4 (without deposit), which is equal to or slightly better than those of the Group-II stainless steels. Similar to the findings in Table 3-2, the corrosion rate of the FeCrAl/T2 system from Test #2 in Table 3-1 (0.05% H_2S at 700°F without the deposit) falls in between those of Group-I and Group-II alloys and is again comparable to the free-standing FeCrAl material.

Reasons for the relatively high corrosion rates obtained from the Al plasma-sprayed coating system (Al/T2) can be easily elucidated by the cross-sectional SEM micrograph in Figure 3-10. This Al/T2 sample is exposed to the retort condition of Test #2. The corrosion products formed on the outer surface of the Al coating is very thin and essentially negligible. However, in the coating layer, there are a large number of second-phase stringers. EDX analysis indicated that the interconnected stringers are primarily aluminum oxide. It is likely that the aluminum oxide was formed by oxidation during the plasma-spray coating process. As a result, the process had consolidated structural defects in the coating layer. Some sulfur was detected by EDX in these stringers, indicating that localized sulfidation has taken place during the retort exposure.

Figure 3-11 is a close-up view of the substrate/coating interface on an Al/T2 sample exposed to the Test #2 condition. The microstructure and EDX analysis revealed the formation of iron aluminide at this interface. In addition, a continuous layer of iron sulfide was found at the Al/T2 interface. The presence of sulfur at this region clearly suggests that the sulfur-bearing species in the mixed gas has penetrated through the coating layer and subsequently reacted with the underlying substrate, despite the relatively thick Al coating layer. The microstructure of the Al coating suggests that the sulfur penetration was facilitated by the presence of the continuous oxide stringers. In other words, the oxide stringers served as short circuits for the inward diffusion of sulfur-containing species. Therefore, higher corrosion rates were measured.

The above analysis again highlights the importance of coating integrity, which can greatly affect the materials performance. The structural defects existing in the Al coating, for example, create preferential corrosion paths in the coating layer for the transport of corrosive species. Therefore, despite the inherently resistant coating materials (e.g., Al), the coating system suffered a noticeable amount of metal loss from the simulated low-NO_x environments.

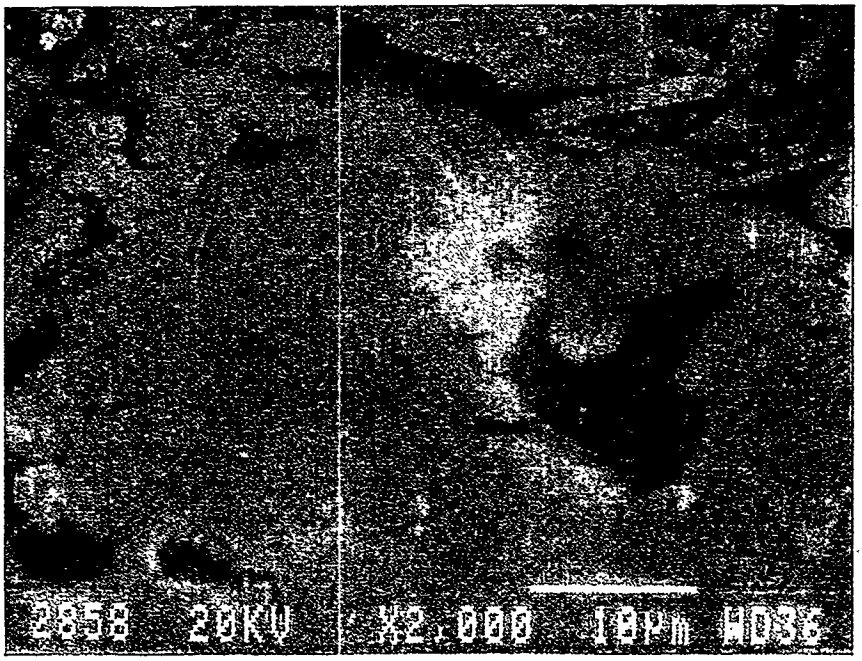

Figure 3-10 Cross-sectional SEM micrograph of an Al/T2 sample after exposure to the Test #2 condition

Figure 3-11 Cross-sectional SEM micrograph of an Al/T2 sample at the coating/substrate interface after exposure to the Test #2 condition

It should be mentioned that the measured high corrosion rate on Al/T2 may have also been escalated by the descaling processes. The inhibited-HCl solution used in the descaling process had a tendency to dissolve Al. Consequently, excessive weight loss was resulted.

Oxide stringers were also found in the FeCrAl plasma-sprayed coating layer. Figure 3-12 is the cross-sectional SEM micrographs of an FeCrAl/T2 sample after exposure to Test #2 conditions. The micrographs show both the microstructures of the coating layer and coating/substrate interface. The existence of oxide stringers throughout the coating layer is again evident. EDX analysis indicated that the corrosion products at the coating/substrate interface consisted primarily of iron sulfide. Therefore, similar to the Al/T2 system, sulfur has penetrated through the coating layer and reacted with the underlying metal. The formation of iron sulfide again stresses the close association of reduced materials performance with coating morphology.

The CrSi/T2 coating system exhibited excellent corrosion resistance to all of the test conditions. Figure 3-13 is the cross-sectional SEM micrograph of CrSi/T2 exposed to Test #2 conditions. Only under very high magnifications, a thin (in submicron) layer of corrosion product could be observed on the coating surface. EDX analysis suggested that this layer was a chromia-base oxide scale containing some silicon. No localized corrosion attack was found in the coating layer. Apparently, the chromia-base scale formed on this coating has provided adequate corrosion resistance to the laboratory reducing environments.

3.1.2 Variation of Corrosion Rate With the Cr Concentration

Carbon and low-alloy steels have been successfully used in conventional pulverized-coal-fired boilers as heat exchanger tubes. The use of these alloys is advantageous because of their 1) low cost, 2) chemical resistance to waterside pitting corrosion, and 3) desired high-temperature mechanical properties. When combustion is controlled to include excess air, carbon and low-alloy steels are generally useful due to the formation of iron oxides..

However, under more severe corrosive environments, such as the reducing combustion gases anticipated in boilers, corrosion protection from iron oxides may no longer be adequate. In fact, based on the previous discussion, iron sulfide is the most stable corrosion product formed on all Group-I alloys in the simulated laboratory environments. Under these conditions, the corrosion resistance of the conventional heat exchanger materials may need to be achieved by forming other types of surface scales, such as chromium oxide (chromia) and aluminum oxide (alumina). As illustrated previously, the Group-II alloys and Group-III coating materials have much better corrosion resistance in the laboratory reducing mixed gases than those of Group-I.

The ability of alloys to form chromia and alumina scales is largely determined by the Cr and Al concentrations in the alloys. While both scales may effectively provide the needed resistance, the use of chromia-forming steels is far more preferred than alumina-forming alloys because of mechanical embrittlement associated with Al addition. Therefore, upgrade of the boiler tubes with a chromia-forming surface composition is a more viable solution to minimize the waterwall wastage in the lower furnace where reducing zone is expected.

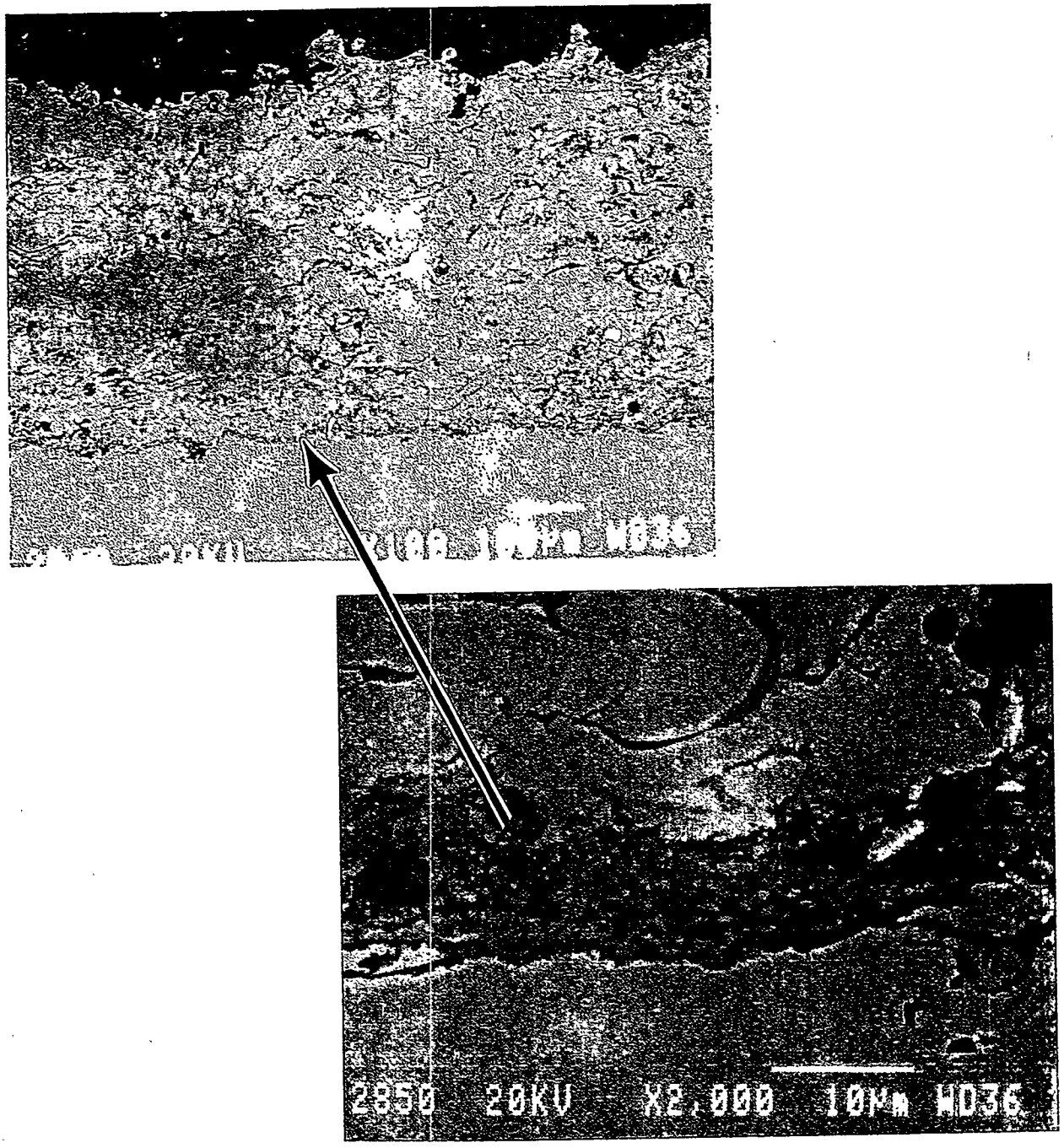

Figure 3-12 Cross-sectional SEM micrograph of an FeCrNiAl/T2 sample at the coating/substrate interface after exposure to the Test #2 condition

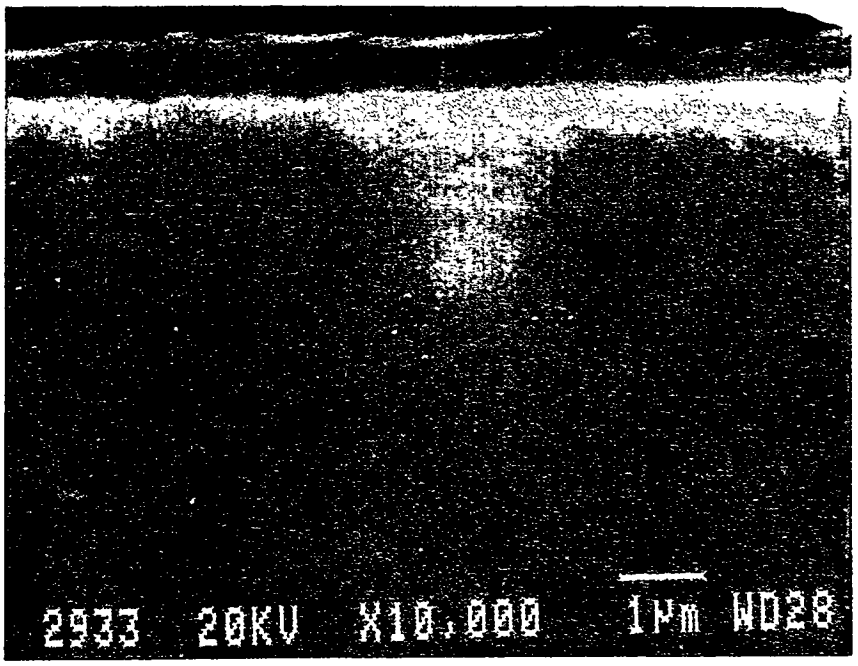

Figure 3-13 Cross-sectional SEM micrograph of a CrSi/T2 sample after exposure to the Test #2 condition

Figures 3-14 and 3-15 show the variations of metal-wastage rates of the alloys as a function of Cr contents *without* and *with* the coverage of simulated deposit, respectively. Apparently, such a correlation assumes that chromium in the iron-base alloys is the only element dictating the materials performance, and the effects from all other elements are negligible. Obviously, these assumptions cannot be always valid because other elements can significantly affect the materials behavior. For example, a large amount of nickel usually promotes sulfide formation which in turn, accelerates the metal wastage. On the other hand, the addition of a small amount of silicon can enhance the corrosion resistance by forming a more protective scale. In fact, effects from other alloying elements may have contributed to the scattering of data in Figures 3-14 and 3-15, especially in the higher Cr% range. Therefore, the simplified correlation must be interpreted with caution.

Figure 3-14 shows that the corrosion rate decreases steadily with increasing Cr concentration in the alloys. For a given Cr content, the corrosion rate under the condition of Test #3 is the highest, followed by Test #5, Test #2, Test #4, and finally Test #1. Because of the unreasonably high metal-wastage rates of the two free-standing coating materials (i.e., FeCrAl and FeCrNiAl) in Group II and the two coating systems (i.e., FeCrAl/T2 and Al/T2) in Group III, their corrosion rates were excluded from this analysis.

Tests #2 and #3 were exposed to the same H_2S concentration in the mixed gas (i.e., 500 ppm) but at different temperatures. As expected, the corrosion rate of Test #3 is higher than that of Test #2. In addition, the metal-wastage rate also increases with increasing H_2S concentration in the mixed gas, as evidenced by Tests #1 and #5. However, the magnitudes of the corrosion-rate change from increasing the metal temperature and H_2S concentration are not proportional. For example, using the corrosion data of Test #2 (i.e., 0.05% H_2S at 700°F) as a baseline, the corrosion rate is far less susceptible to a ten-fold H_2S% increase (i.e., Test #5: 0.5% H_2S at 700°F) than a 200°F metal-temperature increase (i.e., Test #3: 0.05% H_2S at 900°F).

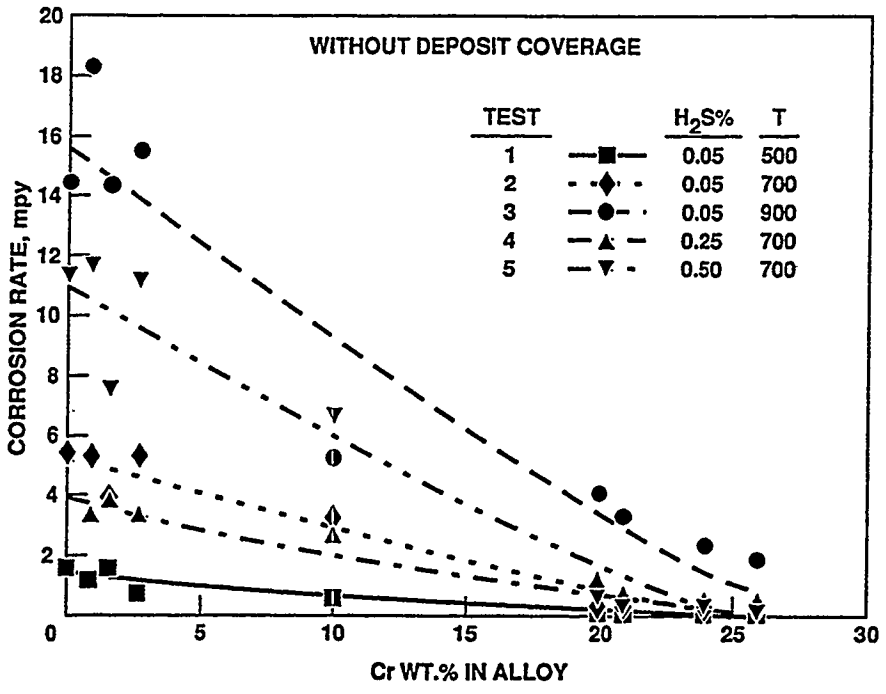

Figure 3-14 Variation of the corrosion rates with Cr concentration in alloys without the coverage of simulated ash deposit

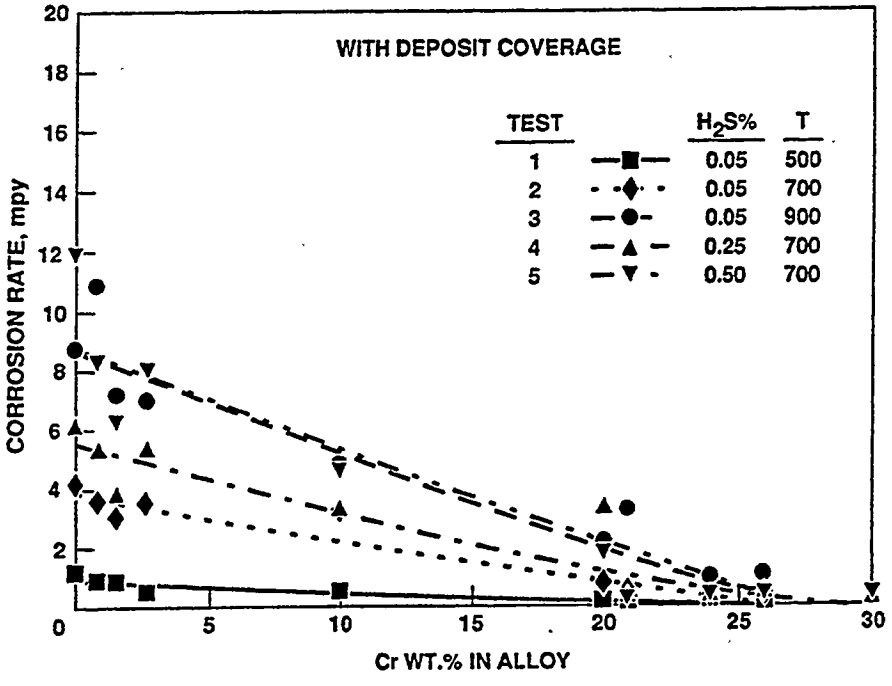

Figure 3-15 Variation of the corrosion rates with Cr concentration in alloys with the coverage of simulated ash deposit

The variations of corrosion rate with Cr% for the alloys in Tests #2 (0.05% H_2S) and #4 (0.25% H_2S), both exposed to 700°F for 1000 hours, are fairly comparable, as shown in Figure 3-14. These comparable corrosion rates indicate that a five-fold increase in H_2S%, while the temperature remains the same, does not noticeably alter the metal-wastage rate. This observation again suggests that the effects from a H_2S% change on the corrosion rate are not as significant as that from temperature, at least within the H_2S concentration and temperature ranges studied.

3.1.3 Variation of the Corrosion Rate With H_2S Concentration in the Flue Gas

The corrosion data from Tests #2, #4, and #5 shown in Tables 3-1 and 3-2, all of which were exposed at the same metal temperature (700°F), are used to correlate the metal-wastage rates with the H_2S concentration in the mixed gas. Figure 3-16 summarizes the results of the Group-I alloys *without* the coverage of the simulated ash deposit.

Although the corrosion rates of these alloys under 0.25% H_2S appear to be slightly less than those under 0.05% H_2S, the differences should fall within the experimental errors. The range of experimental errors will be illustrated by the standard errors of the predictive equations developed in the next section. As a result, the corrosion rates of Group-I alloys at 0.05% and 0.25% H_2S are essentially comparable. This indicates that the corrosion rates of Group-I alloys are relatively insensitive to the H_2S% change, at least from 500 to 2500 ppm. Higher corrosion rates are observed under 0.5% H_2S.

It is likely that, as the H_2S concentration approaches zero, the corrosion rate can be further reduced. That is, as the H_2S concentration becomes very low, sulfidation attack no longer plays an important role in the mixed gases, and the corrosion is dominated by oxidation. Apparently, this involves a change in the corrosion mechanisms. Comparing to sulfidation, the oxidation rates of Group-I alloys would be relatively low. As a result, there should be a sudden decrease in the corrosion rates of these alloys at a low H_2S concentration, as depicted by the dashed lines. The exact H_2S% where the transition takes place cannot be defined based on the available laboratory data in Figure 3-16. However, a decrease in the corrosion rates will be illustrated by the predictive equations in the next section.

Figure 3-17 shows the variations of corrosion rates with H_2S% for the Group-II alloys *without* the coverage of the ash deposit. The variations of these alloys with H_2S% appear to be linear, and they suffered relatively little metal wastage. The corrosion rates of the two free-standing coating materials, i.e., FeCrAl and FeCrNiAl, are higher among these materials. As mentioned previously, the structural defects pre-existing in the rolled sheets have attributed to the higher metal-wastage rates.

Figures 3-18 and 3-19 show the corrosion rates of Group-I and Group-II alloys, respectively, as a function of the flue-gas H_2S concentration *with* the coverage of deposit at 700°F. Perhaps with the exception of the carbon steel (SA178-A), the dependency of corrosion rate upon the H_2S concentration within 0 - 0.5% H_2S is relatively small. It appears that, when covered with the ash deposit, the corrosion rates of the low-alloy steels can be noticeable only at an H_2S concentration above 0.5%, outside the concern of many low-NO_x technologies.

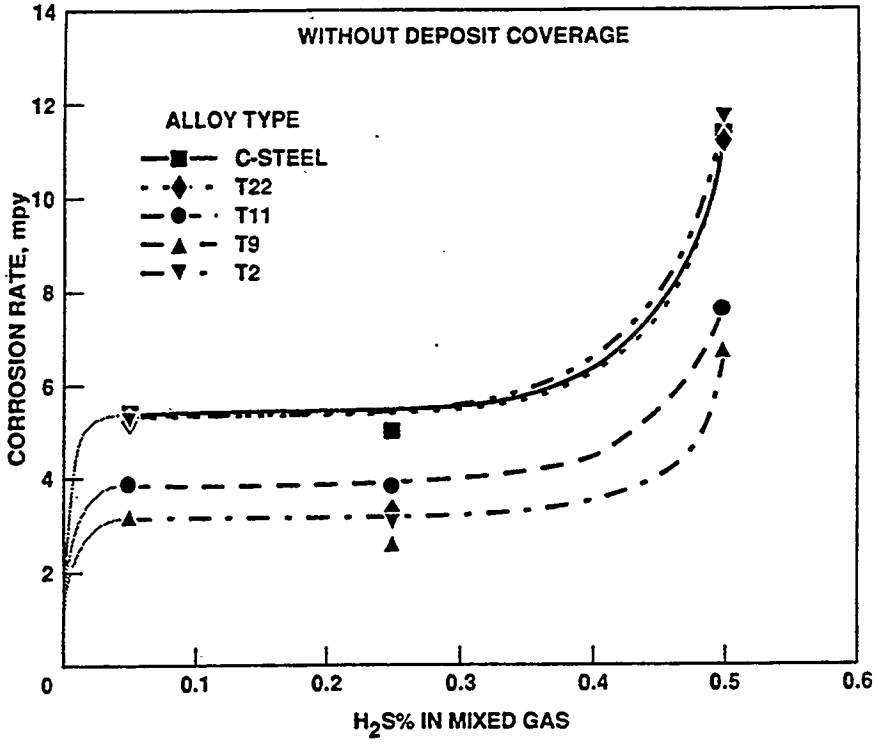

Figure 3-16 Variation of the corrosion rates with H_2S concentration in the mixed gas for the Group-I alloys at 700°F without the coverage of simulated ash deposit

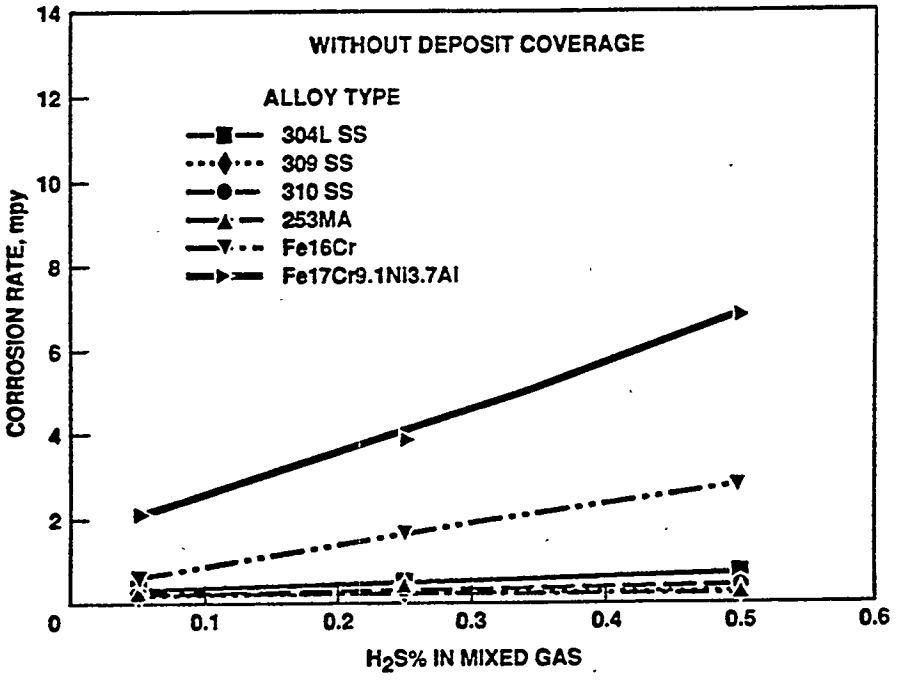

Figure 3-17 Variation of the corrosion rates with H_2S concentration in the mixed gas for the Group-II alloys at 700°F without the coverage of simulated ash deposit

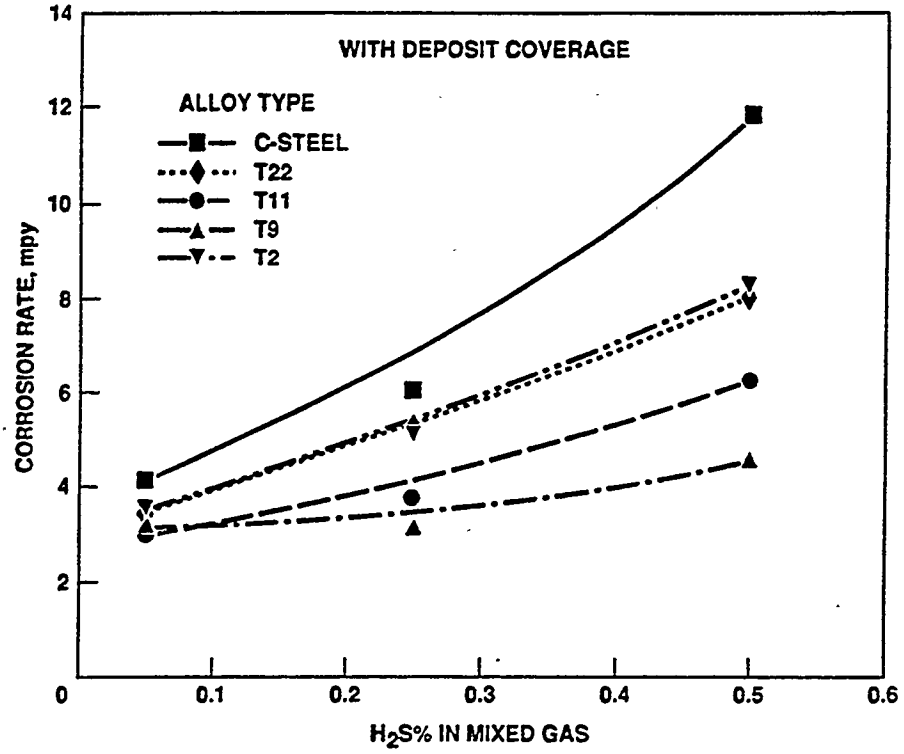

Figure 3-18 Variation of the corrosion rates with H_2S concentration in the mixed gas for the Group-I alloys at 700°F with the coverage of simulated ash deposit

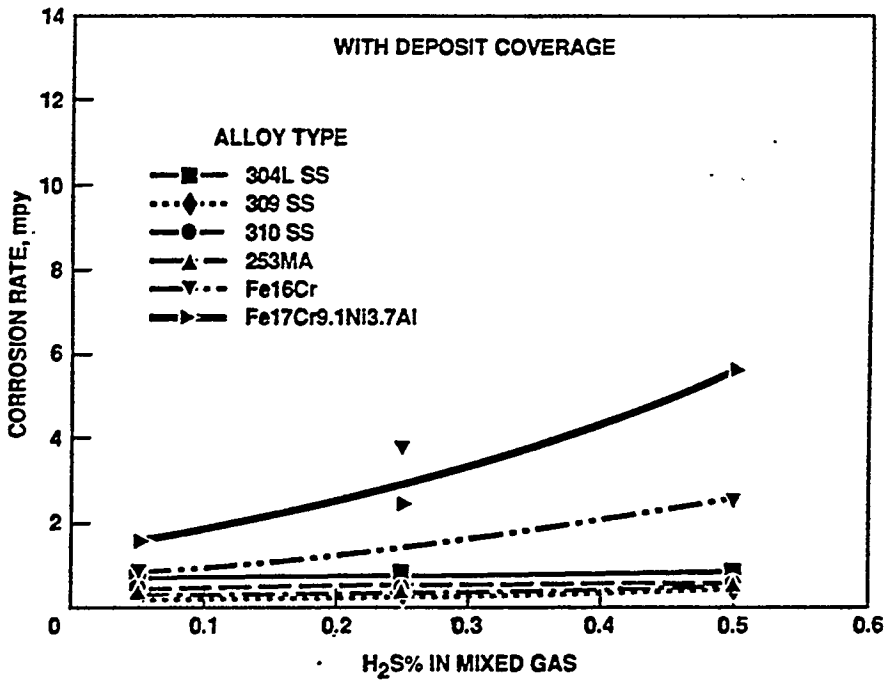

Figure 3-19 Variation of the corrosion rates with H_2S concentration in the mixed gas for the Group-II alloys at 700°F with the coverage of simulated ash deposit

Excellent corrosion resistance of the Group-II high-alloy steels to the simulated reducing combustion environments is once again demonstrated in Figure 3-19. With the ash deposit, the corrosion rates of these alloys fall below 1 mpy at all H_2S levels. Exceptions are the metal-wastage rates for the two free-standing coating materials. Again the higher corrosion rates are associated with the pre-existing defects in the rolled sheets before the exposures.

To understand the corrosion behavior of these alloys within a broader H_2S% range, B&W's previous test data, obtained in mixed gases containing much higher H_2S concentrations, were incorporated in the analysis (Table 3-1). Although limited, these data have extended the corrosion rates up to 5% H_2S in the mixed gas. Using the corrosion data of SA178-A, SA213-T22, SA213-304L, and SA213-310 from the exposures *without* ash deposit at 700°F, Figures 3-20 and 3-21 were constructed.

For carbon and low-alloy steels (Figure 3-20), the variation suggests that a transition in the corrosion rate may occur at an intermediate H_2S concentration, approximately 0.4%. Below 0.4% H_2S, the corrosion rate does not vary significantly with decreasing H_2S concentration in the mixed gas.

Figure 3-21 shows that the corrosion rates of 304SS and 310SS are fairly insensitive to the change of H_2S concentration in the entire H_2S range, and these materials exhibit excellent corrosion resistance to the simulated low-NO_x environments. Essentially, the corrosion rates of these chromia-forming high-alloy steels increase linearly with the concentration of H_2S. The slopes of the variation are very small. Even at 5% H_2S, the corrosion rate is below 1 mpy. Therefore, in the complete range of H_2S concentrations anticipated in the combustion zone of LNCB-retrofitted boilers, the chromia-forming alloys should provide adequate corrosion resistance.

It is noted that the generalizations given above were mostly based on the corrosion data obtained from the laboratory tests conducted at 700°F. A metal temperature of 700°F is quite moderate compared to the highest metal temperature on the waterwalls of modern utility boilers, which is usually in the range of 850° - 900°F. However, this would not be a concern because, based on the measured corrosion data from this laboratory study, mathematic equations are to be developed in the next section. These equations may be used to predict the corrosion rates of alloys exposed to a broad range of temperatures, H_2S%, and Cr% of interests.

3.1.4 Predictive Model Development for Corrosion Rates

Efforts to develop a predictive model capable of simultaneously relating the corrosion rates of alloys to 1) the metal temperature, 2) the H_2S concentration in the flue gas, and 3) the Cr concentration in the alloy are discussed in this section. It is assumed that the corrosion rates of alloys are only functions of the metal temperature, H_2S concentration, and Cr concentration. However, these three functions are independent of each other. Therefore, the following expression for corrosion rate is proposed:

$$\text{C.R.} = f(\text{T}) \times f(\text{H}_2\text{S}) \times f(\text{Cr\%}) \qquad (3\text{-}1)$$

where C.R. is the corrosion rate of any given alloy.

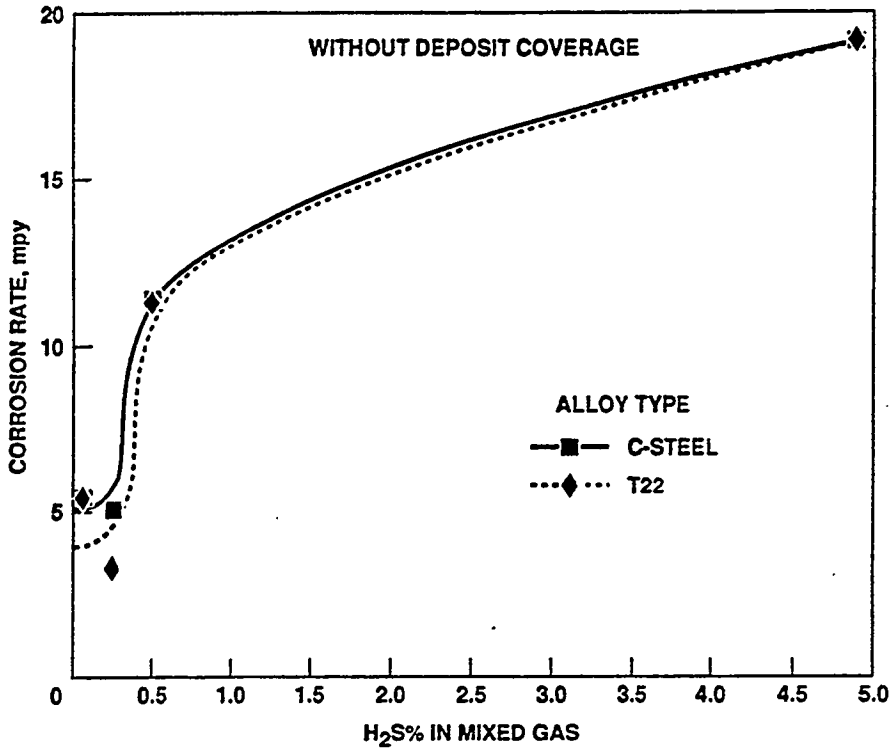

Figure 3-20 Variation of the corrosion rates with H_2S concentration in the mixed gas for SA213-T22 at 700°F without the coverage of simulated ash deposit

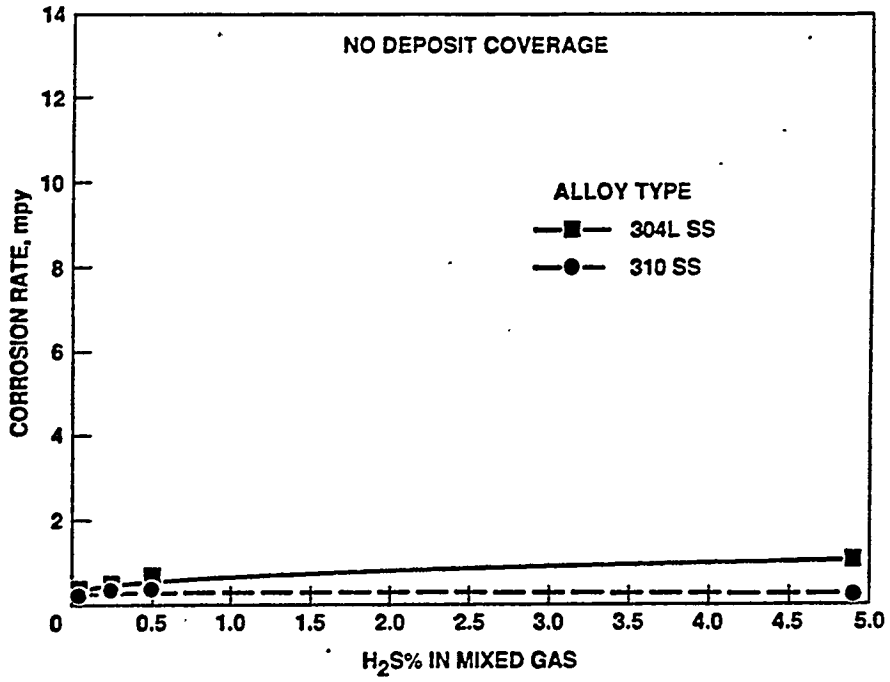

Figure 3-21 Variation of the corrosion rates with H_2S concentration in the mixed gas for SA213-304 and SA213-310 at 700°F without the coverage of simulated ash deposit

Because all corrosion mechanisms are thermally activated, an Arrenius-type relationship can be used to express $f(T)$, i.e.:

$$f(T) = A \times \exp(-E_a / RT) \tag{3-2}$$

where A is a constant, E_a is the activation energy of the corrosion process, R is the gas constant, and T is the absolute metal temperature.

In general, the corrosion rate of alloy is expected to increase with increasing H_2S concentration in the flue gas. However, it is not clear how the change of H_2S concentration affects the corrosion behavior of the boiler alloys, especially in the range anticipated in the combustion zone of LNCB-retrofitted boilers. In other words, the "order" of the corrosion reactions involving H_2S is not known. Therefore, a generic expression for $f(H_2S)$ is given here, i.e.:

$$f(H_2S) = B \times [H_2S]^{\beta} \tag{3-3}$$

where B and β are constants.

Finally, the corrosion rates of alloys would decrease with increasing Cr concentration in the alloys. Such a trend are already demonstrated in Figures 3-14 and 3-15. Again, the improved corrosion resistance from the Cr addition is generally attributed to the higher tendency for chromia-scale formation. Similar to H_2S, the exact relationship between the corrosion rates of alloys and the Cr concentration in the alloys is not known. Therefore, a generic expression is proposed here, i.e.:

$$f(Cr\%) = C / (Cr\% + \gamma)^{\delta} \tag{3-4}$$

where C, γ, and δ are constants. Note that a constant "γ" is introduced here to prevent the value of $f(Cr\%)$ from becoming infinity. In reality, even pure iron exposed to the reducing environments of our investigation will not exhibit an infinite corrosion rate. The addition of constant "γ" therefore provides a ceiling for the corrosion rates of alloys containing very a low Cr%.

Substituting the mathematic expressions of Eqs. 3-2, 3-3, and 3-4 to Eq. 3-1, the corrosion rate of alloy can be represented as:

$$C.R. = \alpha \times \exp(-E_a / RT) \times [H_2S]^{\beta} \times 1 / (Cr\% + \gamma)^{\delta} \tag{3-5}$$

where "α" is a constant having a value of $A \times B \times C$.

If the values of α, β, γ, δ, and E_a are determined, Eq. 3-5 can be used to calculate the corrosion rate of alloy under a condition with known metal temperature, H_2S, and Cr%. To generate the needed constants in Eq. 3-5, the corrosion data in Table 3-1 from the five retort exposures *without* the simulated deposit coverage were used.

The corrosion data in Table 3-1 were chosen because the actual waterwall surfaces in JMSS 4 were covered only with a relatively thin deposit layer, as found in the lower furnace of JMSS 4 during the 1993 Spring outage. The thin deposit coverage on the waterwalls suggest that the deposit-free samples in the

retort tests would better represent the actual field conditions. As mentioned previously, the corrosion rates of alloys in Table 3-2 were reduced possibly due to the overly thick deposit layer acting as a diffusion barrier. Consequently, the use of higher metal wastage rates in Table 3-1 would represent a worse case, thus making the corrosion-rate predictions more conservative.

Similar to the analyses in the previous section, the materials in Table 3-1 were divided into two groups: Group I contains the carbon and low-alloy steels, and Group II includes the high-alloy steels. The two free-standing coating materials were again excluded from Group II. Non-linear regression was performed using a statistical analysis computer program, SAS, to derive the least-square values of these constants. The resulting mathematic expressions for the predictive equations are:

Group I: Carbon and Low-Alloy Steels ($0 \leq$ Cr wt.% ≤ 10)

$$C.R. = 3.2 \times 10^5 \times \exp(-15818 / 1.987T) \times [H_2S]^{0.574} \times 1 / (Cr\% + 10.5)^{1.234} \pm 2.2 \qquad (3\text{-}6)$$

Group II: High-Alloy Steels (Cr wt.% ≥ 16)

$$C.R. = 1.04 \times 10^7 \times \exp(-19230 / 1.987T) \times [H_2S]^{0.29} \times 1 / (Cr\% + 1.40)^{1.37} \pm 1.2 \qquad (3\text{-}7)$$

where C.R. is the corrosion rate of alloy in mpy (mil per year), T is the metal temperature in K, $[H_2S]$ is the H_2S concentration of the flue gas in ppm, and Cr% is the Cr concentration of the alloy in wt.%.

The goodness of fit (or coefficient of determination) for Eq. 3-6 is 93% and for Eq. 3-7 is 70%. The less goodness of fit in Eq. 3-7 may have been attributed to the compositional complication involved in the Group-II alloys, in which other alloying elements must have exhibited noticeable effects on the materials performance. This model development ignored these effects; therefore, a higher degree of uncertainty for the Group-II alloys in Eq. 3-7 is anticipated. Fortunately, because the corrosion rates of the Group-II alloys (Table 3-1) are significantly lower than those of Group-I alloys (Table 3-1), the range of uncertainty becomes relatively small as well. Therefore, the predictive equation of Eq. 3-7 can still be used with reasonable confidence.

Eqs. 3-6 and 3-7 indicate that the activation energy for the Group-II alloys is higher than that of the Group-I alloys. This difference is rational because of the higher tendency for Group-II alloys to form a more protective chromia-base scale on the surfaces than that for Group-I. Both equations are relatively insensitive to the H_2S concentration in the flue gas, again agreeing with the graphic presentations in Section 3.1.3. The low reaction orders of $[H_2S]$ (i.e., constant "β") imply that, under a given condition, the corrosion rates of alloys do not vary significantly with the H_2S concentration in the mixed gas. Both equations are about equally sensitive to constant "δ", although the values of constant "γ" are quite different. Obviously, the difference in constant "γ" is dictated by the ranges of the Cr concentration used in the two equations.

Using the predictive equations of Eqs. 3-6 and 3-7, examples are plotted in Figures 3-22 and 3-23 to demonstrate the corrosion rates of Group-I and Group-II alloys in the mixed gases, respectively. Both figures are in three-dimensional format to illustrate simultaneously the variation of corrosion rates with H_2S concentration in the flue gas and Cr% in the alloys at 850°F. It must be stressed that predictive models are most useful when the ranges of variables are confined to those of actual data points employed

in producing the models. In this case, the H_2S concentration input to Eqs. 3-6 and 3-7 should be confined to 500 - 5000 ppm, Cr concentration to 0 - 30 wt.%, and metal temperature to 500° - 900°F (533 - 755K). The use of input data significantly outside these ranges may lead to large errors.

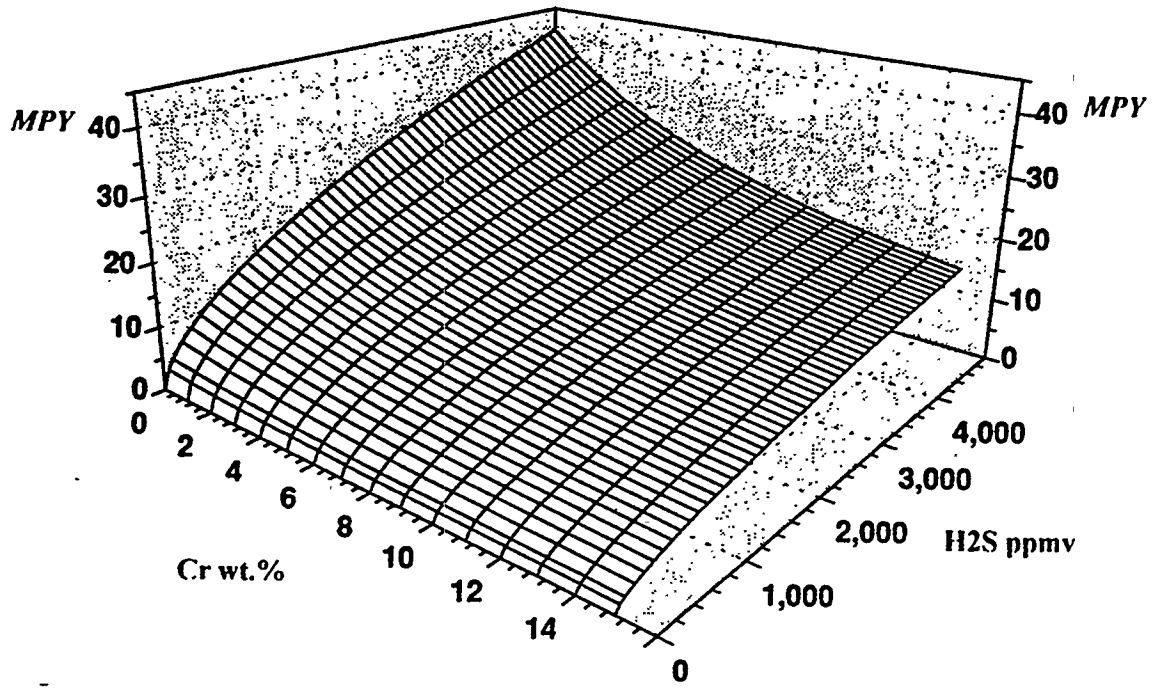

Figure 3-22 Variation of the predicted corrosion rate of alloys containing <15 wt.% Cr with H_2S concentration in the mixed gas and Cr concentration in the alloys at 850°F

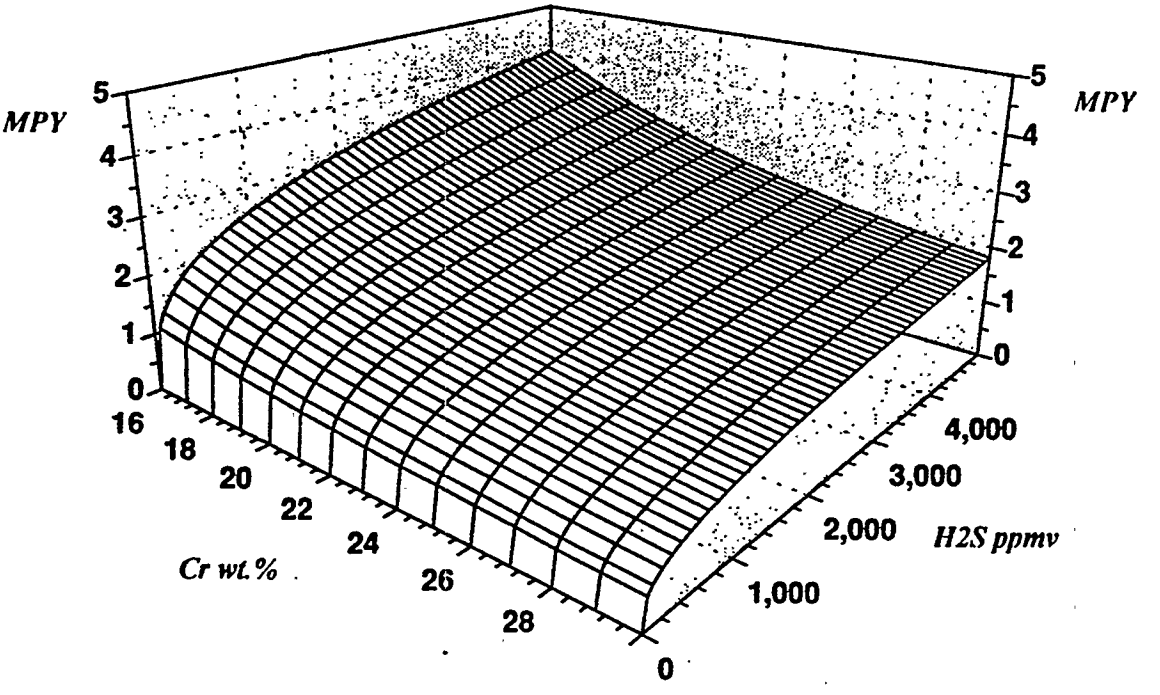

Figure 3-23 Variation of the predicted corrosion rate of alloys containing >16 wt.% Cr with H_2S concentration in the mixed gas and Cr concentration in the alloys at 850°F

The accuracy of these predictive equations, generated solely from the laboratory corrosion test data, will be evaluated in Section 3.3.4 with the field corrosion data determined from the test panel.

3.2 IN-FURNACE PROBING

3.2.1 H_2S Measurements

3.2.1.1 June 1992 Tests. In June 1992, the post-retrofit measurements of H_2S levels were made for Unit 4 of Dayton Power & Light's J. M. Stuart Station (JMSS 4). Measurements were made at the lower burner level through view ports on the west, north, and east walls as well as through corrosion panel ports on the west wall. These measurements were performed at full-load (610 MW) as well as reduced-load (460 MW) operating conditions.

In each view port (note that the north wall's west view port was inaccessible), gas samples were typically taken at 4, 8, 10, 14, and 18 feet into the furnace. For each port on the corrosion panel, samples were extracted at only one position; however within the windbox, 0.5 foot from the furnace.

The H_2S readings were tabulated, and they exhibited substantial spatial variation. H_2S values in the view ports were practically nil (see Table 3-3), and this was supported by the relatively high O_2 values (between 1% and 18%). On the corrosion panel, the H_2S values increased as the sampling location was moved to a higher elevation and southward.

Shown in Table 3-3 are the H_2S as well as CO and O_2 levels during the full-load test condition. Average excess oxygen level at the boiler's economizer outlet was approximately 3.3% at this operating condition. For the corrosion panel, the temporal average H_2S values ranged from less than 20 ppm at the lower left port to 839 ppm at the upper right port. The respective O_2 levels at these two ports varied inversely with H_2S levels as expected — 8.6% and 0.0%. Similarly, the respective CO levels displayed the expected positive correlation with H_2S levels and were 0.42% and 12.7%.

Table 3-4, on the other hand, summarizes gas readings for the reduced-load test condition. For this test condition, the average excess oxygen level at the boiler's economizer outlet was approximately 4.2%. The same spatial trend as for the full-load condition was displayed in the H_2S concentrations. This time, the H_2S levels ranged from 22 ppm at the lower left port to 719 ppm at the upper right port of the corrosion panel. The respective O_2 concentrations were 3.9% and 0.0%, while the CO levels were 0.4% and 10.9%.

3.2.1.2 August 1992 Tests — Burner Optimization Studies. While performing post-retrofit H_2S measurements (June 1992), H_2S concentrations in excess of 200 ppmV were found along the west sidewall of the furnace in the areas measured through the corrosion test panel sample ports. Also, based on data from the post-retrofit burner configuration tests, additional computer modeling was performed and predicted the possibility for high CO concentrations at the west sidewall of the furnace — confirming that furnace conditions conducive to H_2S formation existed. It has been found that CO and H_2S concentrations increase, proportionally, in the furnace when O_2 values approaching zero also exist. Therefore, the emphasis in the optimization study was to minimize H_2S at the west sidewall, as measured through the corrosion test panel taps, without creating undesirable H_2S concentrations elsewhere in the furnace. Modeling results suggested that adjustments to the burners located closest to the corrosion panel (along the west wall) could create a curtain of air to minimize or prevent H_2S formation.

Table 3-3
H_2S DATA — FULL-LOAD CONDITIONS

FULL LOAD TEST CONDITIONS*

PORT I.D.	H2S(ppmV)		O2 (%)	CO (%)
	AVG.	MAX.		
WWNP(A)	<20	<20	10.7 -13.5	0.01 -0.03
EWNP(D)	<20	<20	1.2 -18.1	0.04 -1.2
NWEP(C)	<20	<20	2.8 -6.1	0.08 -2.19
CPLL	<20	<20	8.6	0.42
CPLR	74	105	0.35	5.8
CPUR	839	1015	0.0	12.7
CPUL	68	106	0.05	9.9

LEGEND FOR PORT I.D.

CPLL - Corrosion Port, Lower Left
CPLR - Corrosion Panel, Lower Right
CPUR - Corrosion Panel, Upper Right
CPUL - Corrosion Panel, Lower Right

WWNP(A) - West Wall, North Port
EWNP(D) - East Wall, North Port
NWEP(C) - North Wall, East Port

*Boiler Load 610MW
Excess O2 @ Economizer Outlet - 3.3%

Table 3-4
H_2S DATA — REDUCED-LOAD CONDITIONS

PARTIAL LOAD TEST CONDITIONS*

PORT I.D.	H2S(ppmV)		O2 (%)	CO (%)
	AVG.	MAX.		
WWNP(A)	<20	<20	10.7 -11.5	0.01 -0.02
EWNP(D)	<20	<20	2.6 -15.9	0.08 -0.84
NWEP(C)	<20	<20	N/A	N/A
CPLL	22	32	3.9	0.4
CPLR	294	395	0.04	9.3
CPUR	719	812	0.0	10.9
CPUL	59	103	0.14	9.2

LEGEND FOR PORT I.D.

CPLL - Corrosion Port, Lower Left
CPLR - Corrosion Panel, Lower Right
CPUR - Corrosion Panel, Upper Right
CPUL - Corrosion Panel, Lower Right

WWNP(A) - West Wall, North Port
EWNP(D) - East Wall, North Port
NWEP(C) - North Wall, East Port

*Boiler Load 460MW
Excess O2 @ Economizer Outlet - 4.2%

Since a different coal was used for this testing as compared to the pre- and post-retrofit studies, it was necessary to establish an H_2S baseline before making any burner adjustments. To establish this baseline, H_2S measurements were performed at the four taps of the corrosion test panel, and since the right front test port of the furnace was accessible for this study, the H_2S probe was used through this port.

In a parametric study, lower row burner adjustments were made, and the resultant H_2S concentrations measured at the corrosion test panel taps.

During the optimization study, a switch was made to a lower sulfur coal (0.89%) by Dayton Power and Light. However, a baseline (original burner settings) was not established for this coal.

During post-retrofit and optimization baseline H_2S testing, the upper right corrosion test panel tap (CPUR) consistently had the highest measured H_2S concentrations. By optimizing the burner settings, it was possible to effectively eliminate any measureable H_2S at CPUR. However, this does not suggest that H_2S has been completely eliminated in the furnace.

Listed in Table 3-5 and moving from left to right are the measured H_2S, O_2, and CO values for:

- The four taps of the corrosion test panel during post retrofit testing
- The right front furnace test port and the four taps of the test panel during optimization baseline testing using a higher sulfur coal
- The CPUR at the optimized burner settings using the same higher sulfur coal
- The CPUR during optimization baseline testing using the lower sulfur coal
- The right front furnace test port and the four taps of the test panel at the optimized burner settings using the same lower sulfur coal.

The data are consistent when comparing the H_2S values measured at CPUR to the sulfur content of the three coals at the same burner settings. The H_2S concentration increases as the sulfur content of the coal increases, though not proportionally.

For the higher sulfur coal (1.22%) at the optimized burner settings, the H_2S measured at CPUR was reduced to <20 ppmV as compared to 1653 ppmV for the original post-retrofit burner settings. Similarly, for the lower sulfur coal (0.89%), the H_2S concentration was reduced from 585 ppmV to <20 ppmV.

However, when looking at the H_2S values at the optimized burner settings for the lower sulfur coal, H_2S (95 ppmV) was still detected at the lower right tap of the test panel. This may suggest that instead of eliminating H_2S entirely in the furnace, the high H_2S zone has been redirected to a lower area in the furnace. This is reinforced by the fact that when the H_2S probe was used through the right front furnace test port, appreciable concentrations of H_2S (>200 ppmV) were measured at several locations along the right sidewall of the furnace.

3.2.1.3 March 1993 Tests — Long-Term Optimization Studies. In August 1992, H_2S levels were minimized in the furnace by adjusting burner settings to achieve optimum performance. At that time, the test panel ports, specifically the upper right port (CPUR), were selected as the test locations for monitoring to determine when H_2S concentrations had reached a minimum in the furnace. The purpose of March 1993 testing was to determine if any significant changes had occurred in the H_2S concentrations at the

various test port locations since August 1992. Also, this testing provided additional confidence as to the concentration range of H_2S the external tube surfaces of the test panel were exposed to just prior to its removal for metallurgical examination.

H_2S was measured with the sampling probe through the north wall, west port (NWWP(B)) in order to measure the H_2S concentrations at the same distances into the furnace along the west sidewall as in August 1992. Also with the sampling probe, H_2S was measured through the north wall, east port (NWEP(C)) (measuring H_2S along the east sidewall) and the west wall, north port (WWNP(A)) (measuring H_2S along the right front wall). Coal samples were collected for analysis each day from crushed coal feeder "D" which supplies coal to the burner functioning at the boiler's northwest corner and therefore along the corrosion panel. These samples were analyzed for their sulfur, moisture, and Btu content to document coal composition during the test period.

Listed in Table 3-6 are the H_2S, O_2, and CO concentrations measured at the optimized burner settings through the NWWP(B) and the CORRTP comparing August 1992 to March 1993 data. The March 1993 data shows overall increases in H_2S concentrations compared to August 1992 data.

In prior discussions of the August 1992 data, it was mentioned as a possibility that the H_2S zone had merely been pushed lower into the furnace after the burner settings were changed. One of the known differences in JMSS 4 that did not exist during August 1992 was the fact that the right air heater was partially plugged. Due to this situation, there is the possibility that the reducing zone was relocated higher in the furnace again.

Also listed in Table 3-6 are the H_2S concentrations measured through the four ports of the test panel and the NWWP(B) at full and reduced boiler loads in March 1993. The data show at reduced load a decrease in H_2S concentrations at the two test panel ports (CPUR and CPLR) where H_2S was detected. For the NWWP(B) at reduced load, H_2S concentrations decreased at the 8-foot and 12-foot distances into the furnace. However, at the 16-foot and 18-foot distances, the H_2S concentrations remained essentially unchanged.

Finally, listed in the table (Table 3-6) are the H_2S concentrations measured through the north wall, east port (NWEP(C)) and west wall, north port (WWNP(A)) using the sampling probe. These ports were tested to verify that H_2S concentrations had not changed at locations in the furnace away from the test panel — the primary area of interest. No H_2S was detected (<20 ppmV) at any of the distances into the furnace through WWNP(A); this is consistent with the June 1992 results. However, difficulties were encountered when trying to measure H_2S concentrations through NWEP(C). There was a problem of repeated pluggage of the probe tip in less than 10 minutes once the sampling probe was inserted to a distance of 14 feet into the furnace. The buildup of particles on the probe tip resembled soot rather than the usual coal ash. When the sampling probe was retracted from the furnace, a sooty buildup could be seen on the outside of the probe that corresponded to the distance of 14 to 18 feet inside the furnace. Prior to March 1993 testing, <20 ppmV H_2S was measured at all distances into the furnace through NWEP(C), but 45 and 163 ppmV H_2S were measured at the 14 feet and 16 feet distances into the furnace, respectively, during March 1993.

Table 3-5
MEASURED H_2S, O_2 AND CO PRIOR TO MAKING BURNER ADJUSTMENT AND OPTIMIZING SETTINGS
(Shaded Areas)

		Sulfur, % Dry = 0.91 (6/92)			*Sulfur, % Dry = 1.22 (8/19/92)*						*Sulfur, % Dry = .89 (8/20/92)*					
Port I.D.	Probe Distance Into Furnace, Ft.	H_2S (ppmV) AVG.	O_2 (%) AVG.	CO (%) AVG.	H_2S (ppmV) AVG.	O_2 (%) AVG.	CO (%) AVG.	H_2S (ppmV) AVG.	O_2 (%) AVG.	CO (%) AVG.	H_2S (ppmV) AVG.	O_2 (%) AVG.	CO (%) AVG.	H_2S (ppmV) AVG.	O_2 (%) AVG.	CO (%) AVG.
NWWP(B)																
	4				<20	9.6	0.15							<20	3.30	0.81
	8				952	0.13	11.63							468	0.43	6.3
	12				784	0.13	11.28							824	2.15	9.7
	16				382	0.0	8.6							311	0.96	7.05
	18				70	0.6	5.1							63	0.3	3.25
CPLL		<20	8.1	0.3	<20	6.8	0.54				—			<20	0.96	1.11
CPUL		72	0.0	10.7	55	0.0	6.18				—			<20	4.9	0.38
CPLR		74	0.0	6.5	258	0.22	6.75				—			95	0.07	0.0
CPUR		841	0.0	13.0	1653	0.0	13.03	<20	0.63	1.61	585	0.0	14.0	<20	1.1	1.41

Table 3-6
MEASURED H_2S, O_2, AND CO AT OPTIMIZED BURNER SETTINGS — FULL LOAD AND REDUCED LOAD
(Shaded Areas)

		Sulfur, % Dry = 0.89 (8/20/92)			*Sulfur, % Dry = 0.84 (3/22/93)*			*Sulfur, % Dry = 1.15 (3/30/93)*					*Sulfur, % Dry = 0.96 (3/24/93)*		
Port I.D.	Probe Distance Into Furnace, Ft.	H_2S (ppmV) AVG.	O_2 (%) AVG.	CO (%) AVG.	H_2S (ppmV) AVG.	O_2 (%) AVG.	CO (%) AVG.	H_2S	O_2	CO	Port I.D.	Probe Distance Into Furnace, Ft.	H_2S (ppmV) AVG.	O_2 (%) AVG.	CO (%) AVG.
NWWP (B)	4	<20	3.30	0.81	<20	3.42	0.32	<20	7.94	0.07	NWEP (C)	4	<20	2.21	0.32
	8	468	0.63	5.76	36	1.63	1.85	<20	2.22	1.17		6	<20	3.34	0.31
	12	524	2.13	8.38	1067	0.48	8.56	553	0.18	5.81		8	<20	2.72	1.17
	16	211	0.98	7.05	1068	2.56	8.62	1053	0.21	7.52		10	<20	4.17	0.47
	18	63	0.9	3.25	656	3.24	6.80	665	0.31	7.52		12	<20	3.70	0.53
												14	45	0.30	4.52
												16	163	0.19	9.68
					Sulfur, % Dry = 1.10 (3/23/93)			*Sulfur, % Dry = 1.15 (3/26/93)*					*Sulfur, % Dry = 1.25 3/25/93*		
CPLL		<20	0.98	1.11	<20	0.62	1.53	<20	0.62	1.53	WWNP (A)	2	<20	6.10	0.07
CPUL		<20	4.9	0.38	<20	3.29	0.95	<20	6.92	0.23		4	<20	6.70	0.01
CPLR		95	0.07	8.0	569	0.10	8.15	478	0.08	8.27		6	<20	6.49	0.06
CPUR		<20	1.1	1.41	258	0.14	6.95	25	0.16	4.55		8	<20	7.13	0.03
												10	<20	8.60	0.03
												12	<20	7.92	0.02
												14	<20	7.50	0.02
												16	<20	7.55	0.01
												18	<20	7.30	0.03

3.3 FIELD TEST AT DP&L JMSS 4

Waterwall segments approximately 6 inches long from across the top and bottom portions of the test panel were removed during the April 1993 outage. These segments were sent to B&W's Alliance Research Center (ARC) for metallographic examinations. The primary reason for retrieving the waterwall samples from these locations was that some H_2S% and metal temperature data were measured through the sampling ports and chordal thermocouples on the test panel during the long-term test. Therefore, the metal wastage at these elevations could be better correlated to the corrosive environments. The tube sample numbers were identified according to the tube location on the test panel. Both thickness-loss measurement and cross-sectional metallograph were performed to determine the metal wastage and corrosion performance of the bare T2 and coated T2 tube samples.

3.3.1 Determination of the Metal Loss on Test Panel

To obtain the needed metal-wastage information, three approaches were investigated:

1) Theoretically converting the thickness of the corrosion products back to the metal loss
2) Calculating the differences in the wall thickness on the fireside before and after the corrosion exposure
3) Determining the differences in the ODs before and after the exposure

It was found that approach 1) was not practical because some corrosion products had been lost from the tube surfaces during the long-term test, and therefore could not be accounted for properly. Approach 2) was limited by the large variation in the initial wall thickness, primarily due to the IDs not being round and/or centered. In comparison, the initial T2 tubing ODs were much more uniform. Therefore, the third approach was adopted.

Measurements of the corrosion wastage were determined statistically by the OD changes before and after the 15-month long-term exposure. The original ODs were determined from the archived tube segments cut off from the test panel prior to the panel installation in JMSS 4. The final ODs were measured from the exposed panel samples after the long-term test. The OD measurements were performed by first sandblasting the tube surfaces both on the fireside and windbox side, followed by the OD measurements with a digital micrometer at different tube positions (without hitting the membranes). Extreme care was taken to assure the achievement of an identical sandblasted surface condition. The same technician and equipment were used to perform these tasks.

It should be stressed that the use of statistical approach is essential for this type of field studies. Some variations in the tube ODs are always present. Only the statistic analysis can eliminate or minimize these pre-existing variations. Consequently, the comparison of statistically determined "mean" OD values should better reflect the true metal wastage.

Figures 3-24 and 3-25 show the measured ODs of bare T2 tubing and chromized T2 tubing from the top and bottom locations of the test panel across the test panel. At least seven OD measurements from each tube sample were obtained for each data point. The ranges of variations are indicated by the range bars and their mean values are given by the filled circles.

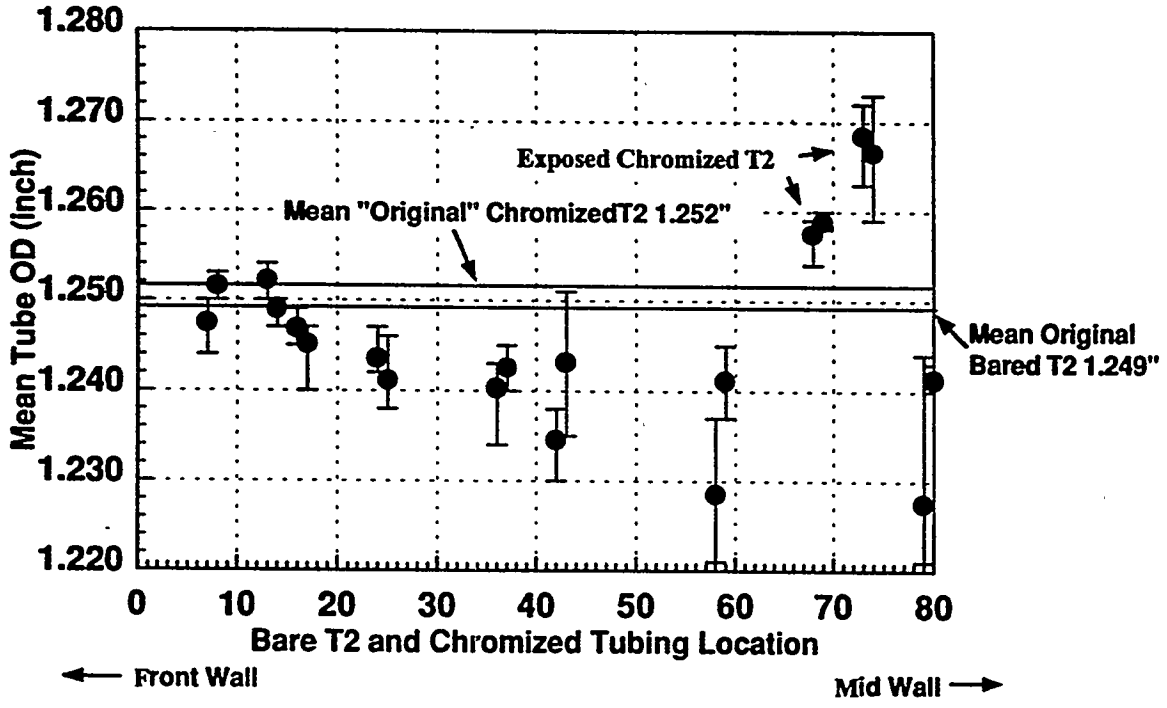

Figure 3-24 Statistical OD values of bare T2 and chromized T2 tube samples from the top segment of the test panel

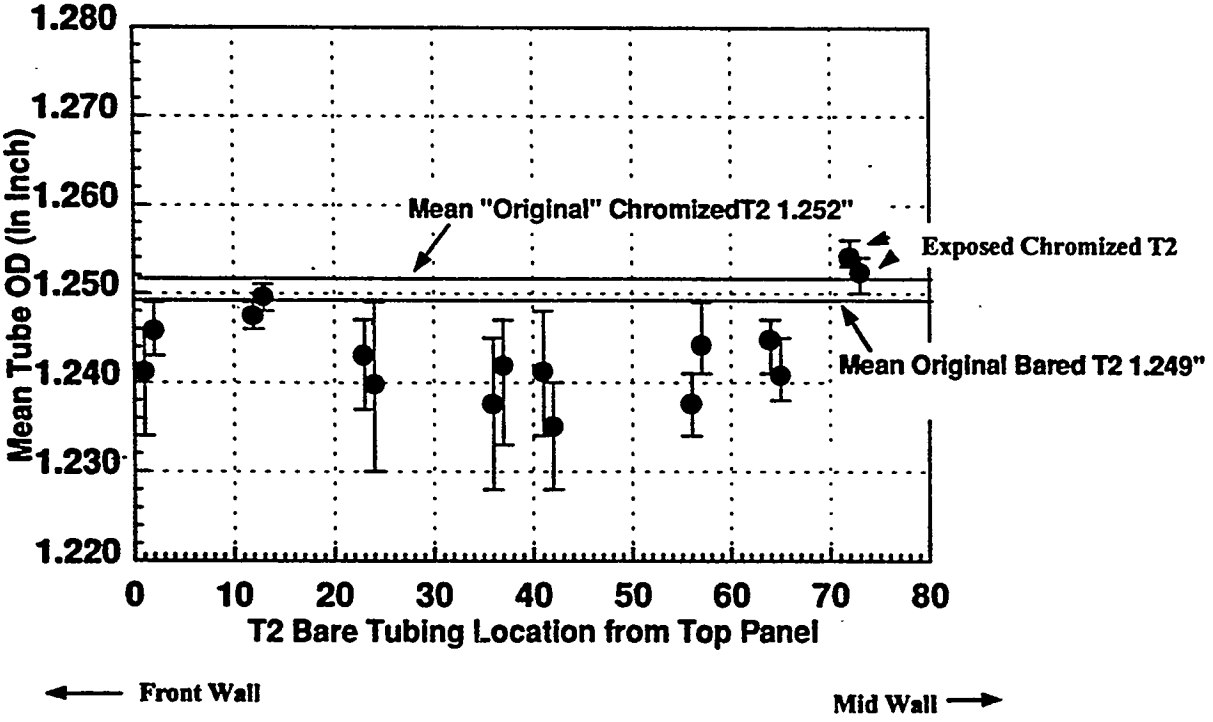

Figure 3-25 Statistical OD values of bare T2 and chromized T2 tube samples from the bottom segment of the test panel

The original "mean" ODs of the bare T2 and chromized T2 tubes are also shown in Figures 3-24 and 3-25 by the two horizontal lines. The original OD value for the chromized T2 was obtained from using the same statistical approach mentioned above, based on the archived chromized T2 panel segment. As discussed previously, the thickness of as-finished chromizing coating was not uniform, and the difference varied up to 10 mils (because of the geometry of the chromizing process, the coating thickness toward the ends of the finished products is usually the thinnest). Since the archieved samples were from an end piece of the chromized segment, it is expected that the "original" mean OD thickness of 1.252 inches in Figures 3-24 and 3-25 represents the minimum OD value for the chromized samples.

Cross-sectional metallographic examinations revealed that the maximum metal wastage of the bare T2 tubing *on the windbox side* was ~1 mil. This wastage was caused primarily by oxidation from the heated air in the windbox. Therefore, the net corrosion wastage on the fireside of a given tube sample is equalevent to the difference in the mean OD values before and after the 15-month field exposure minus 1 mil. Note that only the chromizing coating was applied on both sides of the waterwall surface, and all other coatings had bare T2 on the windbox side. It can be reasonably assumed that the metal loss on the windbox side of the chromized T2 was negligible; thus, no correction was implemented.

Figures 3-26 and 3-27 show the resulting thickness loss of the bare T2 tubing with the tube location. Near the top of the test panel (Figure 3-26), the metal loss varies from approximately zero to 14 mils, with the maximum loss located near Tube 42. On the other hand, the metal loss of the bottom panel (Figure 3-27) ranges from approximately zero to 21 mils, with the maximum loss on Tubes 60 - 80. It is also noted that the metal wastage between two adjacent tubes are different. This difference can be attributed to the fact that JMSS 4 is a two-pass furnace. The metal temperature of the second pass is hotter than that of the first; therefore, the corrosion rate should be higher accordingly.

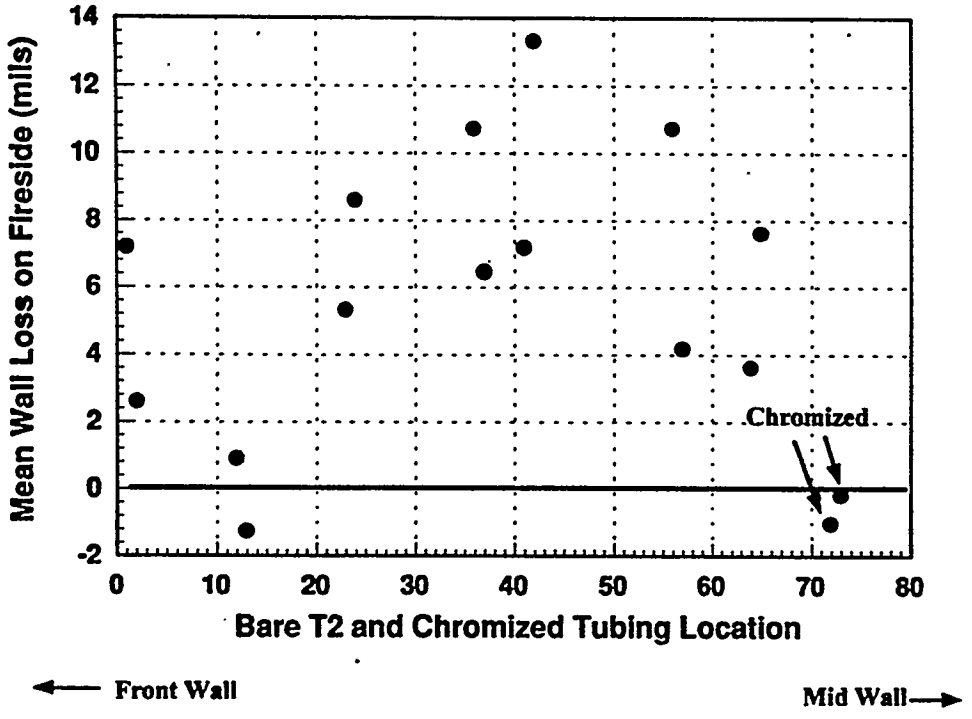

Figure 3-26 Thickness loss of bare T2 tubing along the top segment of the corrosion test panel

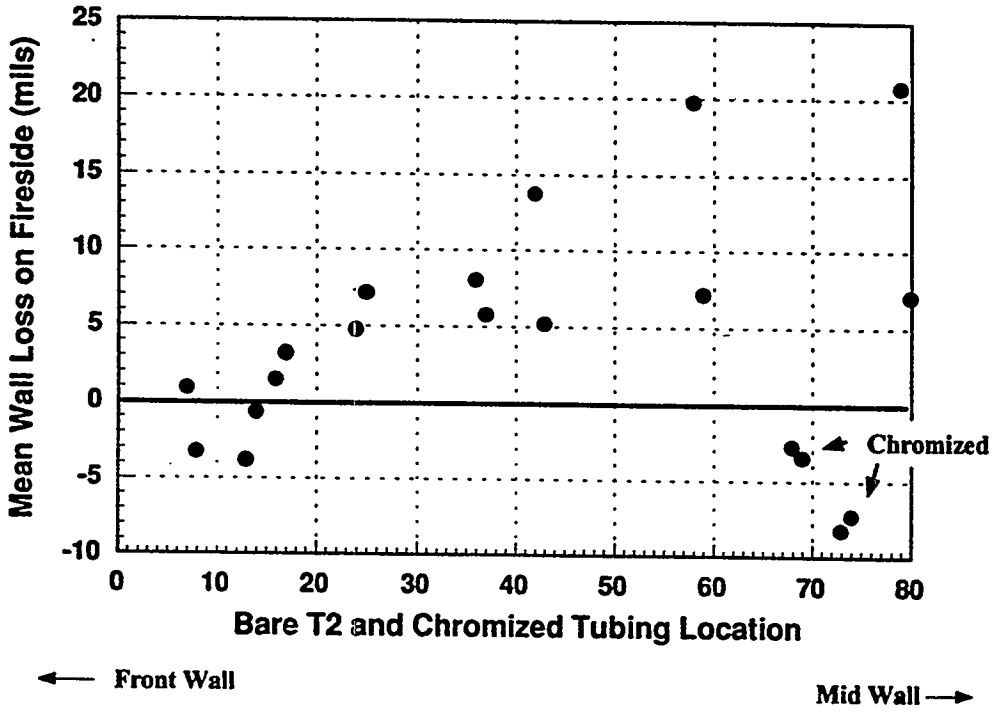

Figure 3-27 Thickness loss of bare T2 tubing along the bottom segment of the corrosion test panel

The mean ODs of the chromized T2 after the field test appear to be thicker than that of the archived samples (1.252 inches). The differences ranges from zero to 16 mils (i.e., 8 mils thicker on one side of the tubing). As mentioned previously, the thickness increase was related to the large variation in the thickness of the as-finished chromizing products. From these data, it can at least be concluded that the chromizing coating shows no sign of metal wastage.

Similar comparison on the ODs of the other coating systems could be easily made due to their extreme roughness on the coated surfaces. Therefore, they are qualitatively evaluated by cross-sectional metallographic analysis.

3.3.2 Metallographic Examination of the Field Exposed Samples

Figure 3-28 is a cross-sectional SEM micrograph of an exposed T2 sample from the test panel. The surface morphology contains a thick corrosion product layer covered with ash deposit. EDX analysis indicated that the corrosion product was primarily iron sulfide with a trace amount of oxide. The formation of a sulfide-rich corrosion product on T2 agrees well with those found in the laboratory study. Therefore, metallographic examinations have confirmed that sulfidation was the predominant corrosion mechanism operating on T2 under the reducing boiler environments.

Unlike the laboratory tests, the surface scale on T2 does not exhibit an apparent multi-layered structure. The growth of a multi-layered sulfide structure usually requires simultaneous inward and outward diffusion of mobile species, such as iron and sulfur. It is likely that the outward growth of sulfide has penetrated into the deposit layer and consequently trapped the deposit in the structure. It is noted that, in the

laboratory study, the simulated ash deposit was loosely placed on top of the sample surfaces; therefore, the loose deposit might not have disturbed the outward growth of iron sulfide. This again implies that the laboratory simulation for the presence of ash deposit was not completely adequate compared to the field condition.

Figures 3-29 through 3-32 show the cross-sectional SEM micrographs of the coated samples from the test panel after the 15-month exposure in JMSS 4. All of the coatings suffered minimal corrosion attack on the coating surfaces, and the wastage was much lower than those on the bare T2. The Al-sprayed coating contains oxide stringers throughout the coating layer, similar to those discussed in the laboratory study. Sulfur was detected in the stringers by EDX. As mentioned previously, these oxide stringers may serve as short circuits for sulfur penetration and lead to localized waterwall failures. Therefore, these stringers should be considered as coating defects. Consequently, Al-sprayed coating is not a desirable choice for applications in boilers where reducing flue gas is expected.

The metal wastage of the two weld-overlaid coatings are essentially negligible. Like the Group-II alloys in Table 2-1, this high corrosion resistance is attributed to the coating's ability to form a chromia-base scale on the outer surfaces. Both of these weld-overlaid layers on T2 are dense and free of structural defects. Therefore, they would not suffer from localized corrosion attack as those of thermal sprayed coatings. The laboratory tests in the present study have already demonstrated that the formation of chromia-base scale can reduce the corrosion rates of alloys to an acceptable level for the low-NO_x applications.

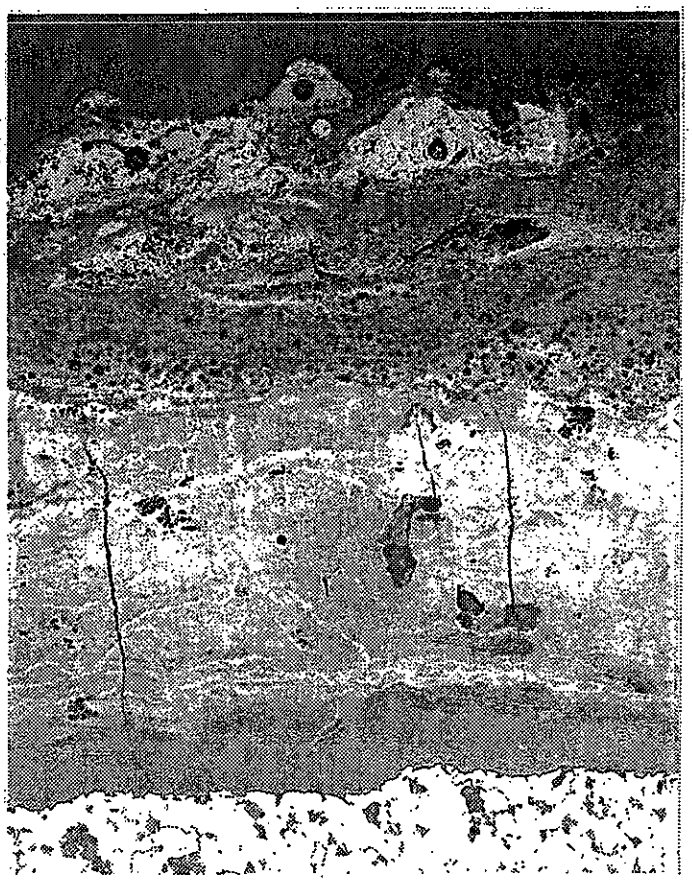

Figure 3-28 Cross-sectional SEM micrograph of a T2 tube sample from the corrosion test panel

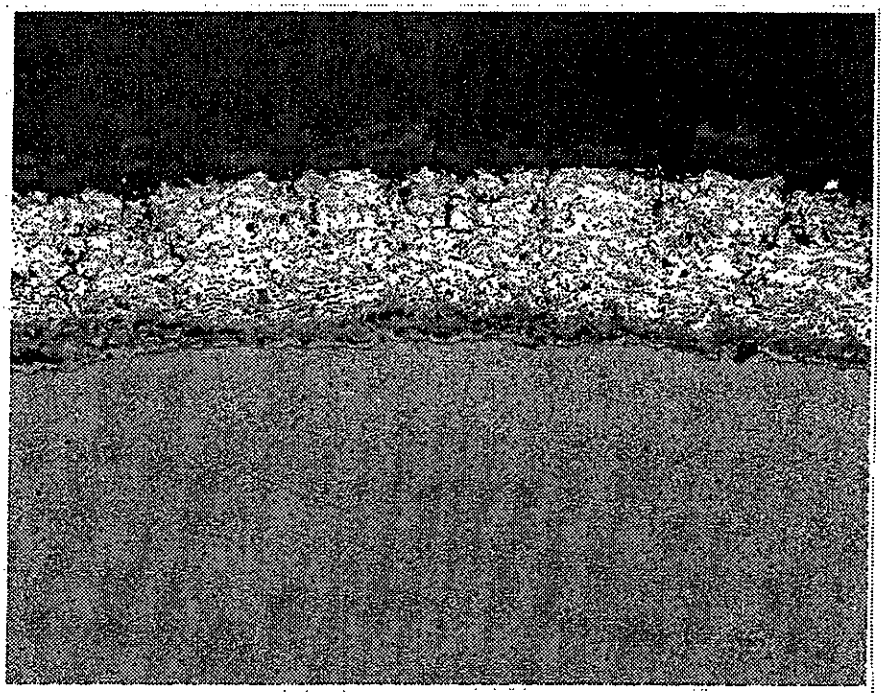

Figure 3-29 Cross-sectional SEM micrograph of an Al-sprayed T2 sample from the corrosion test panel after a 15-month field exposure in JMSS 4

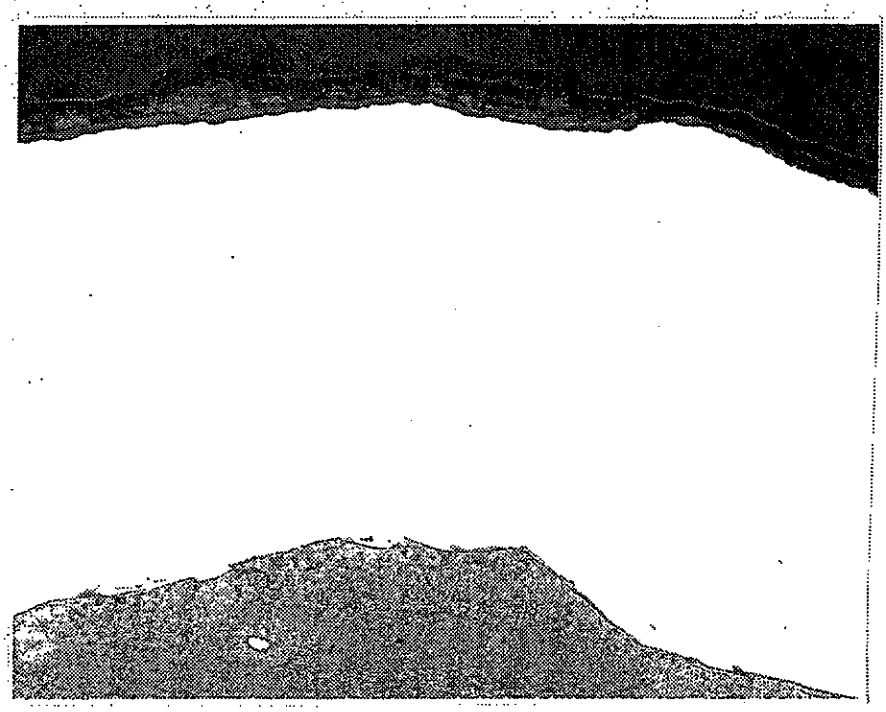

Figure 3-30 Cross-sectional SEM micrograph of a 308L weld-overlaid T2 sample from the corrosion test panel after a 15-month field exposure in JMSS 4

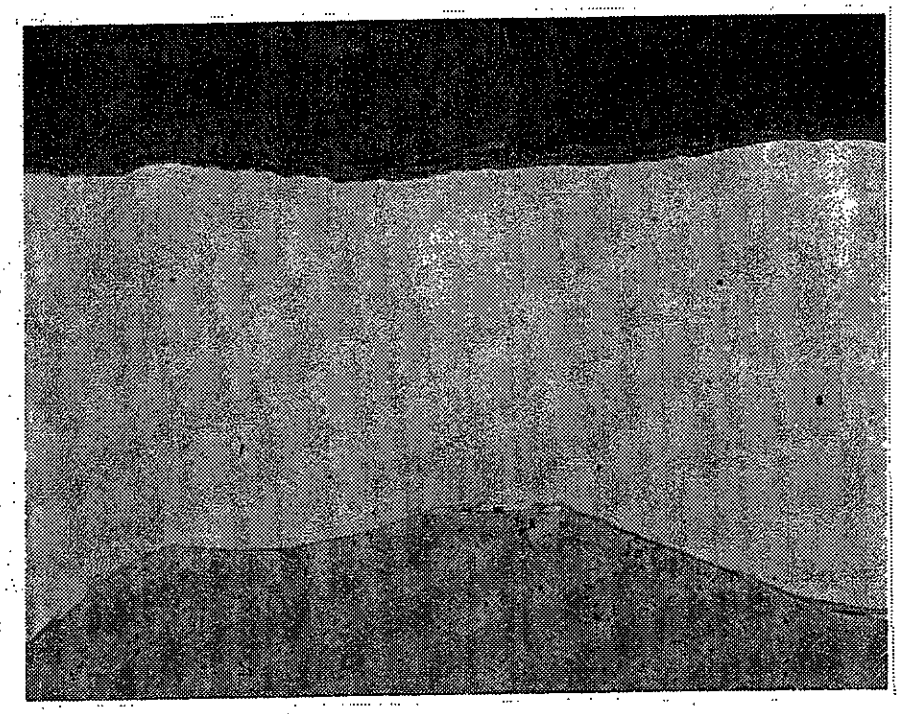

Figure 3-31 Cross-sectional SEM micrograph of a 309L weld-overlaid T2 sample from the corrosion test panel after a 15-month field exposure in JMSS 4

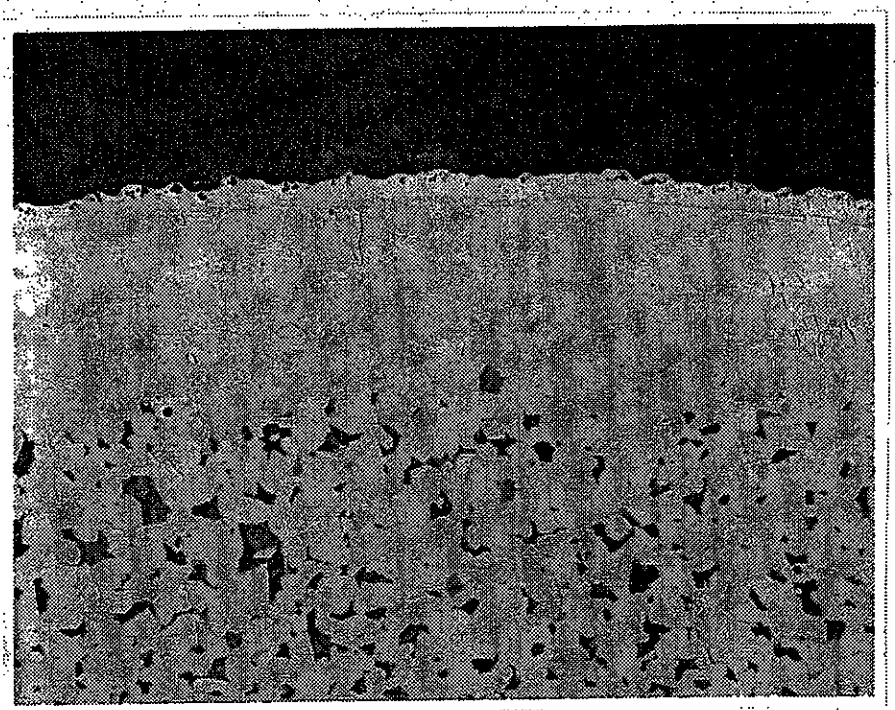

Figure 3-32 Cross-sectional SEM micrograph of a chromized T2 sample from the corrosion test panel after a 15-month field exposure in JMSS 4

Like the weld-overlaid materials, the chromizing coating also exihibits excellent corrosion resistance to the sulfidation attack in JMSS 4. After the 15-month exposure, even the thin, porous chromium carbide outer layer is still found intact on the surface. It appears that the carbide layer is capable of forming the needed chromia scale. As a result, the underlying Cr-rich diffusion zone was not degraded at all by the combustion environments in JMSS 4. This means that the coating may continue to provide adequate corrosion resistance even after the chromium carbide layer is consumed. Overall, the chromizing coating is capable of offering excellent corrosion resistance in boilers where reducing gases are present.

3.3.3 Comparison of Metal Wastage With the Predictive Equations

The sampling ports and chordal thermocouples were only located near the four corners of the test panel. Therefore, the H_2S% and temperature variations across the entire test panel were not available. In addition, many time-dependent variables at JMSS 4 could not be accurately accounted for in this analysis. For example, the gas composition and metal temperature may have varied as a result of boiler operational changes, such as full/partial load changes, coal switching, etc. Consequently, the following analysis assumes that the measured H_2S and metal temperatures were time averaged and were typical for the sulfur level in coal.

The average sulfur content burned in JMSS 4 reported by DP&L was 1.3 wt.%. This sulfur content is most comparable to the coal burned on 8/19/93 (see Tables 3-5 and 3-6) during the probing activities. Therefore, the [H_2S] and tube metal temperatures measured on 8/19/93 in the lower furnace of JMSS 4 were used for this prediction, i.e., the highest H_2S% was 1653 ppm existing at the upper level of the test panel and the highest metal temperature was 816°F. As indicated before, this waterwall surface condition may shift to different locations with time due to changes in boiler operations. As a first approximation, these two values are assumed to be the time-averaged worst case.

Using the predictive equation (Eq. 3-6) and a Cr% of 0.72 for bare T2 tubing (composition in Table 2-1), a corrosion rate of 15 mils per year was calculated. Based on an approximately 15 months exposure period of the test panel, a maximum metal loss of 19 mils was arrived. This estimated maximum metal wastage for T2 agrees fairly well with the worst metal loss shown in Figure 3-27 on the bottom panel. As mentioned before, the equation was derived from the laboratory data without the coverage of an ash deposit and thus, should be used to predict the worst corrosion wastage for a given condition (i.e., T, H_2S%, and Cr%).

Figures 3-33 and 3-34 show the variations of corrosion rates of SA213-T2 in mils per year (mpy) with the tubing location on the test panel. The corrosion rates were calculated based on the measured metal wastage on the fireside and the exposure time. These figures allow direct comparisons of the worst metal wastage rate of T2 on the test panel with the prediction equations developed.

3.3.4 Applicability of the Predictive Equations

The predictive equations were generated using only the results from the laboratory retort tests. When applying these equations to actual boiler environments, the following must be kept in mind. First, it is not always possible to completely simulate the actual boiler environments in laboratory studies. For example, materials tested in the laboratory studies are subjected to simulated gases and deposits, but usually not to any thermal cycling, mechanical stress, and thermal fatigue. It is recognized that these additional factors

commonly existing in boilers can further escalate the metal wastage. Secondly, it is also difficult in the laboratory tests to duplicate the deposit chemistry and its optimal thickness condensed on boiler tubes. As mentioned previously, the deposit chemistry simulated in this laboratory study was derived from thermodynamic calculations based on the assumption of complete system equilibrium on the furnace walls. In addition, the test times employed in the laboratory studies are often insufficient for predicting long-term corrosion behavior.

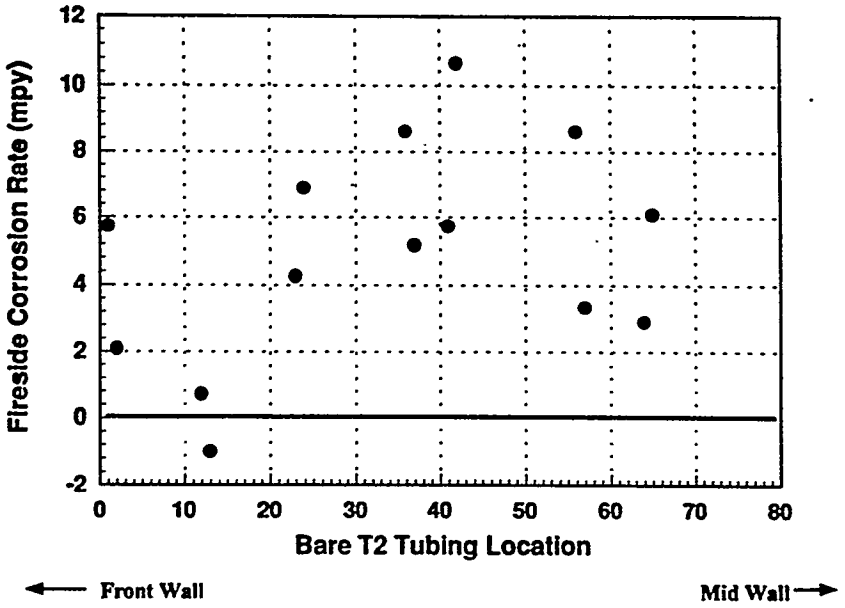

Figure 3-33 Corrosion rate of bare T2 tubing across the top segment of the test panel using the measured metal wastage and exposure time

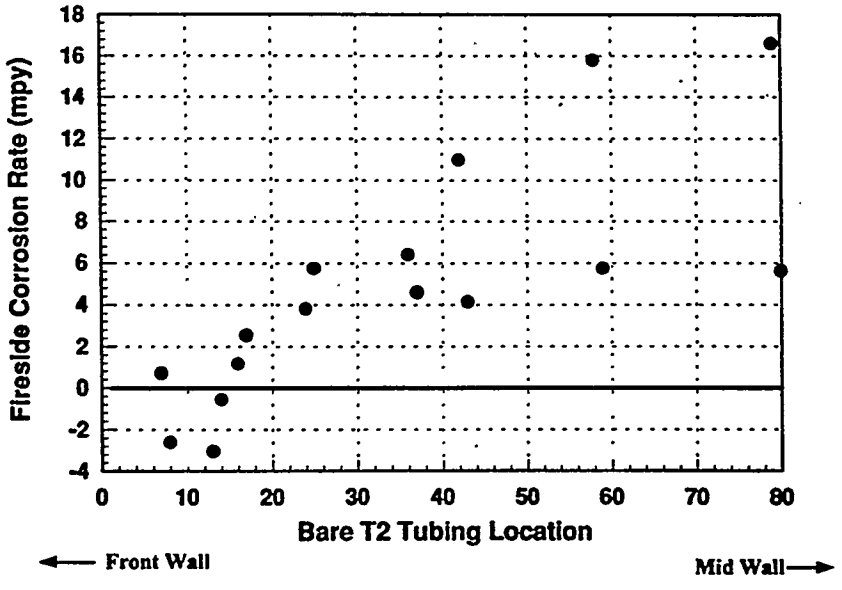

Figure 3-34 Corrosion rate of bare T2 tubing across the bottom segment of the test panel using the measured metal wastage and exposure time

The predictive equations are also generated using the laboratory data without the coverage of the simulated deposit. By using the laboratory corrosion data without the deposit coverage, it assumes that the metal wastage is primarily caused by the gas-solid reactions, and that the thin deposit layer does not participate in the corrosion processes significantly. The cross-sectional metallographic examinations on the field samples do suggest that no melting of the surface deposit has occurred. Therefore, the waterwall materials should not have suffered from the type of accelerated wastage usually associated with molten coal ash. Furthermore, the coverage of a solid deposit layer on the waterwalls, presumably porous as well, would not significantly impede the transport of the corrosive gaseous species. Therefore, the assumption for gas-solid reactions to dominate the corrosion mechanism is probably reasonable. Consequently, the use of the corrosion data from the laboratory study without the simulated deposit coverage should better reflect the actual boiler conditions than those with a thick deposit coverage.

On the other hand, the laboratory tests usually involve exposure of the samples to the worst possible field condition without any compositional fluctuations. In other words, the samples are subjected to the simulated corrosion environment at its maximum strength constantly for the entire test period. However, the corrosivity of the furnace gas in actual boilers tends to fluctuate with time, often reduces from its worst condition. The fluctuations can be caused by various operation changes, such as coal switching and load alteration. Based on this consideration, the corrosion rates of alloys obtained from the laboratory tests should represent the worst case compared to those from the field with compositional fluctuations.

Therefore, the absence of thermal cycling, mechanical stress, and thermal fatigue in the laboratory studies can be offset by the presence of maximum corrosivity in the laboratory condition. The good agreement found in the present study between 1) the metal wastage of T2 calculated from the predictive equation and 2) the metal wastage determined from the test panel is probably attributed to this offset. That is, the two conflicting effects are essentially balanced out. As a result, the 1000-hour laboratory data can reasonably indicate the worst metal wastage in the lower furnace of JMSS 4 after a 15-month operation. However, it is not clear if these equations are equally applicable for predicting the metal loss after longer service times. Therefore, field tests greater than 15 months to verify the applicability of these predictive equations are essential. Such a verification can be achieved by continuing examinations of the existing test panel in JMSS 4, and perhaps evaluation of more furnace wall areas, during the next few outages.

3.3.5 Ultrasonic Thickness Measurement

B&W performed ultrasonic thickness (UT) measurement surveys on the lower furnace walls of JMSS 4 during last three scheduled outages — April 1990, November 1991, and April 1993. The first UT test was conducted in April 1990 to determine the baseline condition of the waterwall tubes prior to the LNCB retrofit. The UT data were taken at several elevations, ranging from 578' -2" (3' - 0" below the center line of lower bottom burners) to 618' -10" (21' - 4" above the upper top burners). Therefore, the range of the UT measurements should have sufficiently covered the entire burner zone. Results of the UT measurements indicated that the majority of the inspected tubes were in relatively good condition. However, significant tube thinning was found on the west side wall at the 583' - 2" elevation. This elevation was in between the upper and lower bottom cell burners. Specifically, Tubes 195 and 205 (counting from left to right inside the boiler) had remaining tube thicknesses at 170 and 160 mils, respectively. These thicknesses were approaching B&W's flagpoint for repair/replacement. Similar tube thickness data were also documented in DP&L's 1990 Plant Betterment Inspection Report, in which UT testing was performed by a DP&L contractor independent of B&W's work.

The severe tube thinning found in this region suggested that reducing combustion gas might have existed locally adjacent to the waterwall surfaces. Although tube thinning in other areas of furnace walls was not as severe, noticeable metal loss was evident at localized locations. As a result, DP&L replaced some of the waterwall tubes in the April 1990 outage.

During the LNCB retrofit outage in November 1991, a series of UT measurements were again performed at various locations. Figure 3-35 shows the exact elevations and locations that the UT measurements were conducted. The measurements included eight furnace bands and twelve points around each burner cell. In addition, after the test panel installation, UT data were also obtained from the test panel at six elevations, ranging from 578' -6¾" to 590' -5¾" at approximately 2-foot intervals. When possible, five UT readings were taken at each location of a given elevation. The five readings were positioned at a 1/2-inch interval, with the center point at the elevation specified. To identify the exact locations tested, the center point of each location was marked with a "B" using a low stress stamp.

The 1991 UT test, in general, did not find any waterwall tubes with remaining wall thickness significantly approaching the flagpoint for replacement in the combustion zone of JMSS 4. Some noticeable tube wastage was found on the rear wall around the cell burners. However, their remaining wall thicknesses were still approximately 215 mils, only slightly less than the minimum wall thickness of 220 mils. It must be pointed out that the actual wall thickness of boiler tubes is typically 20% thicker than the specified minimum. Therefore, the initial wall thickness might have been approximately 264 mils. As a result, significant corrosion attack had occurred on the rear wall between the 1990 and 1991 outages, even thought the remaining wall thickness was still 215 mils.

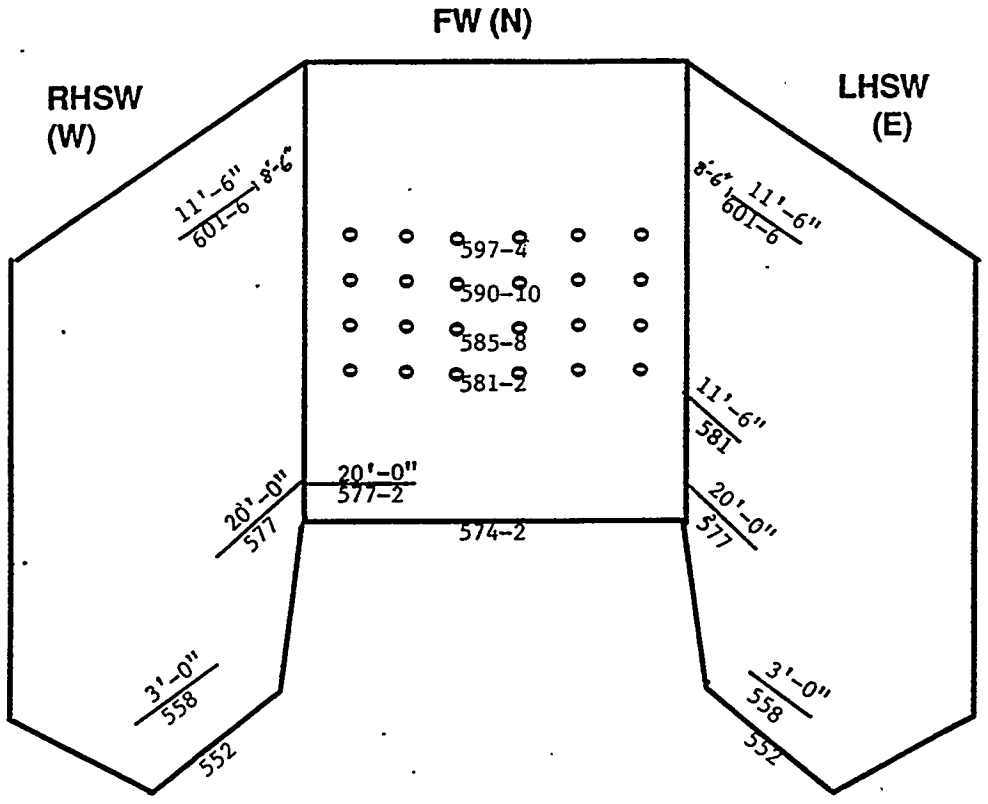

Figure 3-35 Elevations and locations of UT survey performed during the November 1991 and April 1993 outages

Because many areas of the lower waterwalls were replaced during the 1990 outage as a result of the 1990 UT survey, the initial tube thicknesses after the replacements became unknown. The situation was further complicated by the fact that the UT data from the April 1990 outage were taken at different locations compared to those of November 1991. Consequently, the metal wastage rates from April 1990 to November 1991 could not be derived with the available UT data acquired from these two years.

The 1991 UT survey was intended for defining the boiler condition prior to the LNCB retrofit and would be most useful if compared to those from the April 1993 outage, as the locations of both surveys were kept the same. Therefore, comparison between the UT data from the 1991 and 1993 outages should provide a better indication of the JMSS 4 boiler performance after 18 months of low-NO_x operation.

In the April 1993 outage, the UT survey was performed on the lower furnace walls of JMSS 4 at the elevations and locations identical to those of November 1991 (see Figure 3-35). The tube thicknesses on the test panel after the 18 months exposure were also determined in the same fashion described above for 1991. Again, five UT readings were taken at a 1/2-inch interval for each data point when possible.

Table 3-7 summaries and compares the UT data measured on the corrosion test panel at different elevations during the November 1991 and April 1993 outages. The wall thickness changes in mil (0.001 inch) are also given, where negative values stand for wall loss and positive values for gain. Based on the thickness changes, the corrosion rates in mil per year (mpy) are reported. The tube IDs from 1 to 80 are assigned to correspond to the tube numbers on the test panel, with 1 being the bare T2 tubing closest to the front wall. Details of the test panel layout is given in Appendix A. This numbering sequence is identical to those used in Figures 3-24 through 3-27, 3-33, and 3-34.

Unfortunately, as some of the tubing on the test panel exhibit a net loss in wall thickness, others display thickness "gain." The observed thickness changes from the UT measurements range from +33 to -20 mils. The variation tends to be larger on the coated tubing and smaller on bare T2. Apparently, the tube wall thickness cannot grow, and a large margin of error must have been introduced to the UT measurements acquired in November 1991 and April 1993 outages.

The major factors that may have attributed to the error margin include the equipment used, lack of calibration standards for various types of tubing materials tested, and inconsistency in signal interpretation. Other factors, such as surface cleanliness during the UT testing and variation in thoroughness of the sandblasting process prior to the testing, can also affect the accuracy of UT readings.

B&W has identified that the UT surveys during the 1991 and 1993 outages were performed by different technicians using different equipment. The ultrasonic flow detection scope has a readout of oscilloscope "peaks" which need to be subjectively interpreted by the technician. A typical UT measurement involves an error margin of ±5 mils. With the use of different equipment and different technicians, a margin of error at ±10 mils can be easily introduced. In the future outages, such sources of error will be minimized by ascertaining the use of same technician and equipment.

For the coated tubing — 308SS and 309SS overlays, aluminum spray, and chromizing — calibration standards should be established to minimize the error. These calibration standards can be site-specific, when necessary.

Table 3-7
COMPARISON OF TUBE WALL THICKNESS AND CALCULATED CORROSION RATE

RHSW Corrosion Test Panel

Elevation = 588'-3.75"					
TUBE ID on Test Panel	11/91 mils	4/21/93 mils	change mils	Corr Rate mpy	
1	N/A	240			Bare T2
2	N/A	249			Bare T2
3	N/A	241			Bare T2
4	N/A	246			Bare T2
5	N/A	248			Bare T2
6	N/A	270			Al Sprayed
7	N/A	284			Al Sprayed
8	N/A	280			Al Sprayed
9	N/A	282			Al Sprayed
10	N/A	286			Al Sprayed
11	N/A	285			Al Sprayed
12	N/A	270			Al Sprayed
13	N/A	271			Al Sprayed
14	N/A	280			Al Sprayed
15	N/A	270			Al Sprayed
16	N/A	245			Bare T2
17	N/A	233			Bare T2
18	N/A	250			Bare T2
19	N/A	243			Bare T2
20	N/A	236			Bare T2
21	224	222	-2	1.4	Bare T2
22	241	229	-12	8.5	Bare T2
23	236	239	3	*	Bare T2
24	239	237	-2	1.4	Bare T2
25	241	243	2	*	Bare T2
29	316	308	-8	5.6	309SS Overlay
32	312	305	-7	4.9	309SS Overlay
36	240	221	-19	13.4	Bare T2
37	240	239	-1	0.7	Bare T2
38	243	237	-6	4.2	Bare T2
39	236	237	1	*	Bare T2
40	239	229	-10	7.1	Bare T2
41	243	242	-1	0.7	Bare T2
42	236	225	-11	7.8	Bare T2
43	236	243	7	*	Bare T2
44	242	239	-3	2.1	Bare T2
45	245	245	0	0.0	Bare T2
49	330	341	11	*	308SS Overlay
52	333	352	19	*	308SS Overlay
56	236	239	3	*	Bare T2
57	230	242	12	*	Bare T2.
58	236	244	8	*	Bare T2
59	229	241	12	*	Bare T2
60	232	237	5	*	Bare T2
61	235	242	7	*	Bare T2
62	234	244	10	*	Bare T2
63	230	234	4	*	Bare T2
64	238	248	10	*	Bare T2
65	230	238	8	*	Bare T2
66	239	246	7	*	Chromized
67	239	247	8	*	Chromized
68	237	246	9	*	Chromized
69	242	245	3	*	Chromized
70	242	249	7	*	Chromized
71	242	251	9	*	Chromized
72	236	243	7	*	Chromized
73	235	239	4	*	Chromized
74	234	248	14	*	Chromized
75	239	244	5	*	Chromized
76	238	242	4	*	Bare T2
77	230	235	5	*	Bare T2
78	232	239	7	*	Bare T2
79	240	240	0	0.0	Bare T2
80	241	244	3	*	Bare T2

Average Value	
Bare T2	1.5
Weld Overlay	3.8
Chromized	7.3
Total Average	3.0

* These tube wall thicknesses show unrealistic "gain". Therefore, their thickness loss must be determined in future outages.

Table 3-7
COMPARISON OF TUBE WALL THICKNESS AND CALCULATED CORROSION RATE (CONTINUED)

RHSW Corrosion Test Panel

Elevation = 586'-3.75"

TUBE ID on Test Panel	11/91 mils	4/21/93 mils	change mils	Corr Rate mpy	
1	N/A	245			Bare T2
2	N/A	246			Bare T2
3	N/A	246			Bare T2
4	N/A	250			Bare T2
5	N/A	248			Bare T2
6	N/A	250			Al Sprayed
7	N/A	267			Al Sprayed
8	N/A	256			Al Sprayed
9	N/A	287			Al Sprayed
10	N/A	255			Al Sprayed
11	N/A	280			Al Sprayed
12	N/A	270			Al Sprayed
13	N/A	260			Al Sprayed
14	N/A	249			Al Sprayed
15	N/A	254			Al Sprayed
16	N/A	251			Bare T2
17	N/A	237			Bare T2
18	N/A	245			Bare T2
19	N/A	236			Bare T2
20	N/A	236			Bare T2
21	N/A	246			Bare T2
22	239	234	-5	3.5	Bare T2
23	235	236	1	*	Bare T2
24	233	230	-3	2.1	Bare T2
25	236	237	1	*	Bare T2
29	310	295	-15	10.6	309SS Overlay
32	322	338	16	*	309SS Overlay
36	242	231	-11	7.8	Bare T2
37	239	235	-4	2.8	Bare T2
38	237	229	-8	5.6	Bare T2
39	238	239	1	*	Bare T2
40	233	230	-3	2.1	Bare T2
41	236	242	6	*	Bare T2
42	232	234	2	*	Bare T2
43	235	243	8	*	Bare T2
44	237	228	-9	6.4	Bare T2
45	230	235	5	*	Bare T2
49	336	336	0	0.0	308SS Overlay
52	347	354	7	*	308SS Overlay
56	235	238	3	*	Bare T2
57	237	241	4	*	Bare T2
58	232	235	3	*	Bare T2
59	244	244	0	0.0	Bare T2
60	N/A	239			Bare T2
61	N/A	239			Bare T2
62	N/A	246			Bare T2
63	232	238	6	*	Bare T2
64	238	243	5	*	Bare T2
65	230	226	-4	2.8	Bare T2
66	243	245	2	*	Chromized
67	236	248	12	*	Chromized
68	231	245	14	*	Chromized
69	244	246	2	*	Chromized
70	245	249	4	*	Chromized
71	239	249	10	*	Chromized
72	240	249	9	*	Chromized
73	249	251	2	*	Chromized
74	240	245	5	*	Chromized
75	239	250	11	*	Chromized
76	230	242	12	*	Bare T2
77	230	231	1	*	Bare T2
78	237	244	7	*	Bare T2
79	233	240	7	*	Bare T2
80	250	237	-13	9.2	Bare T2

Average Value	
Bare T2	0.5
Weld Overlay	2.0
Chromized	7.1
Total Average	2.1

* These tube wall thicknesses show unrealistic "gain". Therefore, their thickness loss must be determined in future outages.

Table 3-7
COMPARISON OF TUBE WALL THICKNESS AND CALCULATED CORROSION RATE (CONTINUED)

RHSW Corrosion Test Panel

Elevation = 584'-3.75"					
TUBE ID on Test Pane	11/91 mils	4/21/93 mils	change mils	Corr Rate mpy	
1	N/A	240			Bare T2
2	N/A	235			Bare T2
3	N/A	250			Bare T2
4	N/A	245			Bare T2
5	N/A	240			Bare T2
6	N/A	265			Al Sprayed
7	N/A	275			Al Sprayed
8	N/A	265			Al Sprayed
9	N/A	270			Al Sprayed
10	N/A	270			Al Sprayed
11	N/A	280			Al Sprayed
12	N/A	275			Al Sprayed
13	N/A	265			Al Sprayed
14	N/A	270			Al Sprayed
15	N/A	260			Al Sprayed
16	N/A	245			Bare T2
17	N/A	230			Bare T2
18	N/A	240			Bare T2
19	N/A	222			Bare T2
20	N/A	240			Bare T2
21	238	237	-1	0.7	Bare T2
22	239	222	-17	12.0	Bare T2
23	232	227	-5	3.5	Bare T2
24	245	228	-17	22.0	Bare T2
25	237	239	2	*	Bare T2
29	307	308	1	*	309SS Overlay
32	328	314	-14	9.9	309SS Overlay
36	241	221	-20	14.1	Bare T2
37	236	231	-5	3.5	Bare T2
38	240	227	-13	9.2	Bare T2
39	237	236	-1	0.7	Bare T2
40	234	221	-13	9.2	Bare T2
41	238	239	1	*	Bare T2
42	239	221	-18	12.7	Bare T2
43	239	232	-7	4.9	Bare T2
44	238	225	-13	9.2	Bare T2
45	243	235	-8	5.6	Bare T2
49	352	365	13	*	308SS Overlay
52	329	345	16	*	308SS Overlay
56	239	226	-13	9.2	Bare T2
57	233	239	6	*	Bare T2
58	237	228	-9	6.4	Bare T2
59	238	237	-1	0.7	Bare T2
60	240	231	-9	6.4	Bare T2
61	246	242	-4	2.8	Bare T2
62	237	237	0	0.0	Bare T2
63	244	235	-9	6.4	Bare T2
64	235	234	-1	0.7	Bare T2
65	240	232	-8	5.6	Bare T2
66	241	242	1	*	Chromized
67	253	250	-3	2.1	Chromized
68	251	247	-4	2.8	Chromized
69	250	247	-3	2.1	Chromized
70	247	245	-2	1.4	Chromized
71	250	250	0	0.0	Chromized
72	241	245	4	*	Chromized
73	248	243	-5	3.5	Chromized
74	250	251	1	*	Chromized
75	241	238	-3	2.1	Chromized
76	242	240	-2	1.4	Bare T2
77	240	238	-2	1.4	Bare T2
78	227	242	15	*	Bare T2
79	233	230	-3	2.1	Bare T2
80	240	237	-3	2.1	Bare T2

Average Value		
Bare T2	-5.9	
Weld Overlay	4.0	
Chromized	1.4	
Total Average	4.0	

* These tube wall thicknesses show unrealistic "gain". Therefore, their thickness loss must be determined in future outages.

Table 3-7
COMPARISON OF TUBE WALL THICKNESS AND CALCULATED CORROSION RATE (CONTINUED)

RHSW Corrosion Test Panel

Elevation = 582'-3.75"					
TUBE ID on Test Panel	11/91 mils	4/21/93 mils	change mils	Corr Rate mpy	
1	N/A	246			Bare T2
2	N/A	243			Bare T2
3	N/A	248			Bare T2
4	N/A	242			Bare T2
5	N/A	242			Bare T2
6	N/A	284			Al Sprayed
7	N/A	289			Al Sprayed
8	N/A	288			Al Sprayed
9	N/A	287			Al Sprayed
10	N/A	286			Al Sprayed
11	N/A	280			Al Sprayed
12	N/A	289			Al Sprayed
13	N/A	286			Al Sprayed
14	N/A	280			Al Sprayed
15	N/A	287			Al Sprayed
16	N/A	292			Bare T2
17	N/A	278			Bare T2
18	N/A	245			Bare T2
19	N/A	249			Bare T2
20	N/A	244			Bare T2
21	237	247	10	*	Bare T2
22	234	240	6	*	Bare T2
23	234	239	5	*	Bare T2
24	245	235	-10	7.1	Bare T2
25	247	241	-6	4.2	Bare T2
29	302	334	32	*	309SS Overlay
32	315	342	27	*	309SS Overlay
36	235	228	-7	4.9	Bare T2
37	236	238	2	*	Bare T2
38	243	236	-7	4.9	Bare T2
39	247	240	-7	4.9	Bare T2
40	232	232	0	0.0	Bare T2
41	236	237	1	*	Bare T2
42	230	233	3	*	Bare T2
43	238	241	3	*	Bare T2
44	245	231	-14	9.9	Bare T2
45	236	240	4	*	Bare T2
49	324	346	22	*	308SS Overlay
52	320	339	19	*	308SS Overlay
56	240	237	-3	2.1	Bare T2
57	247	245	-2	1.4	Bare T2
58	240	235	-5	3.5	Bare T2
59	233	237	4	*	Bare T2
60	229	228	-1	0.7	Bare T2
61	237	245	8	*	Bare T2
62	239	242	3	*	Bare T2
63	238	238	0	0.0	Bare T2
64	240	243	3	*	Bare T2
65	234	239	5	*	Bare T2
66	234	240	6	*	Chromized
67	248	244	-4	2.8	Chromized
68	247	245	-2	1.4	Chromized
69	240	247	7	*	Chromized
70	244	243	-1	0.7	Chromized
71	236	246	10	*	Chromized
72	250	255	5	*	Chromized
73	245	250	5	*	Chromized
74	243	245	2	*	Chromized
75	246	247	1	*	Chromized
76	237	241	4	*	Bare T2
77	245	241	-4	2.8	Bare T2
78	238	245	7	*	Bare T2
79	239	232	-7	4.9	Bare T2
80	244	242	-2	1.4	Bare T2

Average Value	
Bare T2	-0.2
Weld Overlay	25.0
Chromized	2.9
Total Average	2.8

* These tube wall thicknesses show unrealistic "gain". Therefore, their thickness loss must be determined in future outages.

Table 3-7
COMPARISON OF TUBE WALL THICKNESS AND CALCULATED CORROSION RATE (CONTINUED)

RHSW Corrosion Test Panel

Elevation = 580'-6.75"					
TUBE ID on Test Panel	11/91 mils	4/21/93 mils	change mils	Corr Rate mpy	
1	N/A	242			Bare T2
2	N/A	248			Bare T2
3	N/A	242			Bare T2
4	N/A	238			Bare T2
5	N/A	250			Bare T2
6	N/A	273			Al Sprayed
7	N/A	286			Al Sprayed
8	N/A	275			Al Sprayed
9	N/A	276			Al Sprayed
10	N/A	281			Al Sprayed
11	N/A	288			Al Sprayed
12	N/A	271			Al Sprayed
13	N/A	278			Al Sprayed
14	N/A	273			Al Sprayed
15	N/A	289			Al Sprayed
16	N/A	243			Bare T2
17	N/A	245			Bare T2
18	N/A	241			Bare T2
19	N/A	241			Bare T2
20	N/A	245			Bare T2
21	230	239	9	*	Bare T2
22	238	246	8	*	Bare T2
23	241	242	1	*	Bare T2
24	238	238	0	0.0	Bare T2
25	234	237	3	*	Bare T2
29	309	319	10	*	309SS Overlay
32	326	351	25	*	309SS Overlay
36	242	245	3	*	Bare T2
37	232	242	10	*	Bare T2
38	236	243	7	*	Bare T2
39	234	247	13	*	Bare T2
40	231	238	7	*	Bare T2
41	241	243	2	*	Bare T2
42	239	240	1	*	Bare T2
43	231	241	10	*	Bare T2
44	247	246	-1	0.7	Bare T2
45	237	247	10	*	Bare T2
49	306	339	33	*	308SS Overlay
52	315	342	27	*	308SS Overlay
56	N/A	241			Bare T2
57	242	241	-1	0.7	Bare T2
58	232	238	6	*	Bare T2
59	236	243	7	*	Bare T2
60	236	225	-11	7.8	Bare T2
61	234	242	8	*	Bare T2
62	231	246	15	*	Bare T2
63	248	249	1	*	Bare T2
64	237	248	11	*	Bare T2
65	230	239	9	*	Bare T2
66	248	245	-3	2.1	Chromized
67	240	243	3	*	Chromized
68	238	241	3	*	Chromized
69	247	251	4	*	Chromized
70	253	252	-1	0.7	Chromized
71	254	252	-2	1.4	Chromized
72	238	242	4	*	Chromized
73	248	245	-3	2.1	Chromized
74	246	247	1	*	Chromized
75	247	245	-2	1.4	Chromized
76	238	249	11	*	Bare T2
77	233	240	7	*	Bare T2
78	238	240	2	*	Bare T2
79	239	247	8	*	Bare T2
80	250	249	-1	0.7	Bare T2

Average Value	
Bare T2	5.3
Weld Overlay	23.6
Chromized	0.4
Total Average	5.8

* These tube wall thicknesses show unrealistic "gain". Therefore, their thickness loss must be determined in future outages.

Tables 3-8, 3-9, and 3-10 compare the UT data, thickness changes, and calculated corrosion rates obtained from the right-hand side wall (RHSW), left-hand side wall (LHSW), and front wall (FW) of JMSS 4, respectively. The tests were performed after the aluminum-spray coating was removed by sandblasting to expose the underlying T2 tubing. Again, the elevations and locations from which the data were acquired are shown in Figure 3-35. Similar uncertainty in the accuracy of UT data is observed; however, the margin of error is relatively small compared to that in Table 3-9 for the corrosion test panel.

Based on the 1991 and 1993 UT data, it is not possible to define the exact corrosion rates on the lower furnace walls of JMSS 4, nor pinpoint the problem spots where excessive metal wastage may exist. It is therefore necessary to continue the UT survey during the next few outages, with the implementation of lessons learned from the previous UT activities, so that long-term wall thickness variations can be established.

As discussed in Section 3.1 (laboratory tests) and Section 3.3 (field test), the corrosion rates of bare T2 were found to vary from 0 to 15 mpy in the sub-stoichiometric combustion environments. It should be mentioned that the UT data in DP&L's 1986 and 1987 Plant Betterment Inspection Reports have documented a corrosion rate of approximately 12 mpy on the 104th tube of the rear waterwall at 10 inches above the weld line, and 8 mpy at 14 inches above the weld line. These reports attributed the high corrosion rates to the potential existence of a reducing atmosphere. Therefore, high corrosion rates, comparable to those found in Sections 3.2 and 3.3 for bare T2, did exist prior to the LNCB retrofit. It is noted that the 104th tubing examined in 1986 and 1987 was spray coated with aluminum. If without the coating protection during service, the T2 tube would have suffered an even worse metal loss.

3.4 EMISSIONS PERFORMANCE

3.4.1 N_2O Emissions

Semi-continuous N_2O measurements were performed on the flue gases extracted with the gas sampling system described in Section 2.4 from each economizer outlet duct at two test tap locations. Figure 3-36 shows an overall view where the test taps were located at each economizer outlet duct, and the locations tested.

3.4.1.1 Gas Chromatograph Calibration. The gas chromatograph (GC) was calibrated for N_2O using bottled gas standards (Airco Special Gases, Riverton, NJ) and a N.I.S.T. SRM 2610 (0.33 ppmV N_2O) in the concentration range of 0.33 to 10.5 ppmV. During calibration, each gas standard was delivered to the GC through unheated 1/4-inch OD Impolene tubing connected to the right rear injection port while maintaining a flow rate of 75 ml/min through the gas sample loop. Figure 3-37 shows the calibration curve obtained for nitrous oxide. The relationship between concentration and detector response is linear.

3.4.1.2 Pre- and Post-Calibration — Gas Sampling System. Prior to extracting flue gas samples from the test taps at either economizer outlet duct, the integrity of the gas sampling system was checked using a 0.98 ppmV N_2O gas standard. This standard was chosen because it was the closest available standard concentration to the measured N_2O values found in both economizer outlet ducts during preliminary post-retrofit tests.

Table 3-8
COMPARISON OF TUBE WALL THICKNESS AND CALCULATED CORROSION RATE — RHSW UT DATA ON SANDBLASTED BANDS
(All T2 Tubing)

Elevation = 558'-0"				
TUBE ID	11/91 mils	4/21/93 mils	change mils	Corr Rate mpy
-2	234	240	6	*
-1	236	240	4	*
6	228	238	10	*
7	225	237	12	*
13	229	239	10	*
14	232	239	7	*
20	235	243	8	*
21	236	242	6	*
		Average	7.9	

Elevation = 577'-2"				
TUBE ID	11/91 mils	4/21/93 mils	change mils	Corr Rate mpy
8	240	241	1	*
9	241	241	0	0.0
14	230	242	12	*
15	235	251	16	*
16		240		
20	242	249	7	*
21	237	251	14	*
28	231	251	20	*
29	229	251	22	*
91	250			
92	244			
		Average	11.5	

Elevation = 601'-6"				
TUBE ID	11/91 mils	4/21/93 mils	change mils	Corr Rate mpy
62	247	235	-12	8.5
63	250	244	-6	4.2
72	249	248	-1	0.7
73	249	250	1	*
79	244	237	-7	4.9
80	244	234	-10	7.1
85		252		
90		249		
101		240		
109		246		
115		252		
123		246		
131		246		
139		246		
		Average	-5.8	

* These tube wall thicknesses show unrealistic "gain". Therefore, their thickness loss must be determined in future outages.

Table 3-9
COMPARISON OF TUBE WALL THICKNESS AND CALCULATED CORROSION RATE — LHSW UT DATA ON SANDBLASTED BANDS
(All T2 Tubing)

Elevation = 558'-0"

TUBE ID	11/91 mils	4/21/93 mils	change mils	Corr Rate mpy
1	238	251	13	*
2	220	247	27	*
7	229	243	14	*
8	235	243	8	*
15	239	246	7	*
16	235	249	14	*
22	239	248	9	*
23	230	243	13	*
		Average	13.1	

Elevation = 577'-5"

TUBE ID	11/91 mils	4/21/93 mils	change mils	Corr Rate mpy	
34	254	249	-5	3.5	
41	247	247	0	0.0	
42	249	245	-4	2.8	
69	250	252	2	*	
70	249	249	0	0.0	
76	250	249	-1	0.7	
77	259	252	-7	4.9	
83	245	253	8	*	
84	238	241	3	*	
96		240			
101		250			Al Coating
109		247			
115		252			Al Coating
121		250			
126		242			
134		239			
		Average	-0.4		

Elevation = 581'-0"

TUBE ID	11/91 mils	4/21/93 mils	change mils	Corr Rate mpy	
34	251	250	-1	0.7	
35	247	247	0	0.0	
41	237	248	11	*	
69	241	241	0	0.0	
70	249	247	-2	1.4	
76	239	245	6	*	
77	244	243	-1	0.7	
83	249	248	-1	0.7	
84	243	239	-4	2.8	
88		246			
96		244			
103		257			Al Coating
111		253			*
114		250			*
128		248			*
134		232			*
		Average	0.9		

Elevation = 601'-6"

TUBE ID	11/91 mils	4/21/93 mils	change mils	Corr Rate mpy
59	249	248	-1	0.7
60	237	239	2	*
65	246	243	-3	2.1
66	238	237	-1	0.7
72	245	241	-4	2.8
73	243	242	-1	0.7
80	250	241	-9	6.4
81	249	245	-4	2.8
85		242		
89		249		
92		245		
96		240		
100		247		
104		249		
109		250		
115		246		
120		252		
125		242		
128		248		
135		241		
140		249		
		Average	-2.6	

* These tube wall thicknesses show unrealistic "gain". Therefore, their thickness loss must be determined in future outages.

Table 3-10
COMPARISON OF TUBE WALL THICKNESS AND CALCULATED CORROSION RATE — FW UT DATA ON SANDBLASTED BANDS
(All T2 Tubing)

Elevation = 577'-2"					
TUBE ID	11/91 mils	4/21/93 mils	change mils	Corr Rate mpy	
424		243			
423		245			
417		243			
416		238			
410		243			
404		249			Al Coating
403		258			Al Coating
402		244			
396		236			
395		254			Al Coating
389		246			
388		239			
364		249			
363		247			
353		251			
322		251			Al Coating
321		243			
293		246			
292		247			
		Average			

Elevation = 580'-3"				
TUBE ID	11/91 mils	4/21/93 mils	change mils	Corr Rate mpy
403	236	240	4	*
402	230	239	9	*
396	235	237	2	*
395	238	244	6	*
389	232	239	7	*
388	241	239	-2	1.4
384	248	243	-5	3.5
383	232	247	15	*
354	236	238	2	*
353	234	237	3	*
322		251		
321	232	242	10	*
		Average	4.5	

* These tube wall thicknesses show unrealistic "gain". Therefore, their thickness loss must be determined in future outages.

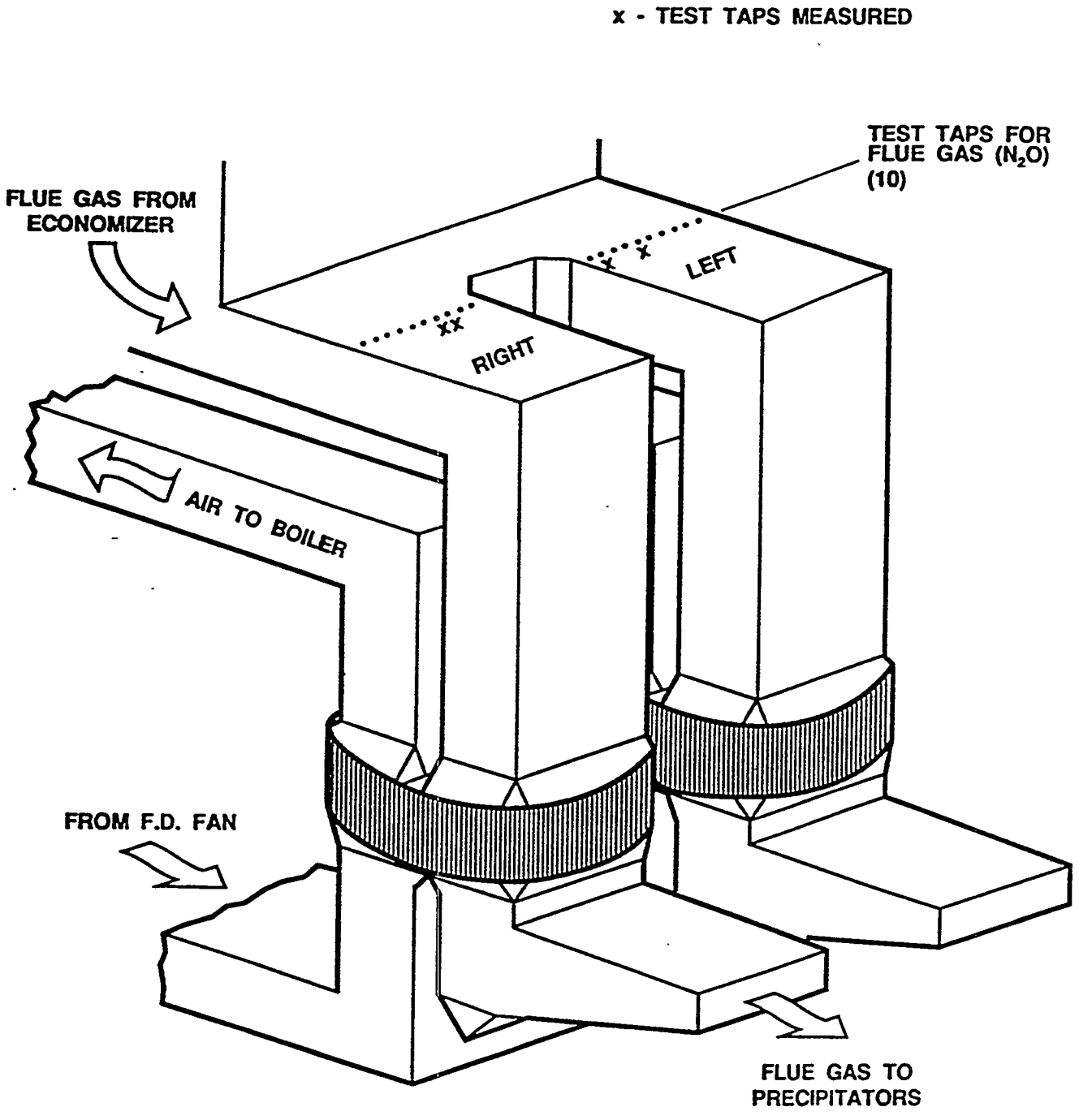

Figure 3-36 Nitrous oxide test port locations on JMSS 4

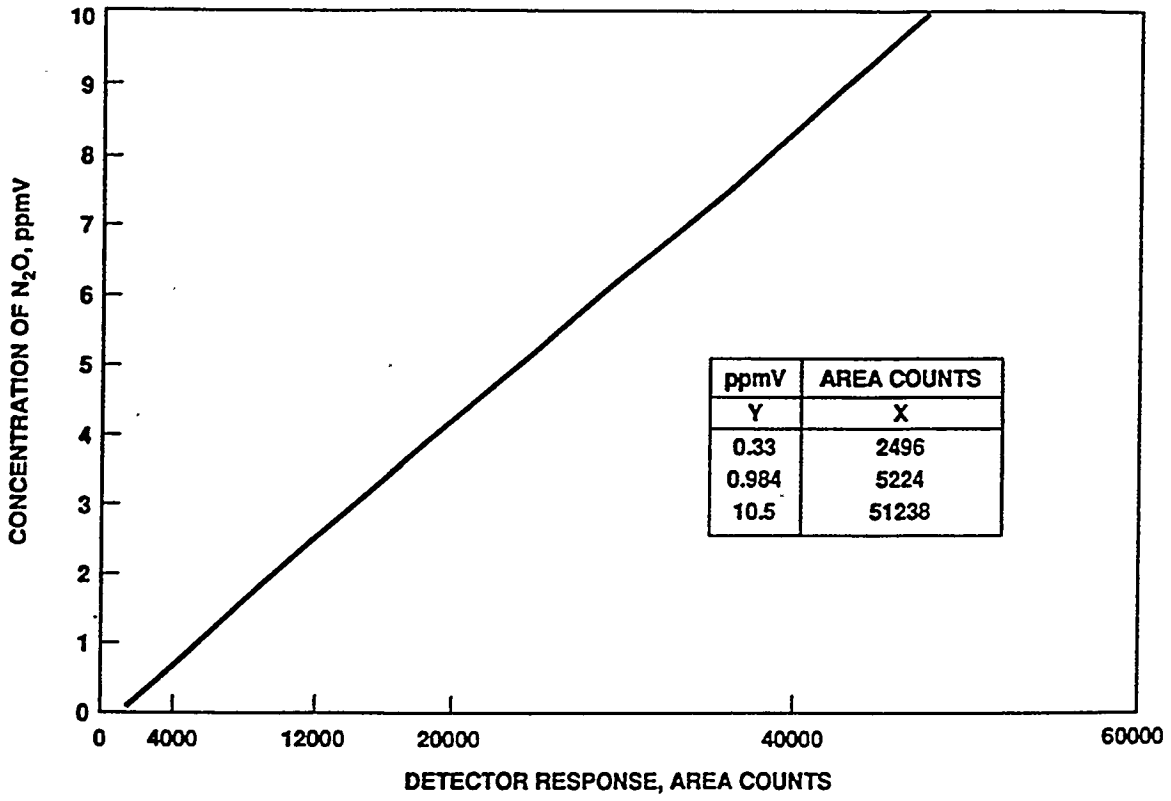

Figure 3-37 Graph of concentration of nitrous oxide against peak area (Data points = 3, correlation coefficient = 0.999; intercept = -0.1465; and slope = 0.0002)

Similarly, after N_2O measurements were performed at each test tap location, the gas sampling system was again checked with the 0.98 ppmV N_2O standard.

During pre- and post-calibrations, the same flow rate through the gas sampling system to the GC was maintained, controlled by adjusting the vacuum gauge pressure (28 p.s.i.) with the vent valve, as during collection of test data. Also, the same flow rate was maintained through the 1 ml gas sample loop (75 ml/min) as during GC calibration and collection of test data.

3.4.1.3 Left and Right Economizer Outlet Ducts — N_2O Measurements. N_2O was measured at two test tap positions from each economizer outlet duct. This meant that instead of taking a composite flue gas sample across the entire width of the economizer duct, just the zone representing one test tap position was being measured. Each test tap position consisted of four pipes that were combined using tees and surgical tubing to yield an output which represented a composite of the height of the duct at that location (see Figure 3-38). However, to be consistent with baseline testing, the gas sampling system was connected to just one tube from each test tap position.

The test tap positions and tubes used for the left economizer outlet duct were:

- The sixth test tap, as measured from the left or east side, using only the longest tube into the duct
- The ninth test tap, as measured from the left, using only the next to the longest tube into the duct

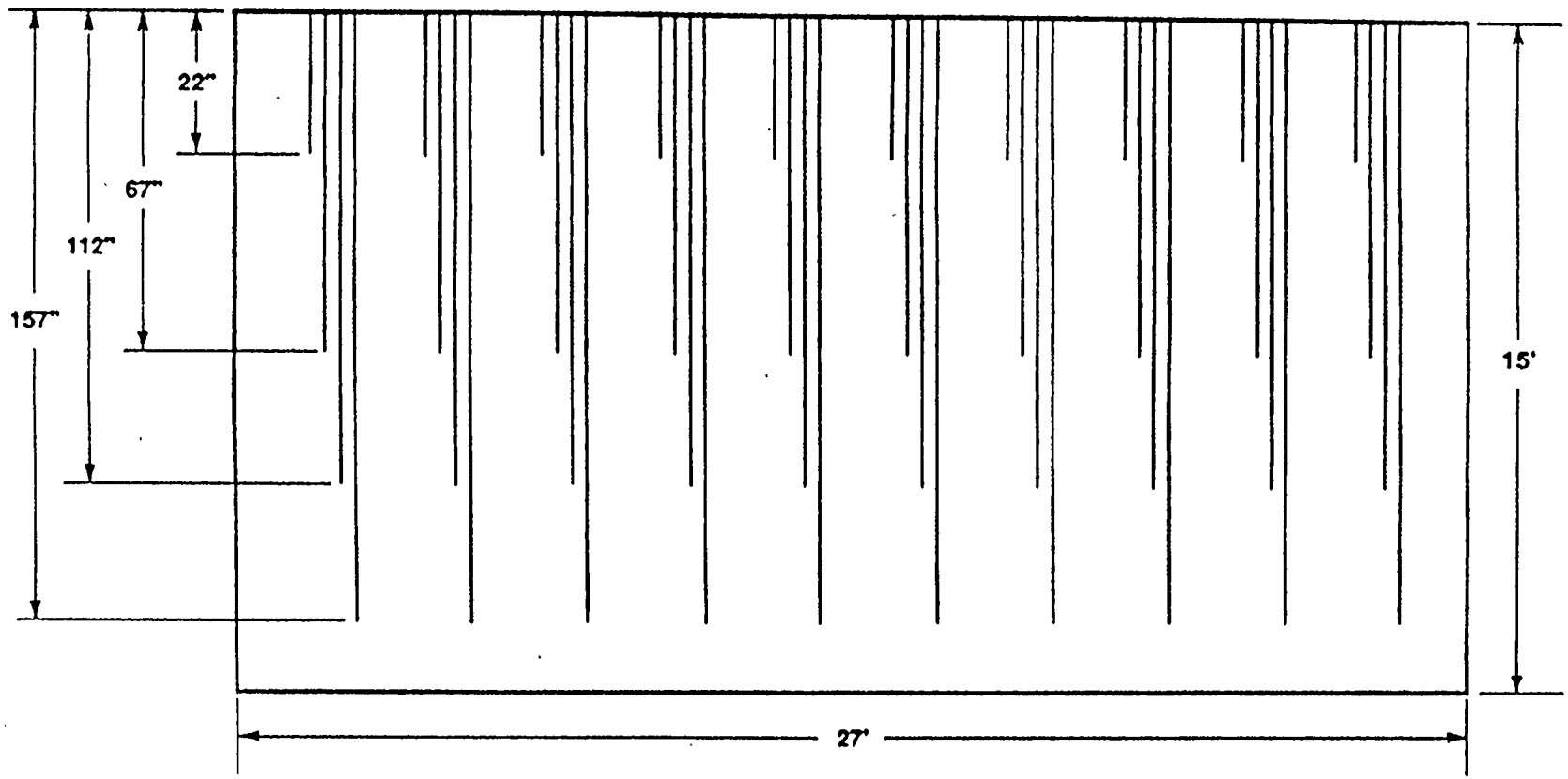

Figure 3-38 Economizer outlet gas sampling grid (1 of 2) 5/16-inch tubing connections to the sample lines

These were the same locations used in baseline testing.

The test tap positions and tubes for the right economizer outlet duct were:

- The third test tap, measured from the left, using only the next to the shortest tube into the duct
- The fourth test tap, measured from the left, using only the longest tube into the duct

Table 3-11 lists the measured N_2O concentrations comparing baseline to post-retrofit testing at each economizer outlet duct. All N_2O values have been corrected to 3% O_2. For the most part, the values obtained with the 0.98 ppmV N_2O gas standard during pre- and post-calibrations were in close agreement to GC calibration values. Therefore, only small differences existed between measured N_2O values and the corrected data listed.

For the locations tested, N_2O concentration increased at each economizer outlet duct after the retrofit as shown in Figure 3-39.

Table 3-11
COMPARISON OF BASELINE TO POST-RETROFIT N_2O RESULTS FROM THE LEFT AND RIGHT ECONOMIZER OUTLET DUCTS

	Left N_2O, ppmV Economizer Outlet Duct				Right N_2O, ppmV Economizer Outlet Duct			
	N_2O, ppmV				*N_2O, ppmV*			
Time, Minutes	*Baseline*	*Post Retrofit*		*AVG.*	*Baseline*	*Post Retrofit*		*AVG.*
0	0.33*	0.98***	0.97***		0.32*	0.98***	0.98***	
5	0.27	0.81	0.74	0.77	0.21	0.93	1.06	1.00
10	0.09	0.83	0.76	0.79	0.21	0.93	1.03	0.98
15	0.16	0.88	0.79	0.84	0.21	0.98	1.06	1.01
20	0.21	0.88	0.79	0.84	0.21	1.01	1.13	1.07
25	0.24	---	---		0.17	---	---	
30	0.50	---	---		0.21	---	---	
35	0.33	---	---		0.21	---	---	
40	0.33	---	---		---	---	---	
---	0.36**	1.07****	1.02****		0.35**	1.03****	1.02****	

* N.I.S.T. SRM 2610 Gas Standard, 0.33 ppmV N_2O, Pre Calibration.

** N.I.S.T. SRM 2610 Gas Standard, 0.33 ppmV N_2O, Post Calibration.

*** Airco Certified Gas Mixture, 0.98 ppmV N_2O, Pre Calibration.

**** Airco Certified Gas Mixture, 0.98 ppmV N_2O, Post Calibration

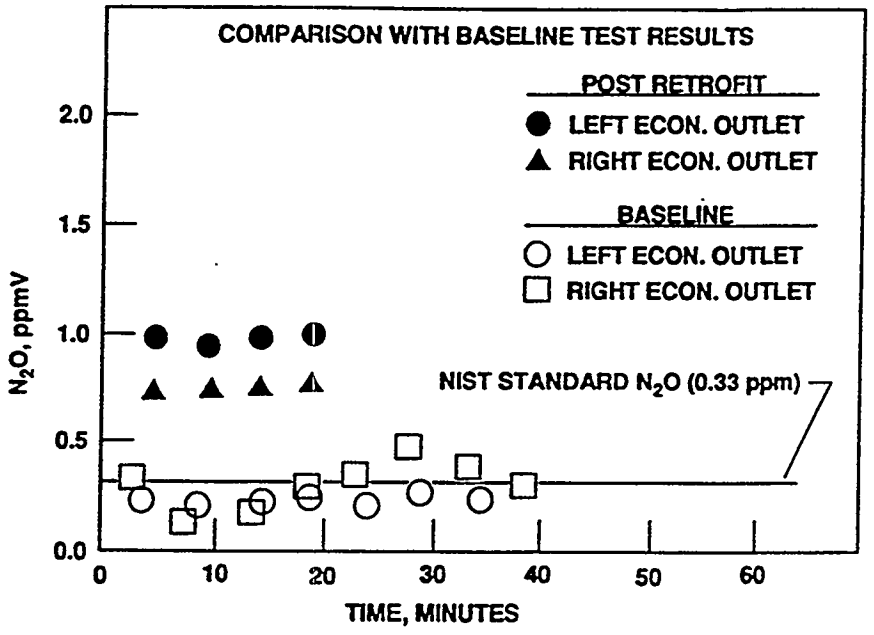

Figure 3-39 N_2O at economizer outlet

3.4.2 Long-Term Emissions Monitoring by Acurex Environmental Corporation

3.4.2.1 Overview. As a follow-up to the Low-NO_x Cell™ Burner (LNCB) test and performance optimization program, a continuous emission monitoring (CEM) system (Dilu-CEM 500) was installed and operated at JMSS 4. This brief discussion was included in *Acurex Environmental Technical Report No. 93-102* entitled "Long-Term Continuous Emission Monitoring Tests: Babcock & Wilcox Low-NO_x Cell Burner Demonstration Project" dated July 1993. See Figures 3-40, 3-41, and 3-42.

A major portion of this report included computer-generated listings of averaged data and their corresponding hourly trend plots. Results of the 8-month monitoring program were summarized as follows:

Table	*Loads*	*Period*
2a	All loads	August - December
2b	All loads	January - March
3a	Full load*	August - December
3b	Full load	January - March
4a	Low load**	August - December
4b	Low load	January - March

* Full load — turbine output ≥ 590 MWe
** Low load — turbine output < 590 MWe

Data from Tables 2a and 2b in the Acurex report were re-formatted for plotting purposes and are shown as Table B-1 in Appendix B. Each of six mills was taken out-of-service as were combinations of mills. With a single mill out-of-service, there was often little need to substantially reduce load. Boiler operation with two or more mills out-of-service was necessary at reduced load.

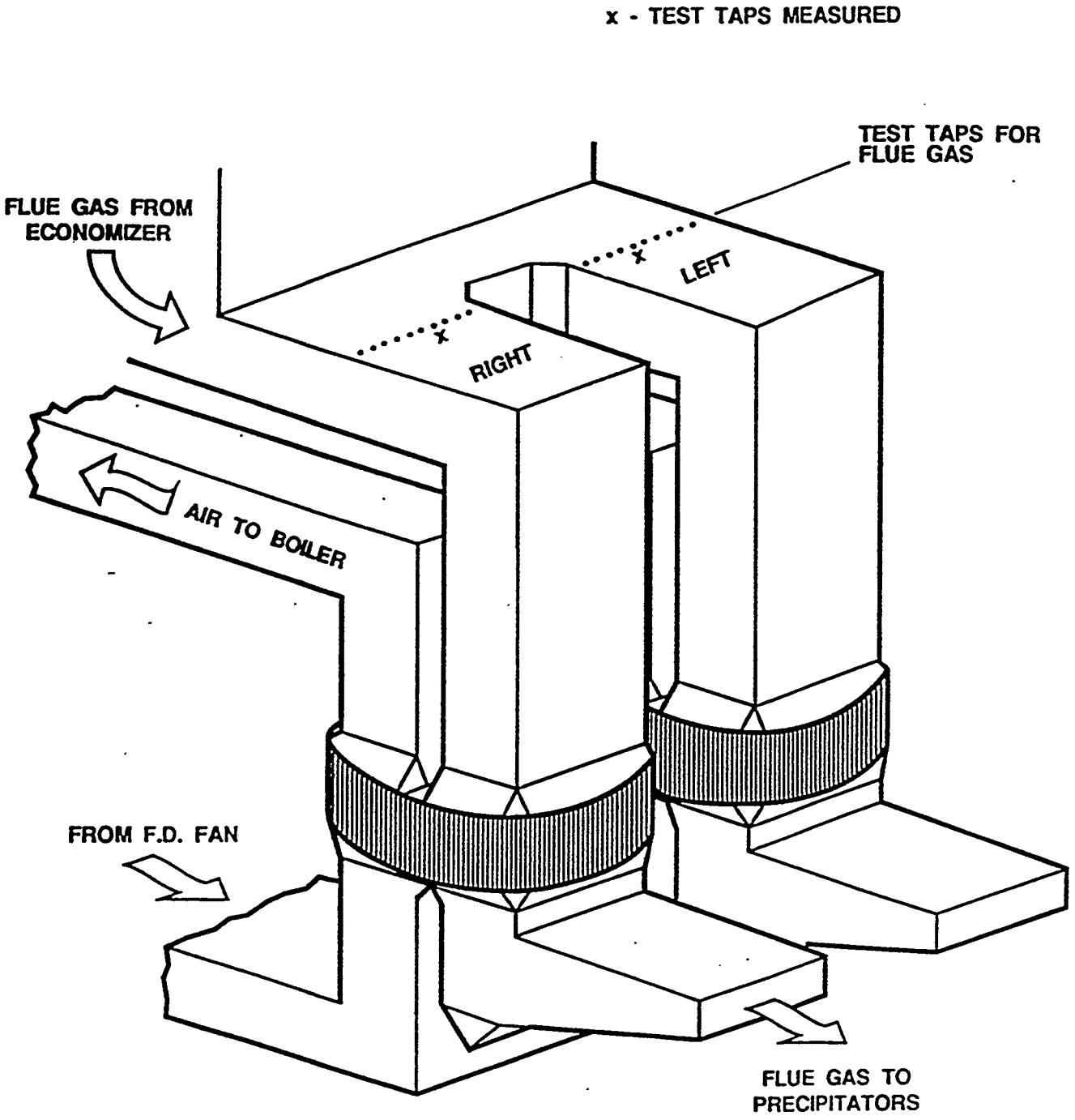

Figure 3-40 Emissions test port locations for Acurex long-term monitoring

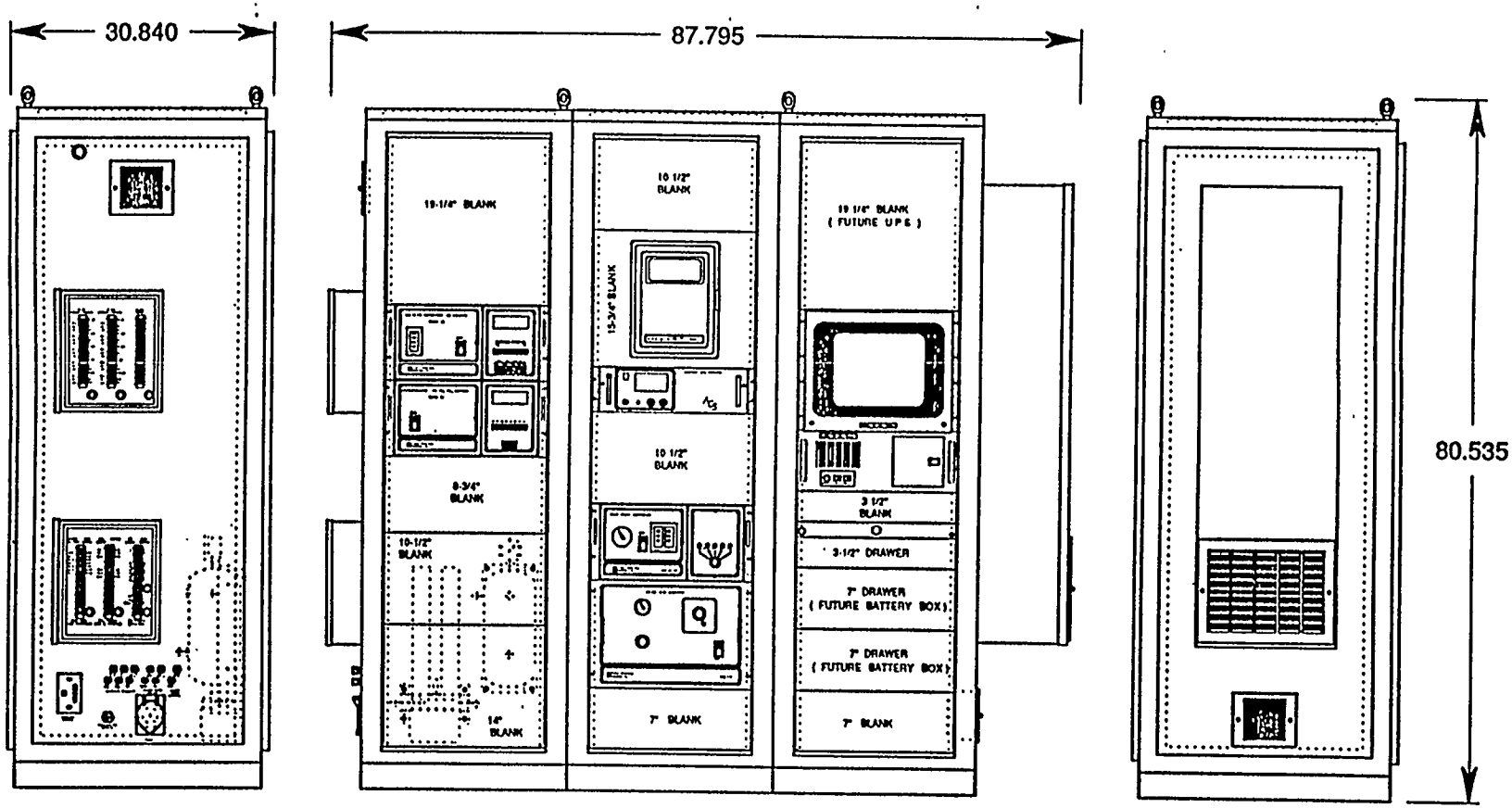

APPROXIMATE WEIGHT = 2110 POUNDS

Figure 3-41 Continuous emission monitoring (CEM) system — Unit No. 4

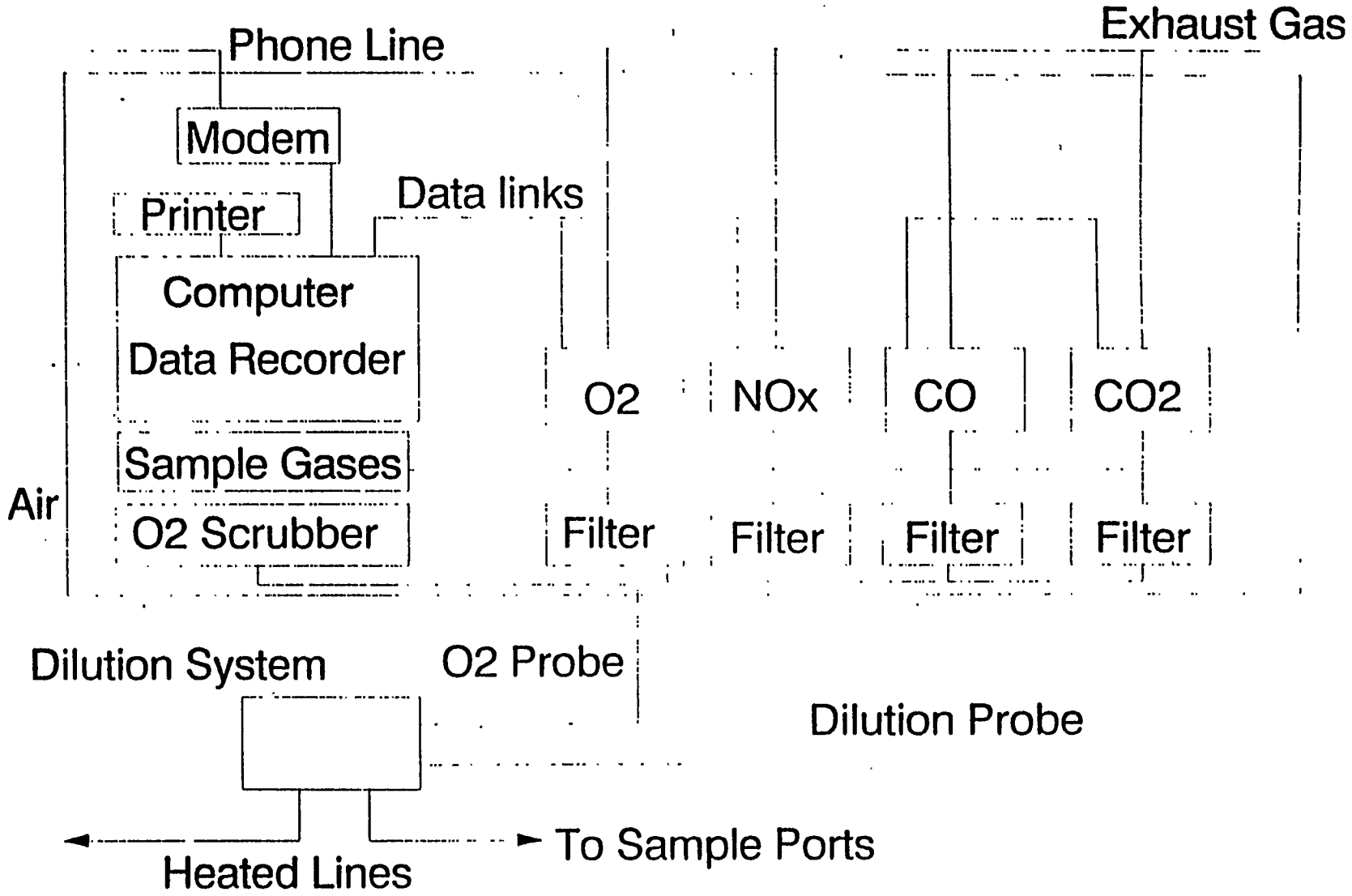

Figure 3-42 Schematic of Dilu-CEM 500

The following discussion will focus on the effects of individual mills being out-of-service as well as operation with all mills in-service. The Acurex report also included data taken with two or more mills out-of-service; however, there was insufficient information available to draw any meaningful conclusions.

Figure 3-43 shows the burner/overfire air port arrangement and burner groups supplied by each mill. Figures 3-44 through 3-49 graphically show comparisons of days out-of-service for each mill, electrical load, excess flue gas O_2 and NO_x with the reference mill in each case being either A- or F-mill. These were selected because an initial review showed that lowest NO_x levels were achieved when these mills were out-of-service regardless of boiler load. Data provided by Acurex are defined as follows:

NO_x	— ppm dry volume basis corrected to 3% O_2
Excess air	— excess O_2 present in flue gas, % volume on a dry basis
Load	— turbine-generator electrical load, MWe
Days out-of-service	— the cumulative number of out-of-service days for each mill or mill combination

The NO_x, excess air, and loads for each mill operating condition are averages corresponding to the cumulative time logged for each mill on a monthly basis. For example, A-mill might have been out-of-service a half-day each week for a given month which would be equivalent to two full days. Each time it was out-of-service, average NO_x, excess O_2, and load levels were logged. At month's end, an overall average for each parameter and an aggregate mill out-of-service time were computed and logged. All other things being equal, this would be equivalent to A-mill being out-of-service all month. As another example, B-mill was out-of-service a total of 3.65 days during December (we do not know how often, when, and for how long each outage was) and during that total out-of-service time, the average NO_x was 365 ppm, excess O_2 was 4.0%, and the turbine load was 561 MWe.

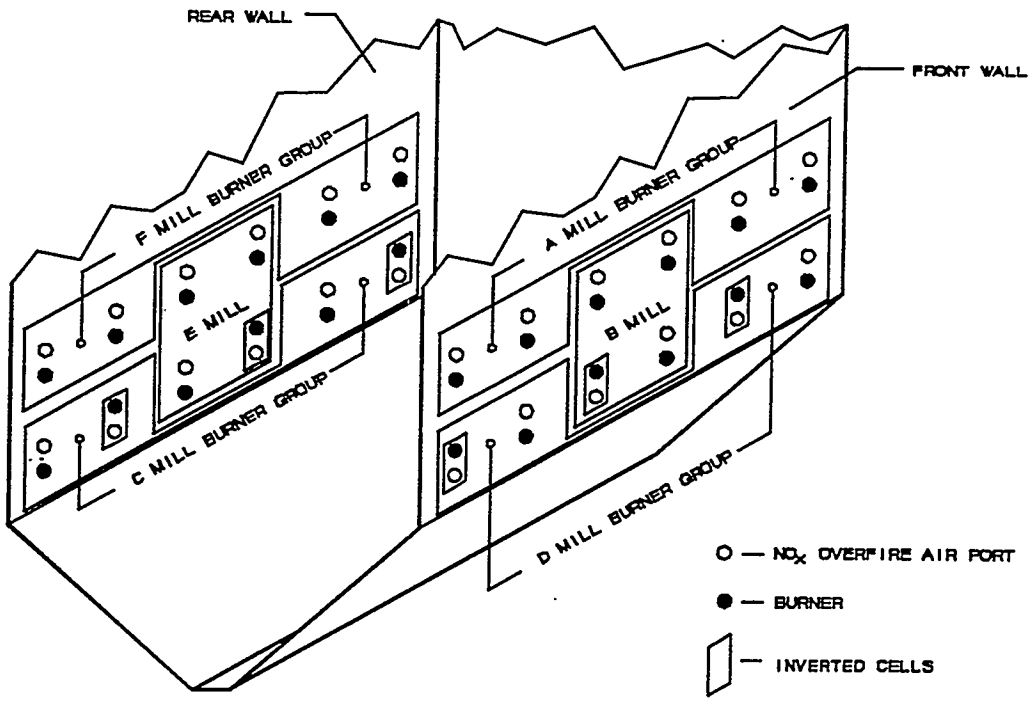

Figure 3-43 Burner, overfire air ports, and mill group layout

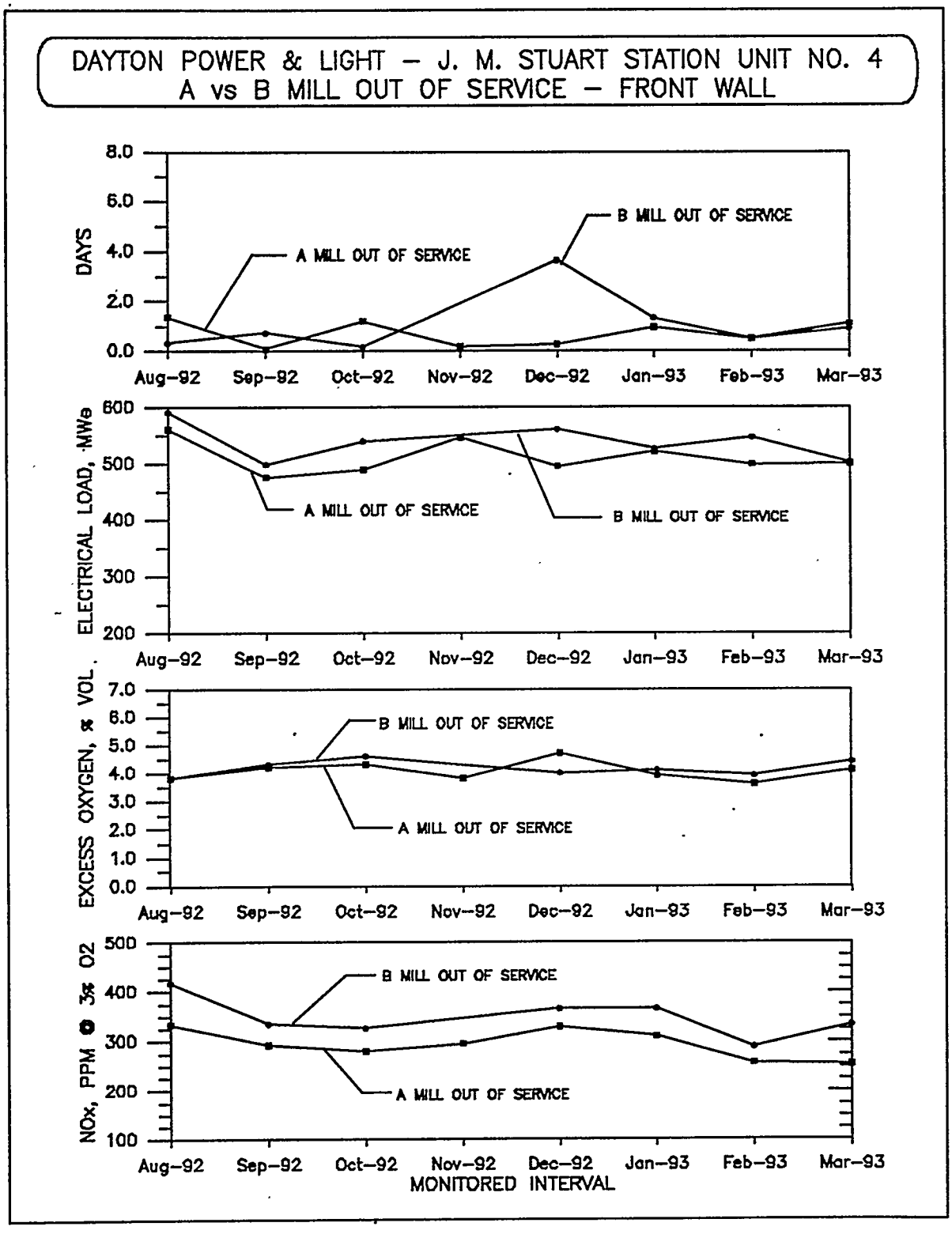

Figure 3-44 NO_x for A-mill out-of-service versus B-mill out-of-service

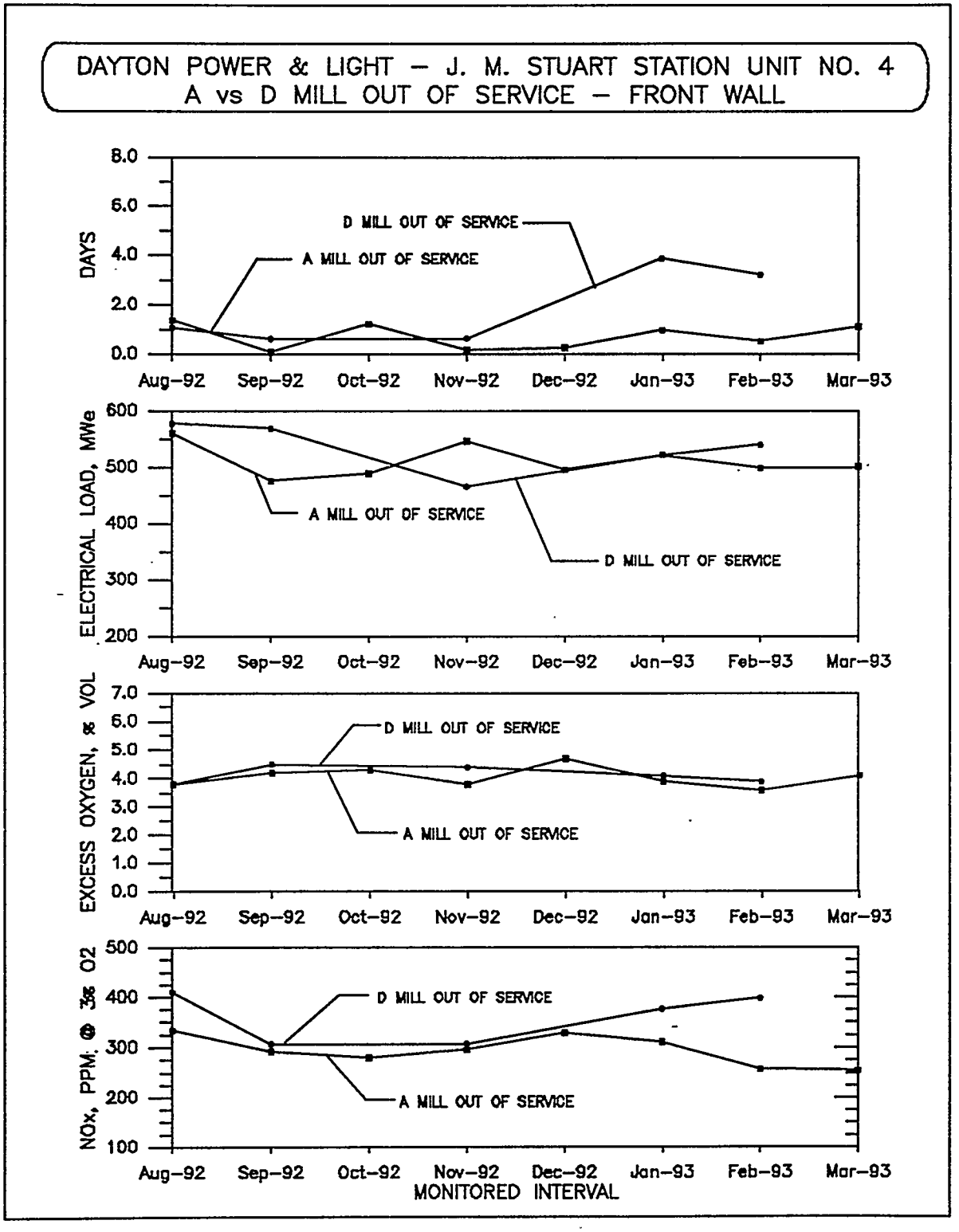

Figure 3-45 NO_x for A-mill out-of-service versus D-mill out-of-service

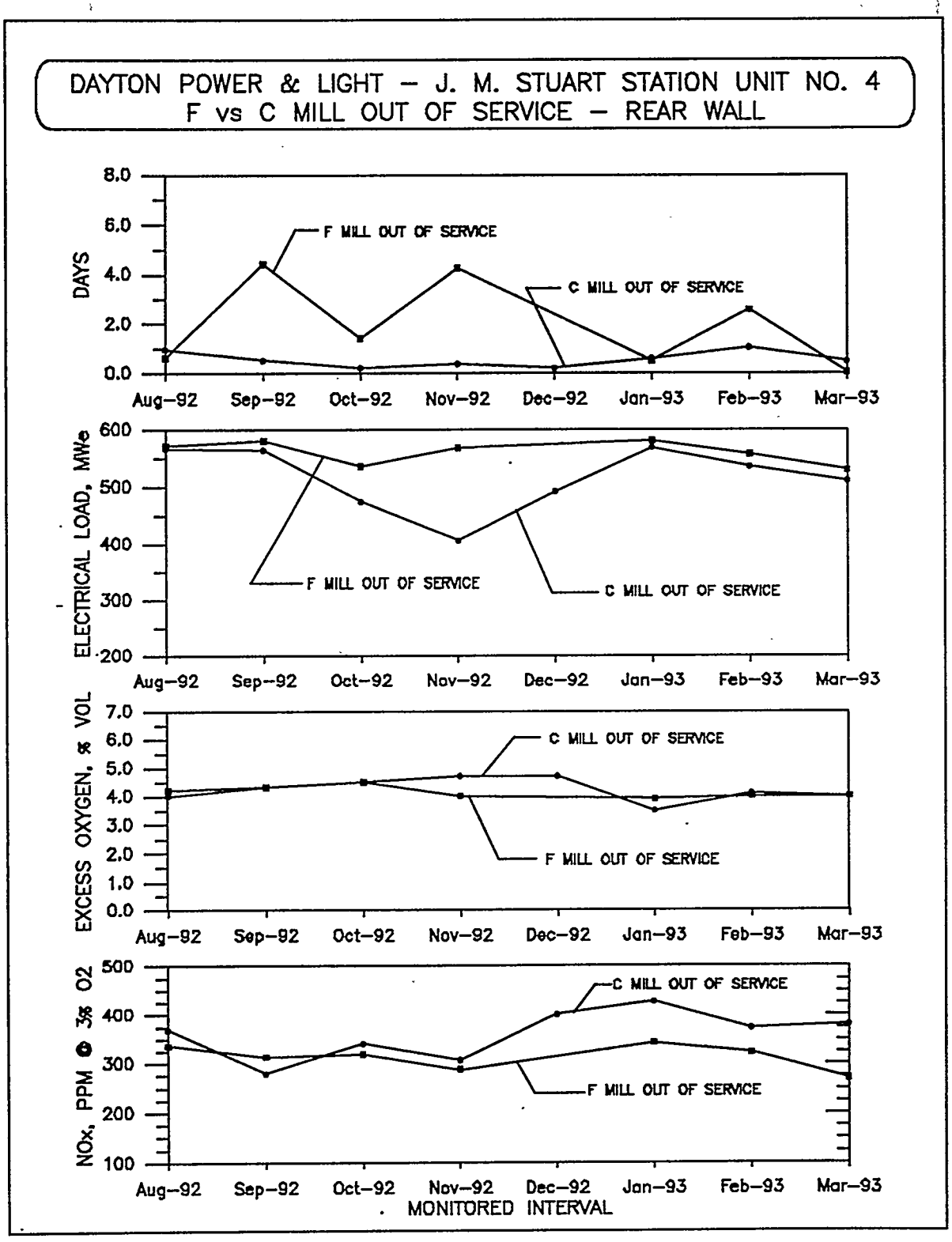

Figure 3-46 NO_x for F-mill out-of-service versus C-mill out-of-service

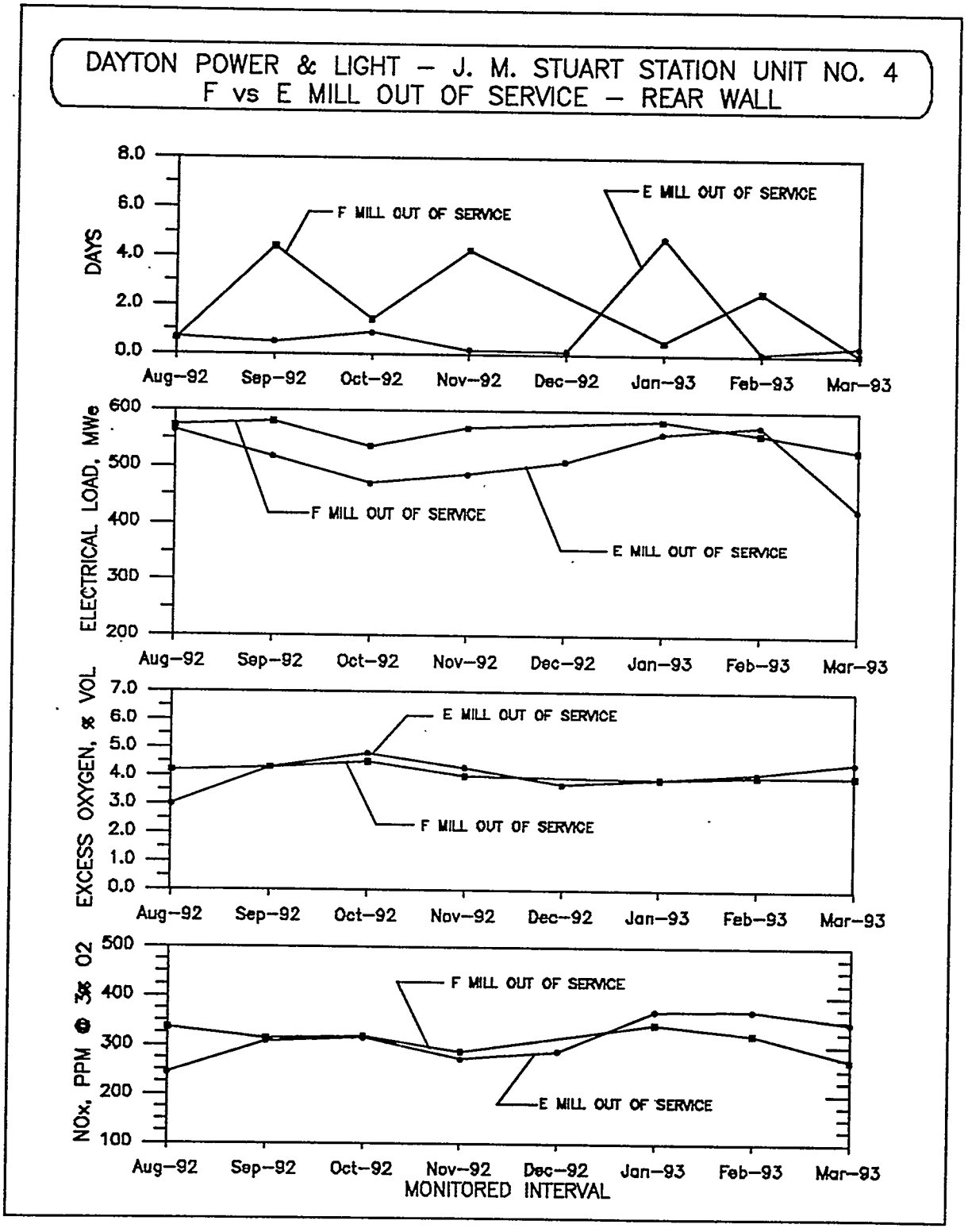

Figure 3-47 NO_x for F-mill out-of-service versus E-mill out-of-service

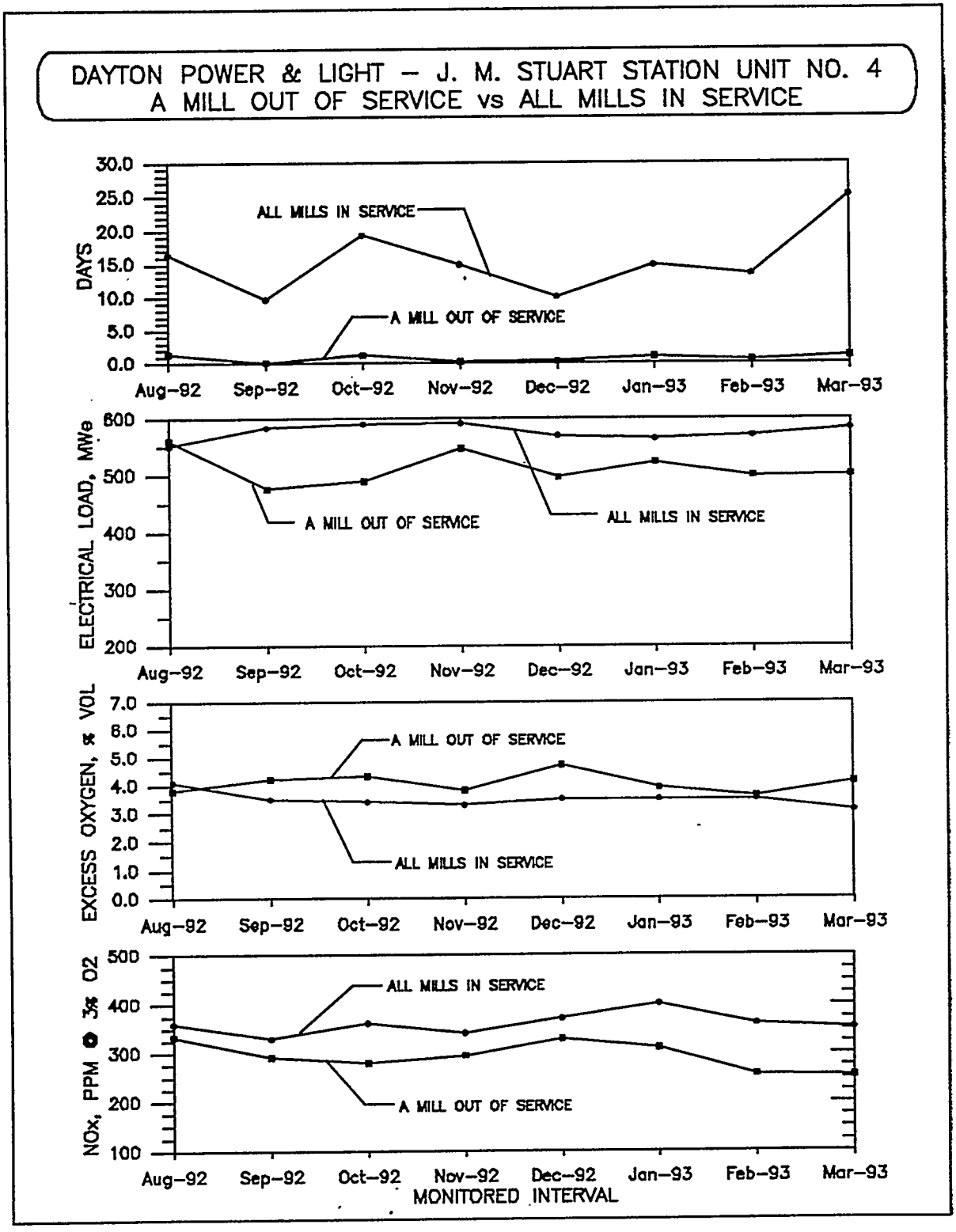

Figure 3-48 NO_x for A-mill out-of-service versus all mills in-service

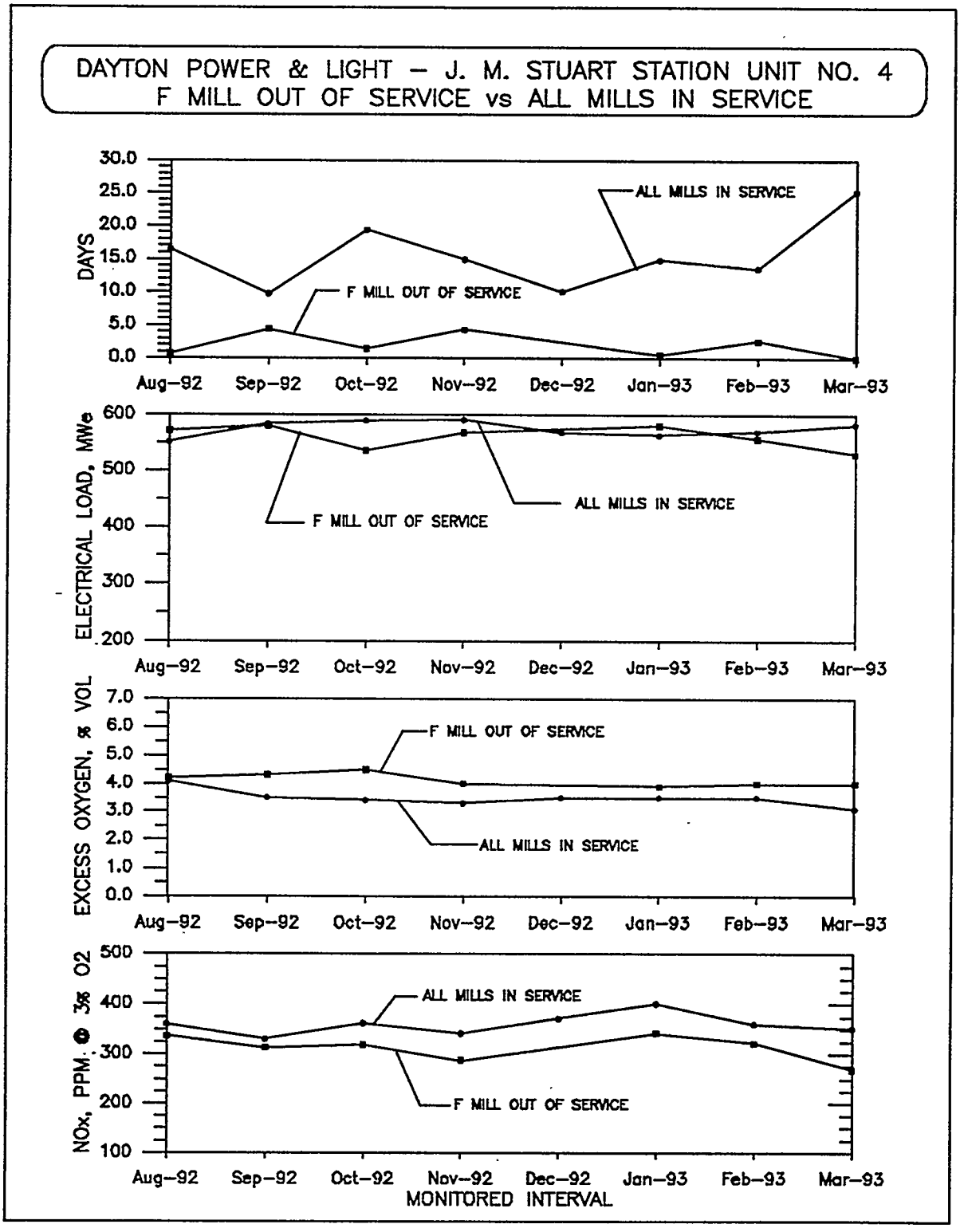

Figure 3-49 NO_x for F-mill out-of-service versus all mills in-service

A-Mill Versus B-Mill Out-of-Service — Front Wall. With A-mill out-of-service, NO_x levels tended to be about 75 ppm less throughout the 8-month period than with B-mill out-of-service. This trend is shown on the bottom plot of Figure 3-44.

A-Mill Versus D-Mill Out-of-Service — Front Wall. As Figure 3-45 shows, NO_x levels parallel each other fairly well over the August to November period with A-mill out-of-service producing about 25 ppm less NO_x. From December through March, D-mill out-of-service showed an upward trend in NO_x while A-mill out-of-service data showed a downward trend culminating in a 75 ppm difference by March. The cause of this phenomenon is not clearly understood. One explanation would be a fuel change magnified by a higher sensitivity to combustion air staging.

F-Mill Versus C-Mill Out-of-Service — Rear Wall. Figure 3-46 shows that regardless of whether F-mill or C-mill is out-of-service, there is little difference in their respective NO_x trends until November/ December. Both show gradual upward trends; however, C-mill increases faster leading to about a 75 to 100 ppm difference by the end of the period.

F-Mill Versus E-Mill Out-of-Service — Rear Wall. Like F-mills and C- mills, F-mills and E-mills in Figure 3-47 show little difference in NO_x levels until January with both showing decreasing levels from January through March. F-mill decreases faster, ending the period about 75 ppm below E-mill.

A-Mill Out-of-Service Versus All Mills In-Service. Figure 3-48 shows A-mill out-of-service produces about 50 ppm less NO_x than when all mills are in-service from August through December. But beyond January, the difference increases to about 100 ppm.

F-Mill Out-of-Service Versus All Mills In-Service. Figure 3-49 shows that when F-mill is out-of-service, NO_x levels decrease about 50 to 75 ppm. This operating condition does not show an increasing difference as A-mill out-of-service versus all mills in-service for the same time period.

3.4.2.2 Conclusions

- Results from eight months of continuous emissions monitoring support earlier conclusions drawn from short-term testing. When mills supplying the top burner rows are taken out-of-service, a significant reduction in NO_x levels occurs. This is more noticeable for burners on the front wall where there is 50 to 75 ppm reduction throughout the 8-month period for A-mill out-of-service versus B-mill out-of-service See Figure 3-43 for burner layout.

  This occurence can be attributed to the effects of air staging. With A-mill out-of-service, cooling air from four burner and four overfire air ports is admitted into the combustion zone across the entire boiler's width. All fuel input through the front wall is through the bottom burner row from D-mill and through a pair of burners in each of the top and bottom rows from B-mill. This firing configuration is almost a fully staged one. Only two of six burners in the top row are supplying fuel.

  With B-mill out-of-service, only two burner and two overfire air ports are available to supply staging air. A-mills and D-mills are supplying all the fuel. This firing configuration provides little to no effective staging since no air is admitted above operational burners.

Similar conclusions can be drawn for burners on the rear wall; however, the difference is not as obvious for similar upper/lower row firing configurations.

- A second observation from a review of CEM data is a very noticeable departure from an overall trend. Except for A-mill versus B-mill out-of-service (Figure 3-44), NO_x levels tend to spread for all other firing configurations after December or January. With A-mills and F-mills out-of-service, NO_x levels decrease while with other mills out-of-service, the decrease is not as great or they increase over this time interval. See Figures 3-45, 3-46, and 3-47. It is not clear why this occurs other than due to some sensitivity to fuel characteristics. We could see no correlation with excess air or load changes.

3.5 LONG-TERM OPERATIONAL PERFORMANCE

The operational performance of the Low-NO_x Cell™ Burner (LNCB) equipment has been good since the final arrangement and impeller modifications were made in April 1992. The LNCBs have been providing stable combustion conditions with good carbon burnout.

The amount of flyash produced appears to have increased while the amount of bottom ash has decreased. The flyash appears to be finer as compared to that produced with the original cell burners. Even though the overall dust loading has increased, the performance of the precipitators has improved.

The cell burners formerly produced a buildup of agglomerated "popcorn" ash on the horizontal convection pass sections of the boiler, particularly on the economizer. This ash buildup and associated tube erosion has been greatly reduced since the installation of the LNCBs. The required maintenance associated with the airheaters, the flyash handling equipment, and the bottom ash handling equipment has been reduced due to the condition of the ash produced by the LNCBs in this boiler.

For the purposes of long-term corrosion evaluation of the furnace waterwall tubes, DP&L has reported that the sulfur level in the as-received coal supplied to the J. M. Stuart Station during the long-term test period of August 1992 through March 1993 averaged 1.24%.

Section 4
CONCLUSIONS

The long-term task of the LNCB project has focused on:

1) Boiler stack emissions monitoring including O_2, CO, NO_x, and CO_2 for the 8-month period as well as measurements of pre- and post-retrofit N_2O levels
2) A corrosion effort in which the corrosion resistance of various alloys and coatings in reducing combustion gases was evaluated by both laboratory retort tests at B&W and field test at JMSS 4
3) In-furnace gas species probing near the burners and waterwall to support the corrosion effort

Conclusions describing the general operation of the Low-NO_x Cell™ Burner technology are as follows:

- Data collected by B&W indicated a 55.5% reduction in NO_x emissions compared to baseline test results. These results were measured with the unit at full load with all mills in-service. Measurements of the same operating condition by the independent testing company (Acurex Environmental Corporation) indicated a 53.0% NO_x reduction.
- Furnace exit gas temperatures averaged about 10°F lower than baseline values (standard cell burners) and more importantly, are more even in distribution than baseline operation. As a result, problems with gas-pass pluggage due to bridging of ash deposits at the furnace exit have been reduced or eliminated.
- A small increase in carbon loss representing about a 0.37% average overall loss of efficiency was measured. Half of this loss was regained through a 0.16% increase in average efficiencies caused by lower economizer gas outlet temperatures.
- No change in ash composition was noted in comparing upper furnace ash samples before and after the retrofit. The original cell burners formerly produced a buildup of agglomerated "popcorn" ash on horizontal convective pass tubes. This ash buildup and associated tube erosion has been greatly reduced since the LNCB installation. Also, required maintenance associated with the airheaters, flyash handling equipment, and bottom ash handling equipment has been reduced since the retrofit.

Conclusions made as a result of the long-term task work are as follows:

- From laboratory and field results, predictive equations were developed which appear to be useful in estimating the expected worst corrosion rate of an alloy under a given combustion environment.
- The long-term corrosion panel test in J. M. Stuart Station Unit #4 (JMSS 4) indicates that the maximum metal wastage of SA213-T2 is approximately 21 mils after the 15-month operating period. This wastage rate is equivalent to a corrosion rate of 17 mpy. Based on predictive equations developed during the long-term test task, maximum metal wastage of T2 was calculated to be 15 mpy.

These equations based their predictions upon: 1) the metal temperature, 2) H_2S concentration in the flue gas, and 3) Cr concentration in the alloys under the test conditions employed.

- All of the commercial high-alloy steels investigated in this task, including a popular and economical steel — SA213-TP304, appear to possess suitable corrosion resistance to the laboratory mixed gases. Their good performance was also confirmed by the field test. Therefore, the selective use of chromia-forming alloys in areas of the boiler where chemically reducing flue gases have wall contact should alleviate the corrosion concern of many low-NO_x technologies.
- By contrast, the corrosion performance of carbon and low-alloy steels commonly used in the lower furnace of utility boilers may suffer due to sulfidation attack under reducing combustion gases. Therefore, these materials require surface protection locally in the lower furnace where reducing gases are present. However, high tube wastage was reported prior to the retrofit in JMSS4 where reducing combustion gases were suspected.
- Results of the field test suggest that a chromia-forming coating relatively free of structural defects may be locally applied to the surfaces of waterwalls to combat the above noted sulfidation attack. However, these corrosion resistant materials can be significantly affected by their microstructure integrity. When pre-existing structural defects, such as cracks, pores, and oxide stringers are present, the corrosion attack can proceed preferentially along these sites. As a result, the metal wastage can be much greater than anticipated when the surface coatings are not applied properly.
- Regarding field measurements, an accurate on-line H_2S monitoring system for the interior of a furnace was successfully developed. Also, an on-line system for monitoring levels of H_2S at the test unit's west wall corrosion panel was developed. This system was not considered as accurate as the in-furnace probe system (since some H_2S may have been destroyed by gas-phase reactions within the probe due to a slow quench rate from 1000°F to 300°F).
- In-furnace H_2S monitoring both before and after the LNCB retrofit indicate that there was no significant increase in H_2S levels on the east and north sides of the boiler between 4 and 18 feet into the furnace interior. These measurements were made at the lower burner level in all instances.
- The temporal average H_2S levels on the corrosion panel ranged from less than 20 ppmV (lower left side) to 839 ppmV (upper right side — near the center of the furnace at the lower burner level) during the post-retrofit testing in June of 1992 (prior to burner optimization for lower H_2S performance). As a result of burner optimization work in August 1992, H_2S levels monitored on the corrosion panel were reduced to less than 20 ppmV (limit of gas chromatograph detection) for three of the four corrosion panel sample ports. H_2S levels of 95 ppmV were measured through the fourth (lower right) port.
- Based on March 1993 probing of the same four ports, the benefit of the burner adjustments was observed to be dependant upon many boiler operating factors. Airheater pluggage had occurred which biased air distribution in the boiler's windbox. This altered burner performance with the effect of increasing H_2S along the corrosion panel. Additionally, it was observed that mills out-of-service alter coal/air mixing to the remaining burners and can change H_2S levels near the furnace walls. For instance, H_2S levels in the 500 ppmV range were measured through one of the corrosion port panels (lower right) in March with the burners in their optimized settings but with airheater pluggage occurring. This compares with an H_2S level of 95 ppmV (lower right port) with no airheater pluggage as measured in August 1992. Burner air distribution is considered the primary cause of this disparity.
- Regarding long-term emission monitoring, economizer outlet emissions by Acurex Environmental Corporation show consistent operation with an average NO_x value of 350 ppmV corrected to 3% excess O_2 over the 8-month monitoring period.

In summary, the JMSS 4 retrofit was successful in fulfilling all of its original objectives and is considered an economical and effective technology for obtaining significant (>50%) NO_x emission reduction for existing cell burner equipped boilers.

Section 5
RECOMMENDATIONS

The following recommendations are made:

- Continue the long-term corrosion evaluation effort at the host site (JMSS 4) over the next 3 to 5 outages (~5 years). Removal of about 1 foot of the corrosion panel material across all 80 tubes should be made with corresponding comparison and analyses. Also, in-furnace sampling for H_2S should be made prior to each boiler outage to measure levels of this gas species near the wall.
- Build an improved probe for sampling through the corrosion panel ports. This would likely require a water-quench system and an internal heater for maintaining the sample above the flue gas dew point (~275°F).
- Test for H_2S using coals of different sulfur content to quantitatively characterize the relationship between coal sulfur content and H_2S levels at the furnace walls.
- For future retrofits of the LNCB technology, application of coatings having compositions similar to commercial high alloy steels is recommended for sections of the boiler's waterwalls in localized areas where high metal temperatures and reducing combustion gases are most likely to co-exist.
- Use numerical modeling techniques developed in other phases of this project to aid in locating potential reducing conditions near the boiler waterwalls.
- The techniques used to apply the coatings with minimum defects proved to be important. Therefore, further work is needed to identify not only the alternative materials, but also the coating techniques. This work should also include economic analyses to optimize the selection of the coating process.

Section 6
REFERENCES

1. L. W. Rodgers, H. Farzan, H. Sarv, and C. F. Eckhart, "Retrofit Combustion Modifications for NO_x Control in Utility Boilers — From Pilot-Scale to Full-Scale Development," presented at the 1990 Fall International Symposium, *AFRC-90 Paper No. 30*, American Flame Research Committee, San Francisco, California, October 8-10, 1990.

2. M. J. Clark, et al., "Development of a Retrofit Low-NO_x Cell Burner," presented at the Joint Power Generation Conference, *ASME Paper 86-JPGC-FACT-G*, Portland, Oregon, October 19-23, 1986.

3. S. F. Chou and P. L. Daniel, "Corrosion in Low-NO_x Staged Combustion Units — A Literature Survey," *Alliance Research Report Center LR:81:2877-01:01*, January 1981.

4. S. F. Chou, P. L. Daniel, and D. Eskinazi, "Fire-Side Corrosion in Low-NO_x Combustion Systems," presented at the EPRI/EPA Joint Symposium on Stationary Combustion, *B&W Technical Paper RDTPA85-36*, Boston, Massachusetts, May 1985.

5. R. A. Rapp, *Corrosion*, NACE, v. 42(10), p. 568, 1986.

6. C. F. Eckhart to T. A. Laursen, "ARC Baseline Test Report for the LNCB Project," *Alliance Research Center Report RDD:4009-01:01:91-01*, July 1991.

7. P. D. Zelanko and G. Simkovich, "High-Temperature Sulfidation Behavior of Iron-Base Alloys in Hydrogen-Sulfide Gas Mixtures," *Oxid. Met.*, v. 8(5), p. 343, 1974.

Appendix A
LAYOUT OF THE TEST PANEL INSTALLED IN JMSS 4

Appendix A
LAYOUT OF THE TEST PANEL INSTALLED IN JMSS 4

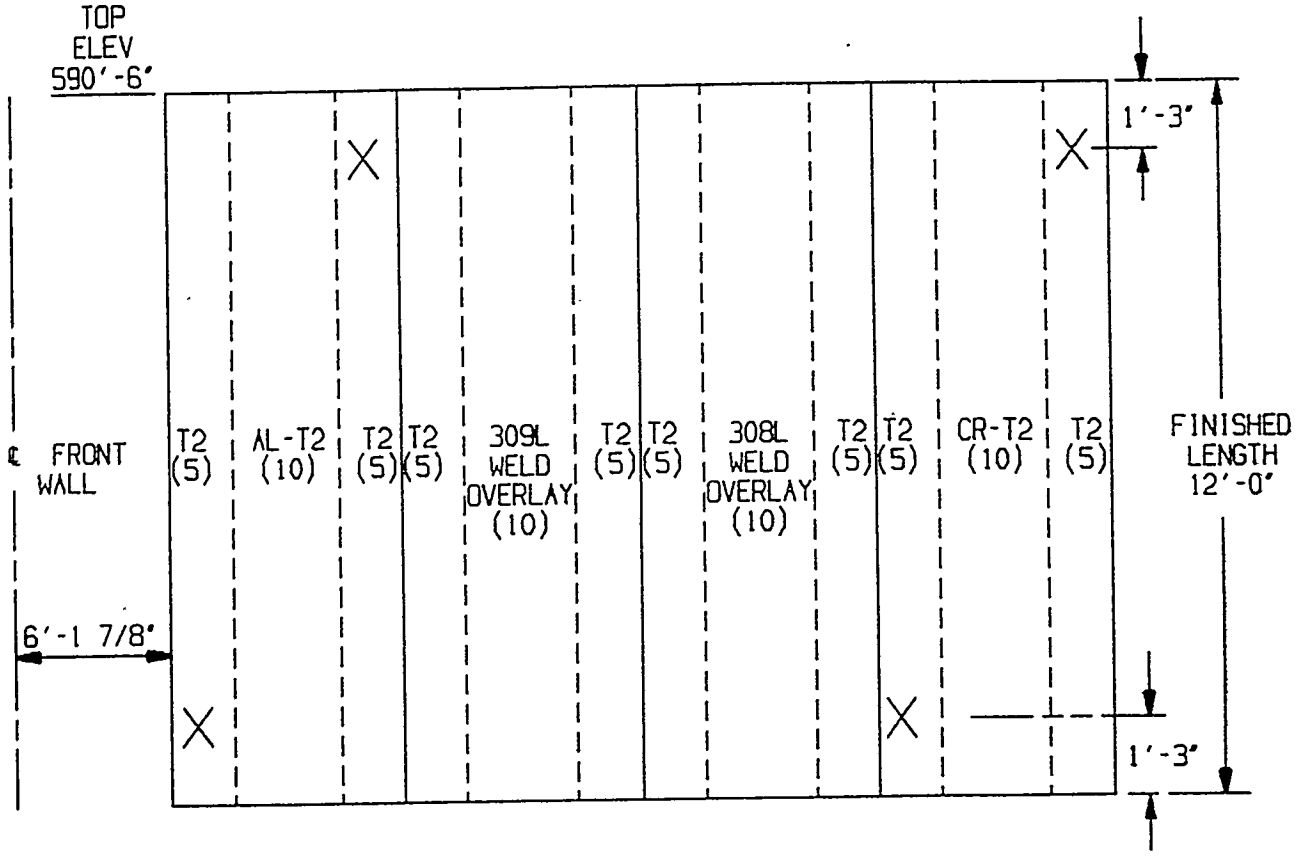

X INDICATES H_2S PORT LOCATION. CHORDAL THERMOCOUPLES ARE ADJACENT TO PORT LOCATIONS

( ) INDICATES QUANTITY OF TUBES IN EACH GROUP

T2 SIGNIFIES SA-213T2 BARE TUBE MATERIAL

AL-T2 SIGNIFIES ALUMINIZED SPRAY COATED T2 TUBE MATERIAL

309L, 308L SIGNIFIES STAINLESS WELD OVERLAY ON T2 BASE METAL

CR-T2 SIGNIFIES CHROMIZED T2 TUBE MATERIAL

Appendix B
ACUREX ENVIRONMENTAL CORPORATION CEM DATA

Appendix B
ACUREX CORPORATION CEM DATA SUMMARY

Table B-1
DP&L STUART STATION UNIT 4 ALL LOADS[a] CEM DATA SUMMARY — AUGUST 1992 TO MARCH 1993

Mills Out of Service	AUGUST				SEPTEMBER				OCTOBER				NOVEMBER			
	NO_x[b]	O_2[c]	MWe	Days[d]	NO_x[b]	O_2[c]	MWe	Days[d]	NO_x[b]	O_2[c]	MWe	Days[d]	NO_x[b]	O_2[c]	MWe	Days[d]
A	334	3.8	561	1.38	292	4.2	476	0.08	280	4.3	489	1.22	295	3.8	546	0.17
B	417	3.8	592	0.33	335	4.3	499	0.75	327	4.6	540	0.17				
C	369	4.0	567	0.96	279	4.3	565	0.54	340	4.5	475	0.22	307	4.7	407	0.39
D	410	3.8	578	1.08	306	4.5	569	0.63					307	4.4	466	0.64
E	244	3.0	564	0.67	308	4.3	518	0.50	315	4.8	470	0.88	272	4.3	486	0.17
F	336	4.2	572	0.63	313	4.3	580	4.42	318	4.5	536	1.41	287	4.0	568	4.26
AE					283	5.6	376	0.21								
AEF					236	6.9	312	0.17								
AF	273	6.1	370	0.71	259	6.0	399	0.63					236	6.3	370	0.40
BC					346	3.9	456	0.38								
BE	397	5.2	419	0.08	295	6.4	366	0.50	289	6.0	426	0.09				
BF	292	4.9	379	0.38	307	5.0	415	0.58					263	4.8	408	0.05
CD	378	5.5	402	0.50	304	5.1	418	1.04					287	5.4	386	0.09
CE	271	5.6	385	0.46												
All Mills In Service	360	4.1	551	16.46	330	3.5	584	9.71	362	3.4	590	19.38	341	3.3	592	14.95
Average for Month	353	4.2	540	23.63	318	4.1	544	20.13	352	3.6	575	23.35	325	3.6	573	21.10

Mills Out of Service	DECEMBER				JANUARY				FEBRUARY				MARCH			
	NO_x[b]	O_2[c]	MWe	Days[d]	NO_x[b]	O_2[c]	MWe	Days[d]	NO_x[b]	O_2[c]	MWe	Days[d]	NO_x[b]	O_2[c]	MWe	Days[d]
A	329	4.7	496	0.26	310	3.9	522	0.97	256	3.6	499	0.52	254	4.1	501	1.10
B	365	4.0	561	3.65	365	4.1	527	1.34	289	3.9	547	0.49	334	4.4	503	0.92
C	400	4.7	492	0.21	426	3.5	569	0.60	372	4.1	536	1.04	379	4.0	511	0.49
D					376	4.1	522	3.88	398	3.9	540	3.23				
E	288	3.7	509	0.14	369	3.9	559	4.78	370	4.1	572	0.08	346	4.5	426	0.35
F					342	3.9	581	0.51	322	4.0	558	2.57	270	4.0	530	0.05
AE					280	5.2	422	0.21					226	5.2	408	0.14
AF	256	4.8	429	0.22					240	4.0	465	0.40	236	4.8	427	0.22
BC					366	5.3	423	0.04					438	4.6	417	0.18
BCE					301	5.9	338	0.14								
BD					376	4.9	443	0.09								
BE									322	4.6	409	0.30	291	5.8	383	0.66
CD	376	5.9	362	0.92	339	5.3	395	0.53					257	4.4	433	0.19
CDF									303	6.1	333	0.05				
CE													409	4.7	405	0.88
CF									304	5.5	364	0.24				
DE					333	5.2	408	0.30								
DF									306	5.3	433	0.04				
EF					288	6.3	378	0.17								
All Mills In Service	371	3.5	569	10.03	401	3.5	564	14.84	360	3.5	570	13.57	352	3.1	583	25.18
Average for Month	367	3.8	550	15.42	383	3.8	546	28.41	355	3.7	553	22.56	347	3.3	562	30.34

[a] Turbine output of all loads
[b] ppm dry, 3 percent O_2
[c] Dry, percent by volume
[d] Cumulative (24-hr) days at load and mill configuration (CEM data for remaining days in each month were not included due to boiler shutdown, CEM maintenance, or questionable data)

Appendix C
INSTRUMENT LIST

Appendix C
INSTRUMENT LIST

PROTOTYPE PROBE EVALUATION

Item	*Manufacturer*	*Mfg #*	*B&W #*	*Status*
Stop Watch	Cole Parmer	0900217	0900217	Certified 12/12/91
Water Meter	Fisher Porter	Ser. #92W340044	0890480	Calibrated
Rotometer	Fisher Porter	8509HC031184/1		Calibrated
Digital Thermometer	Fluke	4540015	880137	Calibrated
Thermocouples			P.O. #01837	5/13/92

VIEWPORT PROBING

Item	*Manufacturer*	*Mfg #*	*B&W #*	*Status*
TC1 to TC10	J-TC		P.O. #01837	5/13/92
TC1 to TC10 and TCB Readout	Fluke	4540015	880137	
TCA Readout	Fluke	3260053	790303	
Probe Heater	Variac	Type 3PN501		
TCC Readout	Barberton			
Pump	Model 19310TC	Ser. #900387		
80 ft Heated Sample Line (b)	Model 80 ft	Ser. #15530-08		
150 ft Heated Sample Line (k)				
Flowmeter	Brooks Instrument	8509HC031184/1	870153	

CORROSION PANEL PROBING

Item	*Manufacturer*	*Mfg #*	*B&W #*	*Status*
TC1				
TC (Heat Tapes)				
TC (Hot Boxes)				
Pump	Model 19310TC	Ser. #900387		
150 ft - Heated Sample Line				
80 ft - Heated Sample Line	Model 80 ft	Ser. #15530-08		
Infra-Heated Sample Line TC				
Intra-Heated Sample Line Readout	Barberton			

ACUREX DILU-CEM 500 CONTINUOUS MONITORING EQUIPMENT

Instrument	Principle of Operation	Manufacturer	Instrument Model	Analyzer Range	Dilution Corrected Range
NO or NO_2	Chemiluminescence Ambient	Thermo Environmental	42	0 to 0.05 ppm 0 to 20.0 ppm	0 to 5 ppm 0 to 100 ppm
CO	Gas Filter Correlation	Thermo Environmental	48	0 to 1.00 ppm 0 to 1,000 ppm	0 to 100 ppm 0 to 10%
CO_2	Nondispersive infrared (NDIR)	Milton Roy	3300A	0 to 0.08% 0 to 0.16% 0 to 0.20%	0 to 8.0% 0 to 16.0% 0 to 20.0%
O_2	Fuel Cell	Yokogawa	Z021D/ZA8C	0 to 21%	0 to 100%
Dilution Air Conditioner	Refrigerant dryer-condenser	Thermo Environmental	111		
Data Collection	IBM-PC Compatible Computer	42 Mb Hard Disk 3.5" 1.44 Mb Floppy Disk 44 Mb Removable Cartridge		Output for: Printer and Modem for remote access	